E.O. Paton Electric Welding Institute of the National Academy of Science of Ukraine
International Association “Welding”

The Paton Welding Journal

09
2024

International Scientific-Technical and Production Journal ♦ Founded in January 2000 (12 Issues Per Year)

Address of Editorial Office
E.O. Paton Electric Welding Institute, 11 Kazymyr Malevych Str., 03150, Kyiv, Ukraine
Tel.: (38044) 205 23 90; E-mail: patonpublishinghouse@gmail.com, E-mail: journal@paton.kiev.ua
https://patonpublishinghouse.com/eng/journals/tpwj

The Journal was registered by the National Council of Ukraine on Television and Radio Broadcasting on 09.05.2024,
carrier identifier R30-04569; ISSN 0957-798X; DOI: http://dx.doi.org/10.37434/tpwj

Subscriptions, 12 issues per year:
348 Euro — annual subscription for the printed (hard copy) version, air postage and packaging included;
288 Euro — annual subscription for the electronic version (sending issues in pdf format or providing access to IP addresses).

Representative Offices of “The Paton Welding Journal”:

BRAZIL, Arc Dynamics
Address: Nova Iguacu, Rio de Janeiro, Brazil
Daniel Adolpho, Tel.: +55 21 9 6419 5703, E-mail: dadolpho@arcdynamics.com.br

BULGARIA, Bulgarian Welding Society
Address: Blvd. Asen Yordanov No.10, Sofia 1592, Bulgaria
Pavel Popgeorgiev, Tel.: +359 899 96 22 20, E-mail: office@bws-bg.org

CHINA, China-Ukraine Institute of Welding, Guangdong Academy of Sciences
Address: Room 210, No. 363 Changxing Road, Tianhe, Guangzhou, 510650, China
Zhang Yupeng, Tel.: +86-20-61086791, E-mail: patonjournal@gwi.gd.cn

POLAND, PATON EUROPE Sp. z o. o.
Address: ul. Kapitałowa 4, 35-213, Rzeszów, Poland
Anton Stepakhno, Tel.: +38067 509 95 67, E-mail: Anton.Stepakhno@paton.ua

The content of the Journal includes articles received from authors from around the world in the field of welding, cutting, cladding, soldering, brazing, coating, 3D additive technologies, electrometallurgy, material science, NDT and selectively includes translations into English of articles from the following journals, published in Ukrainian:

- «Avtomatychne Zvaryuvannya» (Automatic Welding), https://patonpublishinghouse.com/eng/journals/as;
- «Suchasna Elektrometalurhiya» (Electrometallurgy Today), https://patonpublishinghouse.com/eng/journals/sem;
- «Tekhnichna Diahnostyka ta Neruinivnyi Kontrol» (Technical Diagnostics & Nondestructive Testing), https://patonpublishinghouse.com/eng/journals/tdnk.

CONTENTS

ORIGINAL ARTICLES

INFORMATION

*Translated Article(s) from “Avtomatychne Zvaryuvannya” (Automatic Welding), No. 4, 2024.

**Translated Article(s) from “Avtomatychne Zvaryuvannya” (Automatic Welding), No. 5, 2024.

***Translated Article(s) from “Suchasna Elektrometalurhiya” (Electrometallurgy Today), No. 3, 2024.

****Translated Article(s) from “Tekhnichna Diahnostyka ta Neruinivnyi Kontrol” (Technical Diagnostics & Nondestructive Testing), No. 2, 2024.

Indexing: The electronic edition of the Journal is stored in the V.I. Vernadsky National Library of Ukraine (eVerLib), included in the OPEN UKRAINIAN CITATION INDEX database and international databases: CROSSREF, EBSCO, Google Scholar, INDEX COPERNICUS, IET Inspec, ULRICHSWEB.

DOI: https://doi.org/10.37434/tpwj2024.09.01

DEVELOPMENT OF HYBRID TECHNOLOGY OF PRODUCING SPHERICAL POWDERS FROM WIRE MATERIALS USING HIGH-SPEED PLASMA JETS AND ELECTRIC ARC

V.M. Korzhyk, D.V. Strogonov, O.M. Burlachenko, O.P. Gryshchenko, A.V. Zavdoveyev, O.M. Voitenko

E.O. Paton Electric Welding Institute of the NASU
11 Kazymyr Malevych Str., 03150, Kyiv, Ukraine

ABSTRACT

A technological scheme and equipment for hybrid process were developed, which is based on application of the energy of supersonic plasma jet and electric arc to produce high-quality spherical powders at wire material atomization. Performed experimental studies of the particle size distribution, morphology and technological properties of the produced powder showed that the above-mentioned process allows producing spherical powders in the range of 25–160 μm, where the share of finely dispersed fraction of 25–63 μm can be up to 70 wt.% with the coefficient of sphericity higher than 0.8, which results in high technological properties (bulk density, flowability, etc.) of the produced powders, and is extremely necessary for their application in additive technology. It is shown that the hybrid process is characterized by 2.5–6.0 times smaller specific flow rates of gas for producing 1 kg of powder and 1.25–6.0 times higher productivity, compared to other industrial technologies of plasma and electric arc atomization.

KEYWORDS: hybrid atomization, plasma jet, electric arc, productivity, spherical powders, additive manufacturing

INTRODUCTION

Over the recent years, the world has seen significant development of additive manufacturing (AM) technologies of metal product synthesis, which is due to a number of their essential advantages, compared to the traditional (subtractive) technologies of casting, metal treatment, etc. [16]: complete automation of the process and flexibility of the product manufacturing process is achieved; production cycle of component parts from their design stage to manufacturing the final products is significantly shortened; product manufacturing cost is lowered due to a more rational use of materials and production resources; there is a possibility of designing products with a functionally-gradient structure and properties with optimized geometrical, strength and weight characteristics.

It is anticipated that the world market of additive technologies will increase more than 6 times by 2032, from 15 to 95.6 bln USD (Figure 1) [7], where the groups of methods of direct energy deposition (DED) (up to 5 % of the total volume) and powder bed fusion (PBF) (up to 35 % of the total volume) with take up a considerable share of this market [8].

In our time the above-mentioned groups of metal product synthesis methods are used predominantly in high-tech industry segments at manufacture of complex metal components of aviation and aerospace engineering and locally in power industry and medicine. The main factors, limiting the application of additive technologies of metal product synthesis, also in other industry sectors, in addition to complex expensive equipment, is the need to use high-quality spherical powders of a certain particle size distribution as consumable material to form additive layers and granular compositions [9].

So, the above-mentioned group of DED methods includes the processes of direct metal deposition (DMD) and Laser Engineering Net Shaping (LENS), cold atomization (CA) and plasma powder transferred arc atomization (PPTAA), which use powders predominantly in the fraction range of 45–160 μm (15–45 μm for CS process), and the group of PBF methods consists of the processes of selective and direct laser melting and sintering (Selective Laser Melting (SLM), Selective Laser Sintering (SLS), Direct Metal Laser Sintering (DMLS)) and Electron Beam Melting (EBM)), where powders predominantly in the fraction range of 15–45 μm (45–160 μm for EBM process) are used for layer-by-layer synthesis [10]. These powders should also have minimal porosity, high degree of sphericity, stable chemical and phase composition, so that the most promising group of methods, satisfying all the above-listed requirements, and well as allowing adjustment of the particle size distribution of the powders in a broad range of 15–160 μm, are the technologies using the energy of plasma and electric arc.

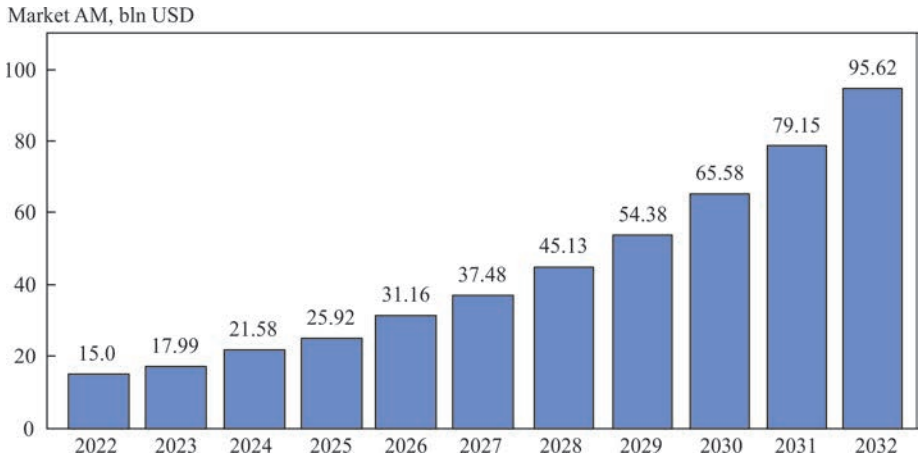

Figure 1. Trends in development of the world market of additive technologies for 2022–2033

ANALYSIS OF PUBLISHED DATA AND PROBLEM DEFINITION

It is known that such promising spheroidization technologies include the processes of plasma and electric arc atomization of the melt, namely plasma rotating electrode process (PREP), electric arc atomization (AA), plasma-arc atomization (PA) of neutral and current-carrying wires [11–13].

At present the PREP technology (Figure 2, *a*) is one of the most wide-spread processes of manufacturing high-quality spherical powders, as it allows producing powders from various materials with the coefficient of sphericity of 0.93 and higher. Here, the powder morphology is characterized by a practical absence of defects in the form of satellites and particles of an irregular shape, internal porosity, etc. [14]. However, operation of the above-mentioned equipment is characterized by considerable difficulties, associated with producing a finely-dispersed fraction of <100 μm, complex process of manufacturing a precision sputtered blank, insufficiently efficient use of this blank material, low process productivity, etc.

Arc atomization (Figure 2, *b*) is a widely applied technology, which is now used predominantly for coating deposition and features simplicity and affordability of the equipment, high productivity, which in some cases can be equal up to 40 kg/h, yield of a large quantity of fine fraction (<63 μm), etc. However, despite the large number of advantages, a significant drawback of arc atomization is use of cold gas for dispersion of the melt, forming at the end face of atomized wires, which leads to formation of powders with a high percentage of irregularly-shaped particles, satellites and with considerable internal porosity, making their application in the field of additive technologies impossible.

Another known technology of wire material spheroidization is the plasma atomization process (Figure 2, *c*), having two variants — atomization of neutral (Plasma non-transferred arc (PNTA)) and current-conducting (Plasma transferred wire arc (PTWA)) wires. A feature of the above technology is application of plasmatrons, generating high-velocity, and in some cases supersonic plasma jets, the velocity of which is in the range of $(2.5–18.5)\cdot10^2$ m/s that greatly intensifies the dispersion processes and increases the quantity of the produced fine fraction of the powder [15]. Known is the equipment of Pyrogen-

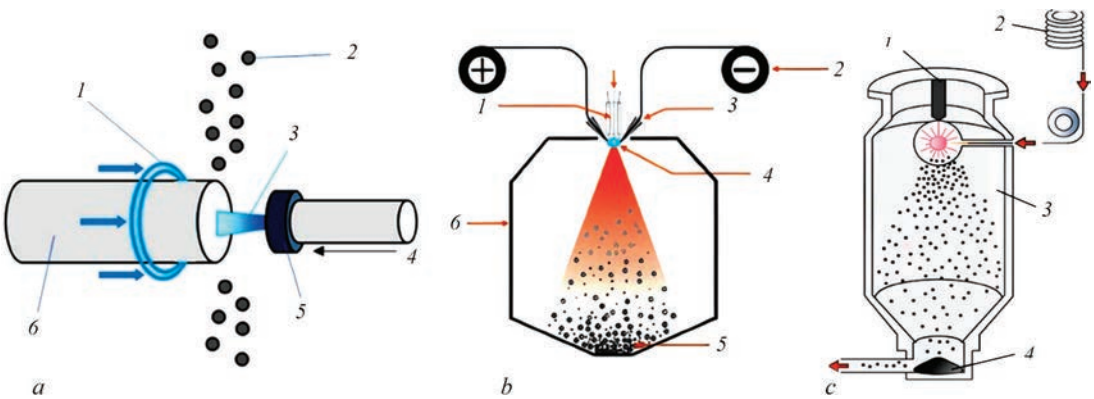

Figure 2. Main plasma and arc technologies of producing spherical powders for additive technologies: *a* — plasma rotating electrode process (*1* — counter gas; *2* — granules; *3* — plasma arc; *4* — plasma-forming gas; *5* — cathode; *6* — rotating blank); *b* — arc atomization of wire (*1* — arc soldering iron; *2* — wire; *3* — wire feeder; *4* — arc; *5* — powder; *6* — atomization chamber); *c* — plasma atomization of wire materials (*1* — plasmatron; *2* — wire; *3* — work chamber; *4* — container for powder collection)

esis Company (Canada), operating by plasma atomization scheme, where the neutral wire is atomized by three plasmatrons, that allows producing high-quality spherical powders from titanium and titanium alloys (Grade 1, Ti6A14V) and other materials, which by their morphology and technological properties correspond to powders, produced by the technology of plasma atomization [16]. The productivity of the process of plasma atomization of neutral wire, however, does not exceed 3 kg/h (up to 5 kg/h in the case of additional heating of atomized wire by an inductor before its feeding into the plasma jet) at 143 kW total power of the plasmatrons. Another approach to solving the above problem of increasing the productivity of plasma atomization process is application of a scheme with current-conducting wire. Corresponding equipment of PLAZER PL-30W [17] and PLAZER PL-50-W brands was developed at PWI, together with "Scientific and Production center "PLAZER"" LLC (Ukraine) [18], and theoretical and experimental investigations of the efficiency of the process of the efficiency of atomized wire heating were conducted [19], which showed that in the case of plasma atomization of current-conducting wire an increase of the quantity of heat applied to the wire by more than 4 times occurs, and this, in its turn leads to increase of the process productivity to 10–12 kg/h.

Thus, the most promising version of further evolution of the above processes is development of a hybrid plasma-arc technology (hybrid plasma-arc atomization (HPPA)), which is based on simultaneous application of the processes of arc plasma atomization for spheroidization of wire materials, as it allows combining the advantages of both the processes and reaching a productivity layer higher than that at application of arc atomization process, with the powder morphology and particle size distribution, inherent to the plasma atomization process. A variant of such a device was proposed in patent [20]. It is noted that this device allows reaching a productivity of up to 28 kg/h for 3.2 mm titanium wire of Ti6A14V grade diameter at atomization at the total power of 113 kW, where the share of the fine fraction of 20–63 μm is equal to 32 wt.%. However, in addition to the need for further increase of the yield of fine powder fraction, the above-mentioned process is characterized by super high flow rates of inert gas (higher than 90 m^3/h) that is much higher than in the known devices for ultra-high speed plasma atomization, where the plasma-forming gas losses are usually not higher than 30 m^3/h.

As there are no open-access data on the design and technological parameters of the process, equipment characteristics, and other technological aspects of hybrid atomization technology, except for the above-mentioned patent, it necessitates performance of investigations for development and evaluation of the suitability of the process of hybrid plasma-arc atomization for spherical powder manufacturing. For this purpose, PWI, in cooperation with "Scientific and Production center "PLAZER"" (Ukraine) where the specialists have extensive experience of operation of equipment for arc atomization, equipment for high-velocity (PLAZER-30, PLAZERT-50) and supersonic plasma atomization (PLAZER-80) [21]) was developed.

RESEARCH OBJECTIVE AND TASKS

The objective of this study is development of the technology and equipment for hybrid plasma-arc atomization and checking the effectiveness of their application to produce spherical powders, where the following tasks should be performed to achieve the defined objective: select the optimal design parameters of the hybrid device, study the particle size distribution, morphology and technological properties of the produced powders, determine the technical-economic characteristics of the above-mentioned method, compare them with other plasma and arc processes.

MATERIALS AND INVESTIGATION PROCEDURE

Solid wire from low-carbon steel of ER70S-6 brand of 1.6 mm diameter was used as model material for investigation of the powder particle size distribution, produced by different atomization technologies and 1.6 mm molybdenum wire of MCh brand was used to investigate the powder morphology and technological properties. Chemical composition of the above-mentioned wires is given in Table 1.

Atomization experiments were performed in air using equipment of PLAZER-50, PLAZERT-80 brand ("Scientific and Production center "PLAZER" LLC, Ukraine), for plasma atomization of current-conducting and neutral wire, respectively (Figure 3), which allows using the subsonic and supersonic modes of

Table 1. Chemical composition of the studied wire materials, wt.%

Wire brand	C	Mn	Si	P	S	Ni	Cr
ER70S-6	<0.07	0.9–1.4	0.4–0.7	<0.025	<0.035	<0.15	<0.15
	Mo	V	Al	Zr	Ti	Cu	–
	<0.15	<0.03	0.05–0.15	0.02–0.12	0.05–0.15	<0.5	–
MCh	Mo		Si			Other	
	>99.92		0.02–0.04			<0.04	

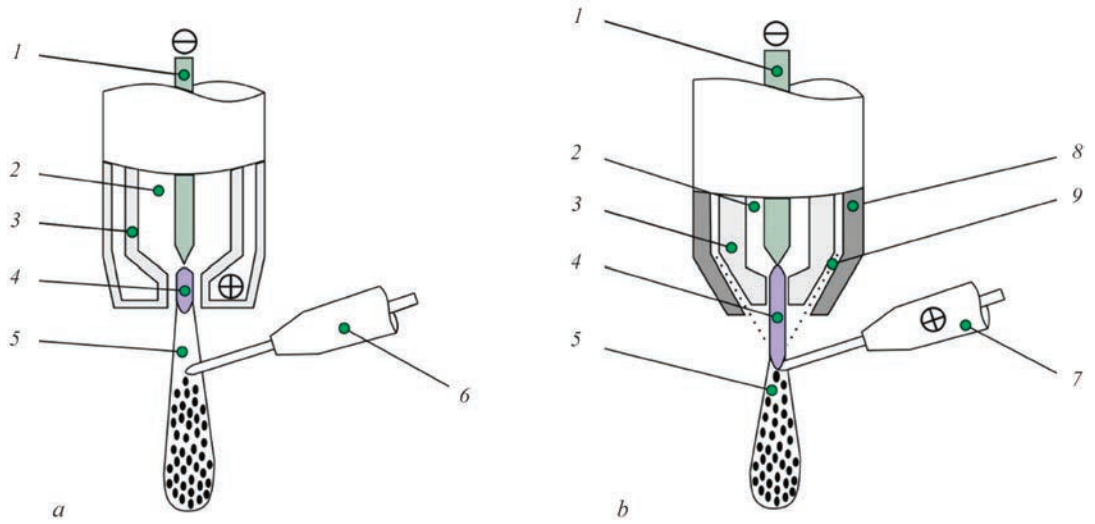

Figure 3. Scheme of the process of plasma atomization of neutral (*a*) and current-carrying wires (*b*): *1* — nonconsumable tungsten electrode (cathode); *2* — plasma-forming gas supply; *3* — plasma-forming nozzle; *4* — plasma arc; *5* — two-phase plasma jet; *6* — neutral atomized wire; *7* — current-conducting wire (anode); *8* — compression nozzle for accompanying gas supply; *9* — accompanying gas supply

plasmatron operation. PLAZER-15AS unit ("Scientific and Production center "PLAZER"", Ukraine) was used for arc atomization.

Technological parameters of the processes of plasma, arc and hybrid atomisation of wires are as follows:

PA (PNTA) — plasma atomization of neutral wire (PLAZER-80 unit):
- plasmatron power, kW 68
- plasma-forming gas flow rate, l/min. 500

PA (PTWA) plasma atomization of current-conducting wire (PLAZER-50 unit):
- plasmatron power, kW 27
- plasma-forming gas flow rate, l/min. 50
- accompanying gas flow rate, l/min 800

AA —— arc atomization (PLAZER 15AS unit):
- electric arc device power, kW. 14
- plasma-forming gas flow rate, l/min. 1000

HPAA — hybrid plasma-arc atomization (PLAZER 15AS + PLAZER 80):
- total power, kW. 82
- plasma-forming gas flow rate, l/min. 500

Note: Atomization of the studied wire materials was conducted in open atmosphere.

Hybrid plasma-arc atomization was performed by the following scheme (Figure 5): plasmatron

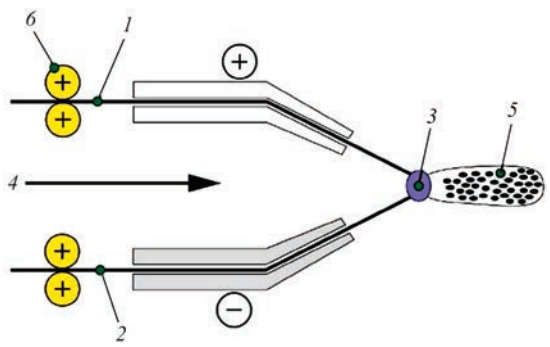

Figure 4. Scheme of the process of arc atomization of wire materials: *1* — anode wire; *2* — cathode wire; 3 — arc; *4* — atomizing gas; *5* — plume with atomized particles; *6* — wire feed mechanism

switching on and supersonic plasma jet formation were performed (Figure 5, *c*) at gas flowing through plasma-forming nozzle *1*, which was followed by switching on feed mechanism *2* of the wires which were under the potential from the arc power source, their feeding and convergence *3* in the axial zone of the plasma jet at 10–15 mm distance from the plasma-forming nozzle edge, where their melting, melt formation and its further fragmentation occurred as a result of aerodynamic influence of the plasma jet (Figure 5, *d*).

Produced particles were collected in a container with water, in keeping with a procedure, given in [22], followed by selection of samples to study the particle size distribution and morphology of powder surface (sample weight was not less than 200 g). Particle size distribution of laboratory powder batches was determined by the method of sieve analysis, in keeping with the procedure of ISO 25911:1988 "Test sieving, Part 1: Methods using test sieves of woven wire cloth and perforated metal plate", using vibro screen RLU-3 (Ukraine) with the following set of sieves: 2545, 4563, 6375, 75100, 100125, 125160, 160200, 200250, 250315, 315400. Investigation of particle shape and coating porosity was performed by the methods of analytical scanning electron microscopy in scanning electron microscope MIRA3 LMU (Ltd TESCAN, Czech Republic) with further analysis of the obtained images in MIPAR program package. Chemical composition of the powder was determined by microprobe analysis using scanning electron microscope MIRA-3 LMU fitted with microanalysis system INCA Energy 450 XMax-80 (Ltd Oxford Instruments, Great Britain). Investigation of the powder technological properties (flowability, bulk and appar-

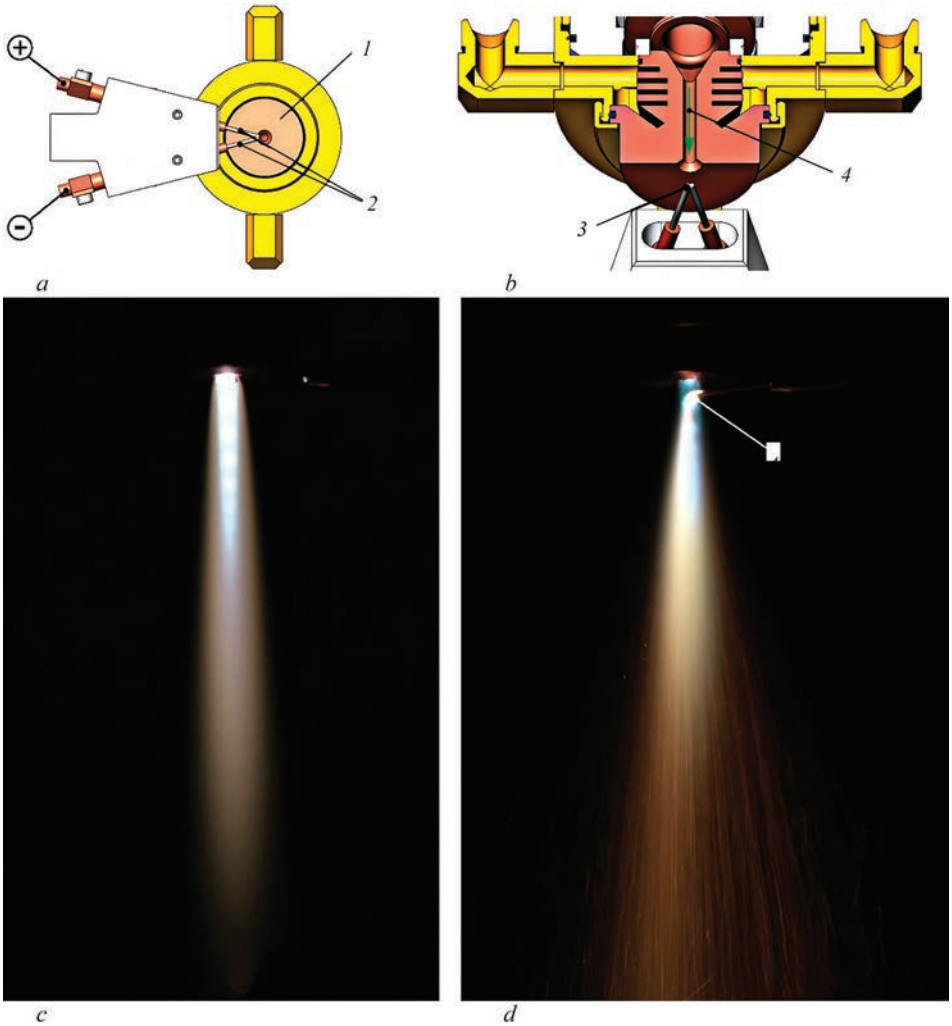

Figure 5. Schemes of plasmatron and arc device arrangement in the process of hybrid plasma-arc atomization (*a*, *b*), appearance of supersonic plasma jet of 1.5 Mach without (*c*) and with wire feed (*d*) into the plasma jet zone: *1* — plasma-forming nozzle of the plasmatron; *2* — atomized wires; *3* — wire convergence in the zone of plasma jet axial outflowing; *4* — direction of plasma-forming gas outflowing; *5* — fragmentation of the melt forming at atomized wire tips

ent density) was performed using Hall instrument, by the procedures of ISO 4490:2018 "Metallic powders — Determination of flow rate by means of a calibrated funnel (Hall flowmeter)" and ISO 39231:2018 "Metallic powders — Determination of apparent density, Part 1: Funnel method". Process productivity, G, and material utilization rate (MUR) were determined by weighing of powder obtained at wire atomization for 5 min, and initial wire weight before atomization in laboratory scales TBE-12-0.5-(250×300)-13P (Ukraine) with up to ±0.5 g accuracy.

INVESTIGATION RESULTS AND THEIR DISCUSSION

INVESTIGATIONS OF THE PARTICLE SIZE DISTRIBUTION, MORPHOLOGY AND TECHNOLOGICAL PROPERTIES OF THE PRODUCED POWDERS

Figure 6 gives the results of studying the particle size distribution of powder, produced at plasma, arc and hybrid plasma-arc atomization of 1.6 mm steel compact wire of ER70S-6 brand.

Investigations of the particle size distribution of the produced powders showed that the hybrid plasma-arc and plasma atomization of the neutral wire provide the largest quantity of the fine powder fraction. Here, much smaller particles are formed than in the processes of plasma atomization of current-conducting wire and arc atomization, with average diameter of 67 and 54 μm, respectively, and the quantity of fine fraction of 25–63 μm may reach 70 wt.% that is attributable to increased gas-dynamic pressure on the melt, formed during melting of the atomized wire tips in supersonic mode of plasma jet outflowing that, in its turn, promotes size reduction of the forming fragments [15].

Figure 7 shows a SEM image, obtained at hybrid plasma-arc atomization of molybdenum wire of MCh brand and the results of its processing in MIPAR program. Application of exactly the refractory metals in the hybrid plasma-arc atomization was due to the

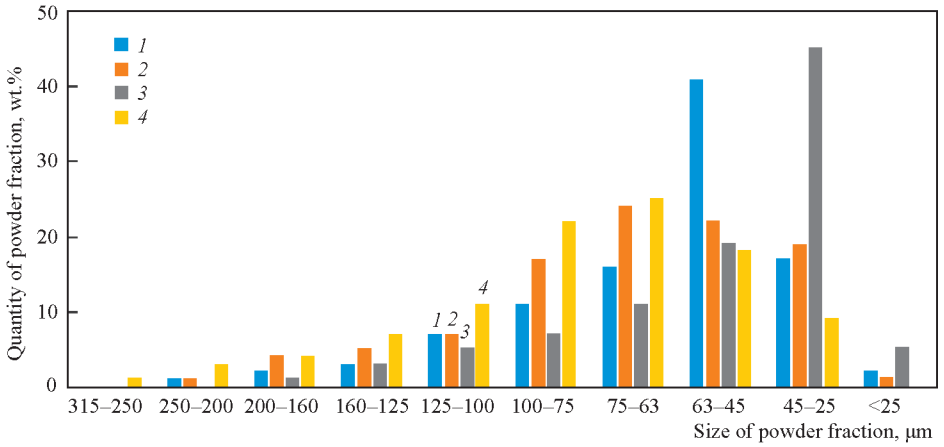

Figure 6. Particle size distribution of powder produced by different technologies of plasma atomization and arc atomization of 1.6 mm steel wire of ER70S-6 brand: *1* — PA (PNTA), G = 4 kg/h; *2* — PA (PTWA), G = 11 kg/h; *3* — HPAA, G = 24 kg/h; *4* — AA, G = 19 kg/h

problems of spheroidization of these materials, because of their physical and thermophysical properties, such as high melting temperature (2620 °C for MO and 3420 °C for W), heat conductivity, etc.

Analysis of powder morphology in MIPAR program showed that the powder is of a spherical shape with average coefficient of sphericity (S = 0.84), defects in the form of satellites and irregularly-shaped particles being practically absent. A more detailed consideration of powder morphology showed the presence of oxide film in some local zones of its surface, which may form during movement of molten particles as a result of their intensive interaction with oxygen, present in the air and may lead to deterioration of the coefficient of sphericity. To study this phenomenon energy-dispersive X-ray spectroscopy (EDX) of the mentioned local zones of powder surface was performed (Figure 8, Table 2).

Oxygen content on the studied powder surface is explained by the fact that the process of molybdenum

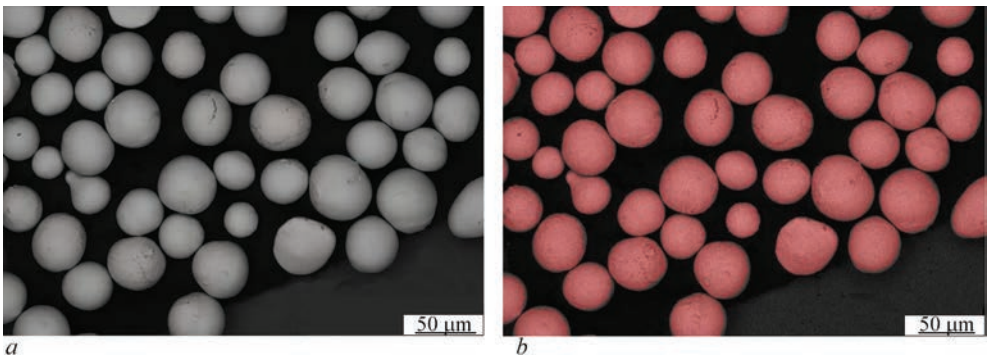

Figure 7. SEM image of powder of 15–45 μm fraction produced at hybrid plasma-arc atomization of 1.6 mm molybdenum wire of MCh brand before (*a*) and after (*b*) processing in MIPAR program

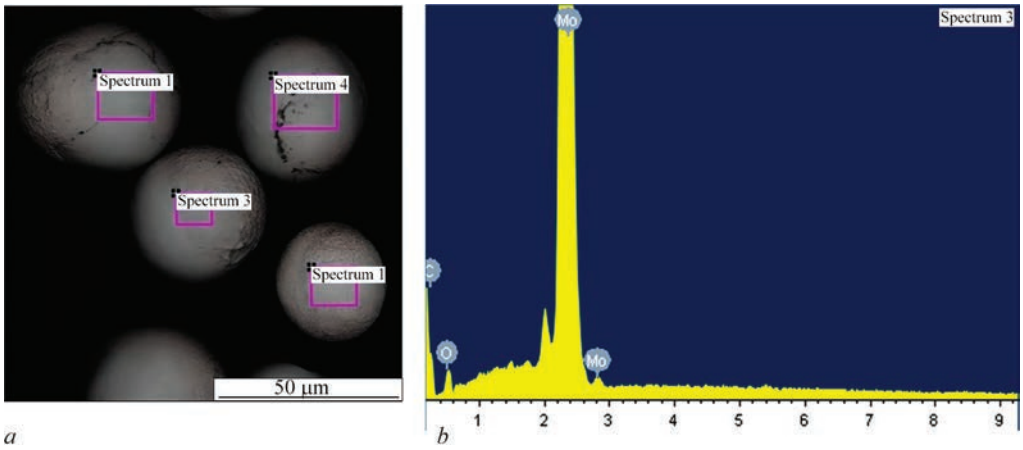

Figure 8. SEM image (*a*) and results of analysis of elemental composition (*b*) in local zones of molybdenum powder surface by EDX method

Table 2. Results of EDX of local zones on the surface of powder produced in the hybrid process of plasma-arc atomization of 1.6 mm molybdenum wire of MCh grade

Local zone	Chemical composition of local zones, at.%	
	Mo	O
Spectrum 1	97.32	2.68
Spectrum 2	98.73	1.27
Spectrum 3	98.29	1.71
Spectrum 4	97.04	2.96

Table 3. Technological properties of molybdenum powder produced by the technology of spheroidization of irregularly-shaped particles in induction plasma (ICPS) and hybrid plasma-arc atomization (HPAA)

Production method	Fraction size, μm	Bulk density, g/cm^3	Tap density, g/cm^3	Flowability, s/50 g
ICPS	2553	6.25	6.80	11
HPAA	2545	6.05	6.45	14

wire atomization was conducted in an open atmosphere with cooling in water, leading to interaction of the surface layers of molten particles with oxygen with oxide formation on their surface.

Investigations of technological properties (bulk density, tap density and flowability) of molybdenum powder produced by the technology of hybrid plasma-arc atomization, showed that the above powders do not essentially differ by these characteristics (Table 3) from commercial powders made by the technology of spheroidization of irregularly-shaped powders in induction plasma (Induction Coupled Plasma Spheroidization (ICPS), Tekna Company, Canada). Lower technological characteristics of the powder can be due to presence of oxide film on the particle surface and narrower range of the particle size distribution, shifted towards the finely-dispersed fraction, which impairs the sphericity characteristics, and furtheron can be eliminated when performing atomization in chambers with a shielding atmosphere.

DETERMINATION OF THE TECHNICAL-ECONOMIC CHARACTERISTICS OF THE HYBRID PROCESS OF PLASMA-ARC ATOMISATION AND ITS COMPARISON WITH OTHER COMMERCIAL PROCESSES

Studying the productivity (Figure 6) of the above-mentioned processes showed that its highest values are achieved at application of the processes of hybrid plasma-arc atomization and arc atomization, and they are equal to 24 and 19 kg, respectively. Improvement of productivity of the hybrid plasma-arc process relative to arc atomization by 25 % can be due to additional heating of the atomized wires as a result of their convective heat exchange with the plasma jet [17]. Calculations of the material utilization rate for the hybrid plasma-arc process showed that the above coefficient is equal to 0.97, i.e. up to 3 % of the total weight of the wire evaporates during atomization.

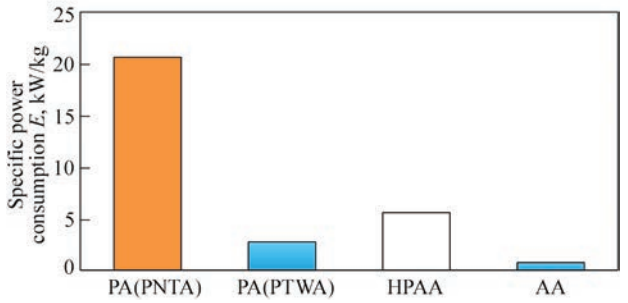

Figure 9. Specific power consumption E to produce 1 kg of steel powder at atomization 1.6 mm wire of ER70S-6 brand produced by different atomization technologies

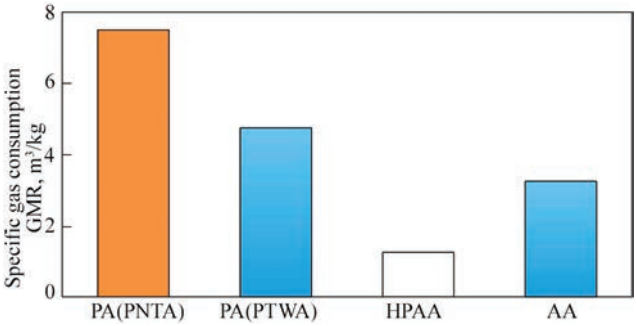

Figure 10. Specific gas consumption (GMR) to produce 1 kg of steel powder at atomization 1.6 mm wire of ER70S-6 brand produced by different atomization technology

Determination of specific power consumption (Figure 9) showed that in terms of its economy the most rational is application of the processes of arc and plasma atomization of the current-conducting wire, where power consumption is equal to 0.75 and 2.75 kW/kg, respectively, while the process of hybrid plasma-arc atomization is characterized by higher values of power consumption equal to 5.5 kW/kg.

Determination of specific gas consumption (gas to metal ratio (GMR)) to produce 1 kg of steel powder of ER70S-6 grade at HPAA atomization (Figure 10) showed that gas flow rate is the lowest in the processes of hybrid plasma-arc atomization and arc atomization, where the value of specific gas consumption is equal to 1.25 and 3.25 m^3/kg, respectively.

CONCLUSIONS

1. A scheme and equipment for hybrid plasma-arc atomization process was developed, which uses the arc for heating and melting of the atomized material, and the supersonic plasma jet is applied predominantly for melt fragmentation at the atomized wire tip at radial feeding of the wires into it.

2. The effectiveness of application of the hybrid process of plasma-arc atomization to produce high quality spherical powders, meeting the requirements by their particle size distribution and technological properties, to powders used in additive technologies (SLM/SLS, CS, EBM, PPTAA and LENS) was confirmed in the case of a compact steel and molybdenum wires of ER70S-6 and MCh brands of 1.6 mm diameter. It is shown that the above process allows producing powders with average diameter (less than 70 μm), where the share of the fine fraction of 25–63 μm can reach 70 wt.%. Studies of powder morphology showed that the above process allows producing powders with the coefficient of sphericity of 0.8. This, in its turn, ensures the high technological properties of the powder (bulk density, tap density and flowability), compared to the technological properties of powders produced by the method of spheroidization of irregularly-shaped particles in induction plasma.

3. Studies of technical-economic characteristics of the hybrid process of plasma-arc atomization showed that the above process has a number of advantages relative to other plasma atomization and arc atomization processes, namely: increase of productivity by 25 %, compared to the process of arc atomization, which may reach 24 kg/h for steel and reduction of specific gas consumption to produce 1 kg of powder by 2.5 times: from 3.25 up to 1.25 m^3/kg are achieved.

REFERENCES

1. Dev Singh, D., Mahender, T., Raji Reddy, A. (2021) Powder bed fusion process: A brief review. *Materials Today: Proceedings*, **46**, 350–355. DOI: https://doi.org/10.1016/j.matpr.2020.08.415
2. Ahn, D.G. (2021) Directed energy deposition (DED) process: State of the Art. *Int. J. of Precis. Eng. and Manuf.-Green Tech*., **8**, 703–742. DOI: https://doi.org/10.1007/s40684-020-00302-7
3. Svetlizky, D., Das, M., Zheng, B. et al. (2021) Directed energy deposition (DED) additive manufacturing: Physical characteristics, defects, challenges and applications. *Materials Today*, **49**, 271–295. DOI: https://doi.org/10.1016/j.mattod.2021.03.020
4. Dezaki, M., Serjouei, A., Zolfagharian, A. et al. (2022) A review on additive/subtractive hybrid manufacturing of directed energy deposition (DED) process. *Advanced Powder Materials*, **1**, 100054. DOI: https://doi.org/10.1016/j.apmate.2022.100054
5. Vaz, R.F., Garfias, A., Albaladejo, V. et al. (2023) A review of advances in cold spray additive manufacturing. *Coatings*, **13**, 267. DOI: https://doi.org/10.3390/coatings13020267
6. Dimitrov, D. (2018) Manufacturing of high added value titanium components. A South African perspective. *Proc. of IOP Conf. Ser.: Mater. Sci. Eng*., 430012009. DOI: https://doi.org/10.1088/1757-899X/430/1/012009
7. *Additive manufacturing market size, trends, report by 2032*. https://www.precedenceresearch.com/additive-manufacturing-market
8. Shanthar, R., Chen, K. Abeykoon, C. (2023) Powder-based additive manufacturing: A critical review of materials, methods, opportunities, and challenges. *Adv. Eng. Mater.*, **25**, 2300375. DOI: https://doi.org/10.1002/adem.202300375
9. Sun, P., Fang, Z., Zhang, Y. et al. (2017) Review of the methods for the production of spherical Ti and Ti alloy powder. *JOM*, **69**, 1853–1860. DOI: https://doi.org/10.1007/s11837-017-2513-5
10. Korzhyk V.M., Strogonov D.V., Burlachenko O.M. et al. (2023) Development of plasma-arc technologies of spherical granules production for additive manufacturing and powder metallurgy. *Avtomatychne Zvaryuvannya*, **11**, 37–52. DOI: https://doi.org/10.37434/as2023.11.04
11. Chen, G., Zhao, S., Tan, P. et al. (2018) A comparative study of Ti6Al4V powders for additive manufacturing by gas atomization, plasma rotating electrode process and plasma atomization. *Powder Technology*, **333**, 38–46. DOI: https://doi.org/10.1016/j.powtec.2018.04.013
12. Chen, D., Daoud, H., Scherm, F. et al. (2020) Stainless steel powder produced by a novel arc spray process. *J. of Materials Research and Technology*, **9**, 8314–8322. DOI: https://doi.org/10.1016/j.jmrt.2020.05.076
13. Yurtukan, E., Unal, R. (2022) Theoretical and experimental investigation of Ti alloy powder production using low-power plasma torches. *Transact. of Nonferrous Metals Society of China*, **32**, 175–191. DOI: https://doi.org/10.1016/S1003-6326(21)65786-2
14. Cui, Y., Zhao, Y., Numata, H. et al. (2020) Effects of plasma rotating electrode process parameters on the particle size distribution and microstructure of Ti6Al4V alloy powder. *Powder Technology*, **376**, 363–372. DOI: https://doi.org/10.1016/j.powtec.2020.08.027
15. Yin, Z., Yu, D., Zhang, Q. et al. (2021) Experimental and numerical analysis of a reverse-polarity plasma torch for plasma atomization. *Plasma Chem Plasma Process*, **41**, 1471–1495. DOI: https://doi.org/10.1007/s11090-021-10181-8
16. Entezarian, M., Allaire, F., Tsantrizos, P. et al. (1996) Plasma atomization: A new process for the production of fine, spherical powders. *JOM*, **48**, 53–55. DOI: https://doi.org/10.1007/BF03222969
17. Korzhik, V.N., Korab, M.F. (2012) Mechanized line PLAZER 30PL-W for plasma-arc wire deposition of coatings on large-sized parts of "shaft" type. *Svarshchik,* **4**, 13–15 [in Russian].
18. Korzhyk, V.M., Strogonov, D.V., Burlachenko, O.M. et al. (2023) New generation unit for plasma-arc deposition of coatings and atomization of current-conducting wire materials. *Suchasna Elektrometal.*, **3**, 19–27.DOI: https://doi.org/10.37434/sem2023.03.04
19. Korzhyk, V.M., Strogonov, D.V., Burlachenko, O.M. et al. (2023) Effectiveness of the process of plasma-arc spheroidization of current-conducting titanium wire. *Suchasna Elektrometal.*, **1**, 33–42. DOI: https://doi.org/10.37434/sem2023.01.05
20. Proulx, F., Dion, C., Carabin, P. (2023) *Method and apparatus for producing high purity spherical metallic powders at high productions rater form one or two wires*. Pat. US, 11839918 B2. Dec. 12, 2023.
21. Petrov, S.V., Korzhik, V.N. (2012) PLAZER 80-PL unit for plasma spraying. *Svarshchik,* **4**, 22–25 [in Russian].
22. Strogonov, D.V., Korzhyk, V.M., Jianglong, Yiet al. (2022) Influence of the parameters of the process of plasma-arc spheroidization of current-conducting wire from low-carbon steel on the particle size distribution of the produced powders. *Suchasna Elektrometal.*, **3**, 29–37. DOI: https://doi.org/10.37434/sem2022.03.05

ORCID
V.M. Korzhyk: 0000-0001-9106-8593,
D.V. Strogonov: 0000-0003-4194-764X,
O.M. Burlachenko: 0000-0003-2277-4202,
O.P. Gryshchenko: 0000-0003-2640-8656,
A.V. Zavdoveyev: 0000-0003-2811-0765,
O.M. Voitenko: 0000-0003-4946-6517

CONFLICT OF INTEREST
The Authors declare no conflict of interest

CORRESPONDING AUTHOR
V.M. Korzhyk
E.O. Paton Electric Welding Institute of the NASU
11 Kazymyr Malevych Str., 03150, Kyiv, Ukraine.
E-mail: vnkorzhyk@gmail.com

SUGGESTED CITATION
V.M. Korzhyk, D.V. Strogonov, O.M. Burlachenko, O.P. Gryshchenko, A.V. Zavdoveyev, O.M. Voitenko (2024) Development of hybrid technology of producing spherical powders from wire materials using high-speed plasma jets and electric arc. *The Paton Welding J.*, **9**, 3–11.
DOI: https://doi.org/10.37434/tpwj2024.09.01

JOURNAL HOME PAGE
https://patonpublishinghouse.com/eng/journals/tpwj

Received: 13.03.2024
Received in revised form: 17.06.2024
Accepted: 24.09.2024

DOI: https://doi.org/10.37434/tpwj2024.09.02

PHASE AND STRUCTURAL TRANSFORMATIONS DURING HEATING OF MULTILAYER Ti/Cu FOILS OF EUTECTIC COMPOSITION OBTAINED BY THE EBPVD METHOD

S.O. Demchenkov, T.V. Melnychenko, A.I. Ustinov, O.E. Rudenko, O.V. Samofalov

E.O. Paton Electric Welding Institute of the NASU
11 Kazymyr Malevych Str., 03150, Kyiv, Ukraine

ABSTRACT

Phase and structural transformations in multilayer Ti/Cu foils of eutectic Composition I (Ti50–Cu50 wt.%) and Composition II (Ti22–Cu78 wt.%), obtained by layer-by-layer electron beam physical vapor deposition of components in vacuum, were investigated using differential thermal analysis (DTA), X-ray diffraction (XRD), and scanning electron microscopy (SEM) methods. It was found that during heating of the multilayer foils in the temperature range of 400–600 °C, due to the diffusion interaction between Ti and Cu layers, the following intermetallic compounds are formed: Cu_4Ti, Cu_4Ti_3, CuTi, and $CuTi_2$ in Composition I foils, and Cu_4Ti and Cu_4Ti_3 in Composition II foils. Upon further heating, melting of the multilayer foils of both eutectic compositions occurs. The Composition II foils begin to melt at a temperature of 879 °C, close to the equilibrium melting temperature of the eutectic alloy of the same composition (875 °C), while in the case of Composition I foils, the onset of melting occurs at a temperature of 915 °C, which is lower compared to the melting temperature of the eutectic alloy of Composition I (960 °C). Considering that Cu_4Ti and Cu_4Ti_3 metastable phases are formed in multilayer Composition I foils, which are components of the more fusible eutectic of Composition II, the reduction in the melting temperature of the foil may be due to its metastable structure. Such behavior of multilayer Ti/Cu foil of eutectic Composition I may facilitate softening of the temperature conditions required to establish physical contact in the material bonding zone during their reactive brazing.

KEYWORDS: Ti–Cu alloys, eutectic, electron beam physical vapor deposition, vacuum condensates, multilayer structures, phase transformations, melting

INTRODUCTION

It is known that multilayer foils (MF), consisting of interlayers of reactive components, are characterized by a pronounced heterogeneous structure and a considerable margin of internal energy: excess chemical energy, energy of elastic stresses in the layers, free energy of interphase boundaries [1, 2]. MF heating promotes solid phase reactions in it, running at a high rate. Nature of phase transformations in MF is determined by reaction interaction of the layer components, layer thickness, method of producing the foil, and it differs from the equilibrium one due to a considerable area of the contact zone between the components and a large number of grain boundaries in the layers [3]. The features of phase transformations and formation of the specific structural-phase state (presence of metastable phases, multiphase composition, structural elements of the nanoscale size, defects of vacancy type and pores) determine the physical properties of the foil and direction of its practical application. So, considerable heat evolution at running of SHS reaction, initiated by foil heating, which consists of layers of intermetallic forming components, allows using such MF as a local heat source at high-speed brazing [4, 5]. Formation of the nanostructured components and pores at MF heating ensures low-temperature plastic deformation of the foil under the conditions of thermomechanical loading, which determines the possibility of its application as an interlayer at diffusion welding of materials that are difficult to deform [6, 7]. On the other hand, formation of nanostructured and metastable components can lead to lowering of the temperature of phase and structural transformations at MF heating [8]. It may be useful at application of MF, which consists of layers of components of eutectic systems, as braze alloy at brazing of materials sensitive to thermal impact. From this viewpoint, MF of Ti–Cu system should be noted, the components of which are the base of the known braze alloys (for instance, Ticuni 70, BTi-1, MBF 5012, etc.) for brazing various materials.

The authors of [9] showed that in Ti/Cu contact reaction pair at its heating an interlayer of liquid based on a copper-enriched eutectic forms first, in keeping with the constitutional diagram. In view of that it can be assumed that the beginning of Ti/Cu MF melting will occur at the temperature of low-temperature eutectic transformation (875 °C in keeping with the constitutional diagram). Thus, it is possible to optimize the brazing process: lower the brazing temperature, reduce the braze alloy thickness through application of thin foil, and reduce the concentrational inhomo-

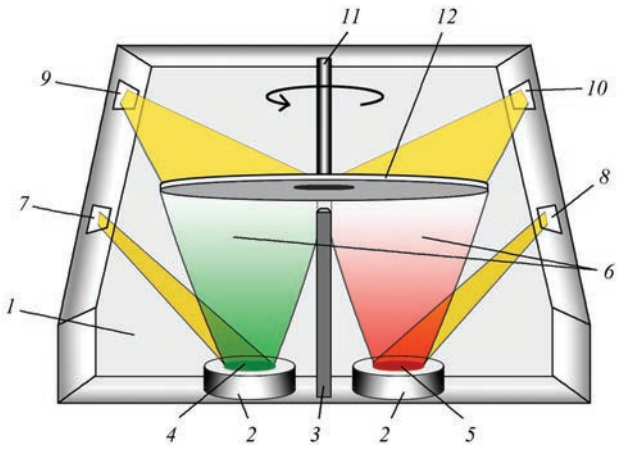

Figure 1. Scheme of electron beam deposition of condensates with a multilayer structure: *1* — work chamber; *2* — water-cooled crucibles; *3* — screen non-transparent for the vapour phase; *4*, *5* — titanium and copper ingots, respectively; *6* — vapour flows; *7*, *8* — electron beam guns for evaporation; *9*, *10* — electron beam guns for substrate heating; *11* — substrate holders; *12* — rotating substrate

geneity of the joint. In order to determine the nature of phase transformations in Ti/Cu MF, a study of the influence of layer thickness (layer period) and chemical composition of the foil produced by electron beam deposition of the component vapour phases, on the regularities of formation of its structure and phase composition at heating.

EXPERIMENTAL STUDIES

Ti/Cu MF were produced by the method of electron beam deposition of the components, in keeping with the scheme given in Figure 1.

Vapour flows, forming at evaporation of Ti and Cu ingots, are simultaneously deposited on a substrate rotating around the vertical axis in a vacuum chamber. An impermeable screen is mounted between the crucibles to prevent mixing of their vapour flows. As the substrate rotates, each section of it sequentially passes over the crucibles, which is accompanied by the deposition of the corresponding metal layer onto the substrate surface. The ratio of thicknesses of the layer components with such a deposition scheme is determined by the ratio of their evaporation velocities, and the period of modulation of the multilayer structure (sum of thicknesses for the two adjacent component layers) is determined by the speed of substrate rotation. Multilayer foils with the required component ratio were produced by changing the ratio of evaporation rates of each of the ingots, and the structure modulation period was varied at the change of the speed of rotation. To prevent diffusion interaction of the components during the deposition of vapor flows, the substrate temperature was stabilized at 200 °C.

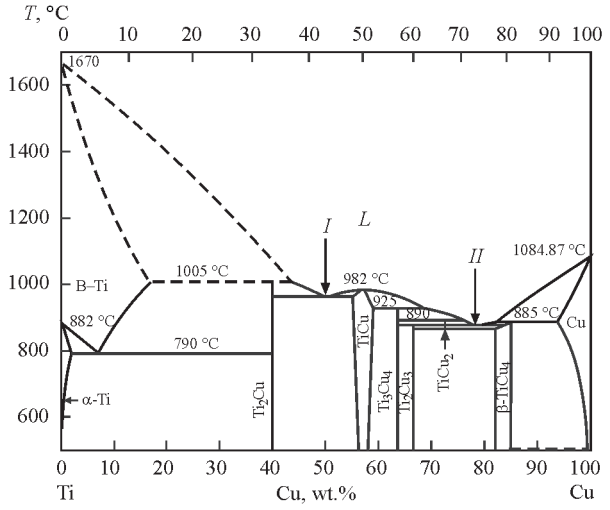

Figure 2. Ti–Cu binary alloy phase diagram [11]

Microstructural characteristics of the materials were studied by SEM method, using CamScan 4 electron microscope, fitted with energy-dispersive spectrometer EDS-200, on transverse sections prepared by the standard procedure of machining the surfaces in Struers Company equipment. Phase composition was studied by the method of XRD analysis in DRON-4M diffractometer in K_α radiation of the copper anode.

Temperature ranges of the phase and structural transformations in the investigated materials were studied by the method of differential thermal analysis in VDTA-2000 unit [10]. Specimens heating was conducted in the helium atmosphere at the rate of 20 °C/min.

In keeping with the phase diagram (Figure 2) [11], Ti–Cu system is characterized by existence of two alloys of an eutectic composition: eutectic I — at Ti50–Cu50 (wt.%) ratio with melting temperature of 960 °C and eutectic II with Ti22–Cu78 (wt.%) and melting temperature of 875 °C. In view of that, MF with component ratio corresponding to eutectic I and eutectic II were prepared for investigations (Table 1).

Table 1. Characteristics of manufactured MF and ingots

Eutectic alloy type	Foil/ingot number	Layer alternation period (Ti + Cu), nm	Ti		Cu	
			wt.%	at.%	wt.%	at.%
Eutectic I	Ingot I	–	49.9	56.9	50.1	43.1
	No. 1	500	48.7	55.8	51.3	44.2
	No. 2	150	47.5	54.6	52.5	45.4
Eutectic II	Ingot II	–	21.8	27.0	78.2	73.0
	No. 3	700	20.4	25.4	79.6	74.6

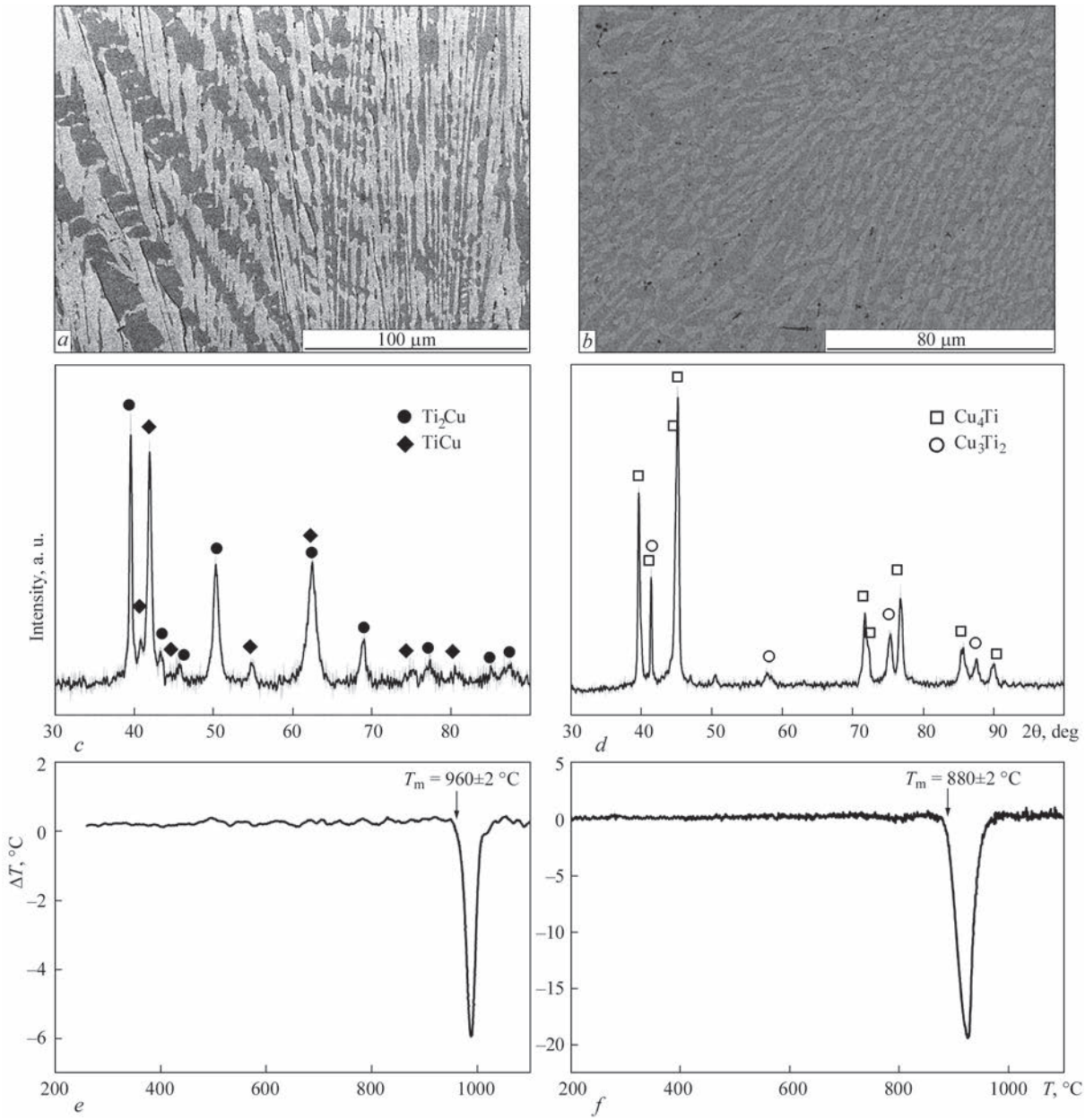

Figure 3. SEM image (*a*, *b*), diffraction patterns (*c*, *d*) and DTA thermograms of the produced Ti–Cu ingots of eutectic composition I and eutectic composition II, respectively

Investigations of the features of running of phase and structural transformations were conducted in comparison with cast ingots of Ti–Cu alloys of eutectic composition I and II (Figure 2, Table 1). Ingots were produced by the method of double electron beam remelting. Copper of M0k grade and VT1-0 titanium were used as the charge.

Cross-sectional microstructure of the prepared ingots is given in Figure 3, *a*, *b*. One can see that both the ingots have a microstructure characteristic for eutectic alloys and have two components, differing by their contrast. Chemical analysis of the sections showed that in the case of ingot 1 (Figure 3, *a*) the light-coloured regions have $Ti_{43.4}Cu_{56.6}$, composition, dark-coloured regions are $Ti_{60.2}Cu_{39.8}$, and in the case of ingot 2 (Figure 3, *b*) $Ti_{17.5}Cu_{82.5}$ composition corresponds to light regions, and $Ti_{25.7}Cu_{74.3}$ — to dark regions. X-ray diffraction analysis showed that ingot 1 consists of two phases: Ti_2Cu and TiCu (Figure 3, *c*) and ingot 2 consists of Cu_4Ti and Cu_3Ti_2 phases (Figure 3, *d*). DTA showed that the melting temperature of ingot 1 is equal to 959±2 °C (Figure 3, *e*), and that of ingot 2 is 880±2 °C (Figure 3, *f*). Maximal melting rate is observed at the temperature close to 900 °C. Complete melting of the ingot occurs at heating up to 920 °C temperature.

Thus, in keeping with the equilibrium phase diagram of Ti–Cu system, the chemical phase compositions of the produced ingots 1 and 2 correspond to eutectic alloys I and II, respectively (Figure 2).

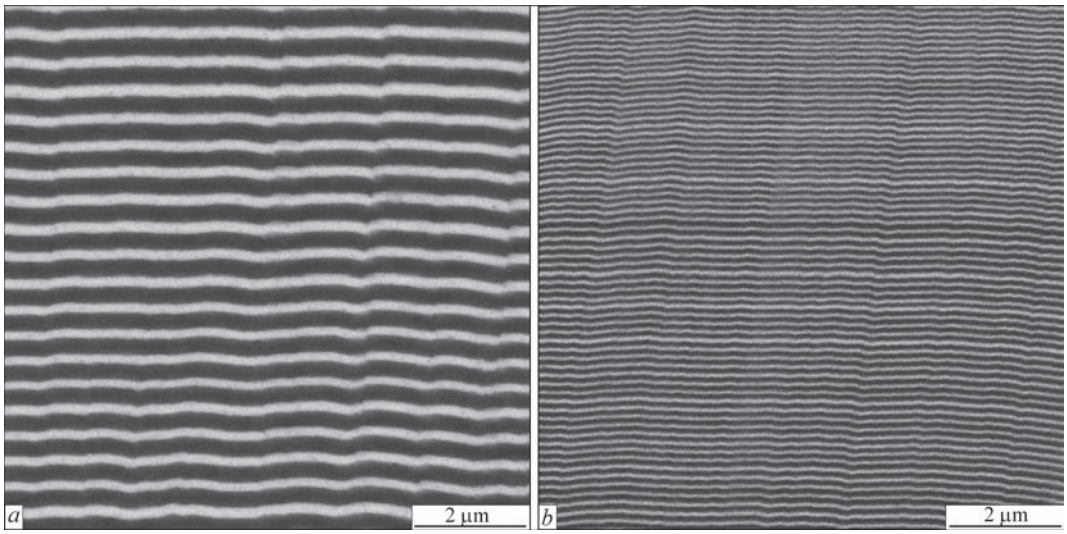

Figure 4. SEM images of the cross-section of Ti/Cu MF No. 1 (*a*) and No. 2 (*b*): dark layers — Ti; light layers — Cu

RESULTS AND THEIR DISCUSSION

Electron microscopic image of the characteristic microstructure of the produced Ti/Cu MF with different period of component layer alternation is given in Figure 4. One can see that the foil structure consists of layers with clearcut boundaries. There are no precipitates of other phases or structural defects such as pores or cracks on the layer interfaces.

X-ray diffraction analysis of as-deposited MF revealed the presence of diffraction peaks from just copper and titanium (Figure 5). This is indicative of a perfect physical contact between the layers of titanium and copper. The discrepancy between the experimentally revealed and theoretical intensity of the diffraction peaks is the consequence of formation of the crystallographic texture in the layers during deposition.

Figure 6, *a* gives a thermogram of Ti/Cu MF No. 3, in which the ratio of the components corresponds to eutectic composition II. One can see that unlike the ingot thermogram of the same chemical composition (Figure 3, *f*), a heat evolution peak is observed in the temperature range of 450–520 °C. In keeping with the diffraction studies after foil heating up to the temperature of 700 °C (higher than the heat evolution maximum), a change in its phase composition takes place compared with the initial condition. Diffraction peaks from titanium disappear, and peaks correspond-

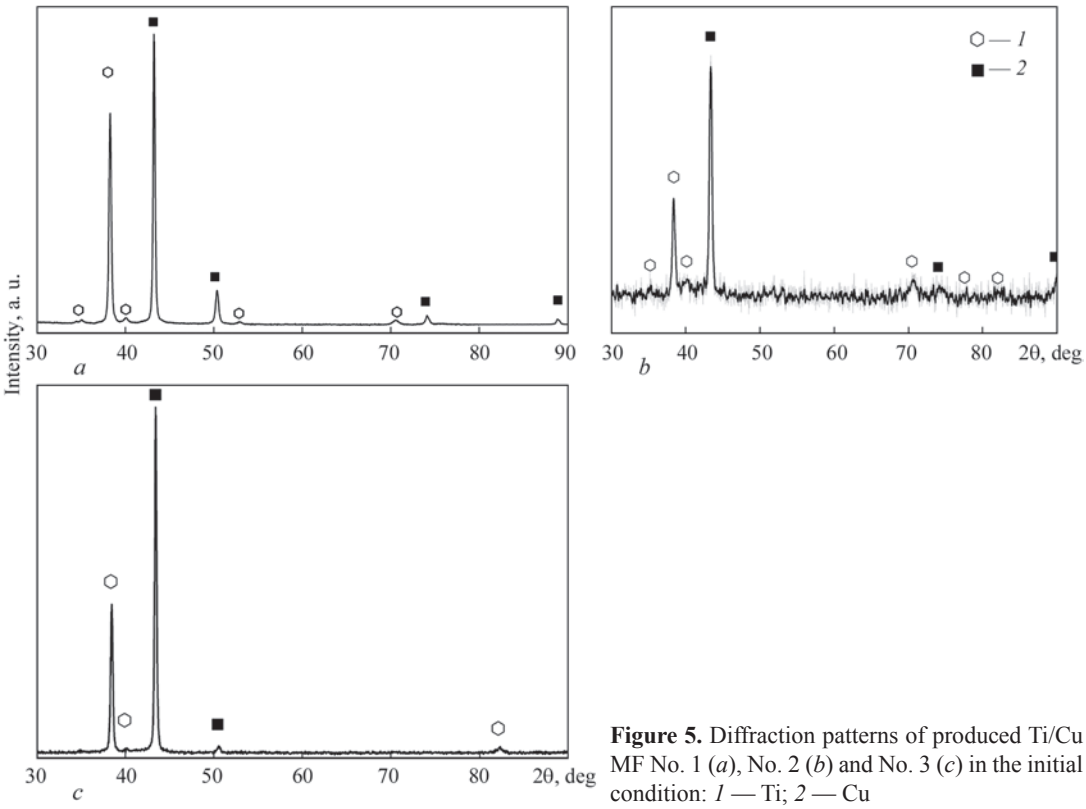

Figure 5. Diffraction patterns of produced Ti/Cu MF No. 1 (*a*), No. 2 (*b*) and No. 3 (*c*) in the initial condition: *1* — Ti; *2* — Cu

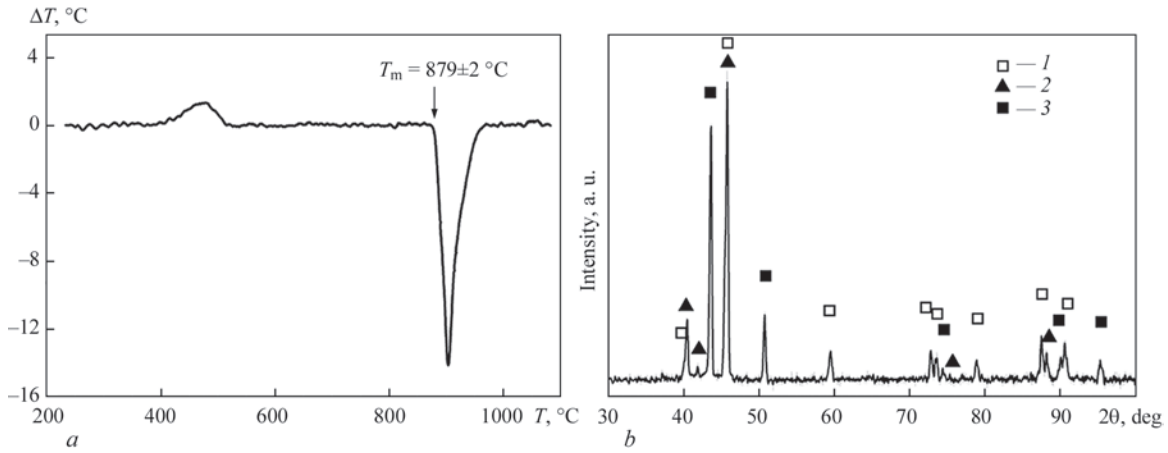

Figure 6. DTA thermogram of MF No. 3 (*a*) and its diffraction pattern after heating to the temperature of 700 °C (*b*): *1* — Cu_4Ti; *2* — Cu_4Ti_3; *3* — Cu

ing to Cu_4Ti and Cu_4Ti_3 intermetallic compounds are formed. Peaks from copper are also present in the diffraction pattern, which may be indicative of incomplete running of phase transformations, because of short duration of annealing or the need for heating to a higher temperature. At the same time in keeping with the phase diagram, Cu_4Ti_3 and Cu_3Ti_2 intermetallics have close chemical composition and crystalline structure, so that it can be assumed that longer annealing or heating to higher temperatures ensures an interaction of residual copper with Cu_4Ti_3 phase. As a result of such an interaction, a phase composition of Cu_4Ti and Cu_3Ti_2 forms, which corresponds to components of eutectic of composition II. This is confirmed by DTA data, according to which melting of MF No. 3 occurs at the temperature of 879±2 °C, which practically coincides with melting temperature of ingot No. 2 of the same chemical composition.

At heating of MF No. 1, where the ratio of the components corresponds to eutectic composition I a heat evolution maximum is also observed in the temperature range of 450–600 °C on DTA thermogram (Figure 7). At further heating, unlike an ingot of the same chemical composition (Figure 3, *e*), MF melting begins at the temperature of 915±2 °C, and at the temperature of 959±2 °C the melting process becomes much more intensive. The melting process is over at the temperature close to 1060±2 °C.

In keeping with the data of X-ray diffraction analysis at heating of MF No.1 to the temperature of 700 °C synthesis of a number of intermetallic compounds occurs through solid-phase reactions: $TiCu_4$, Ti_2Cu_3, Ti_2Cu and TiCu. Thus, the start of melting of MF No.1 with an averaged chemical composition, corresponding to eutectic I, at a lower temperature (compared to the ingot) can be the result of interaction between regions in MF, where $TiCu_4$ and Ti_2Cu_3 intermetallic compounds formed, which are the components of eutectic II. As the volume fraction of these phases is much smaller than that of Ti_2Cu and TiCu, the volume of molten metal and the respective thermal effect in the thermogram will be small.

In keeping with the theoretical models of melting of eutectic alloys, formation of the liquid phase occurs in regions of physical contact of the eutectic components at temperature lower than the melting temperature of each of the components [12, 13]. Formation of regions of physical contact creates the nec-

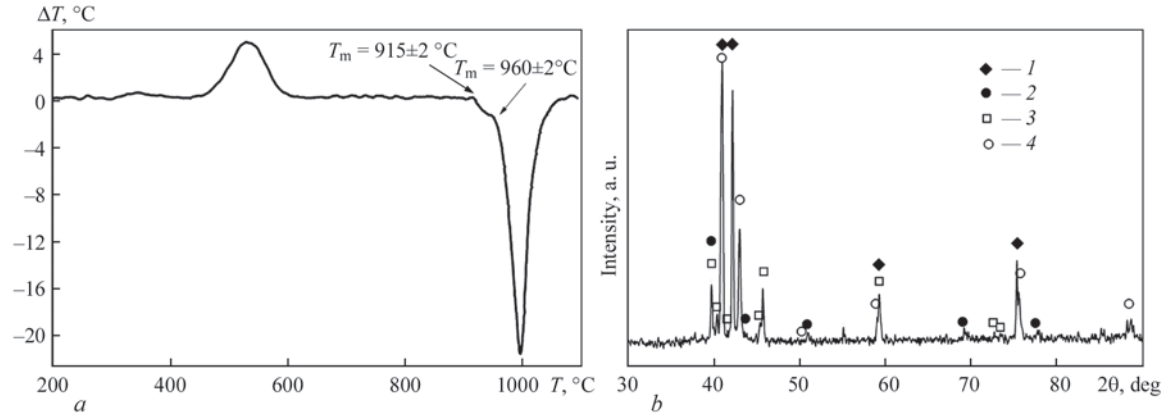

Figure 7. DTA thermogram of MF No. 1 (*a*) and its diffraction pattern after heating to the temperature of 700 °C (*b*): *1* — TiCu; *2* — Ti_2Cu; *3* — Cu_4Ti; *4* — Cu_3Ti_2

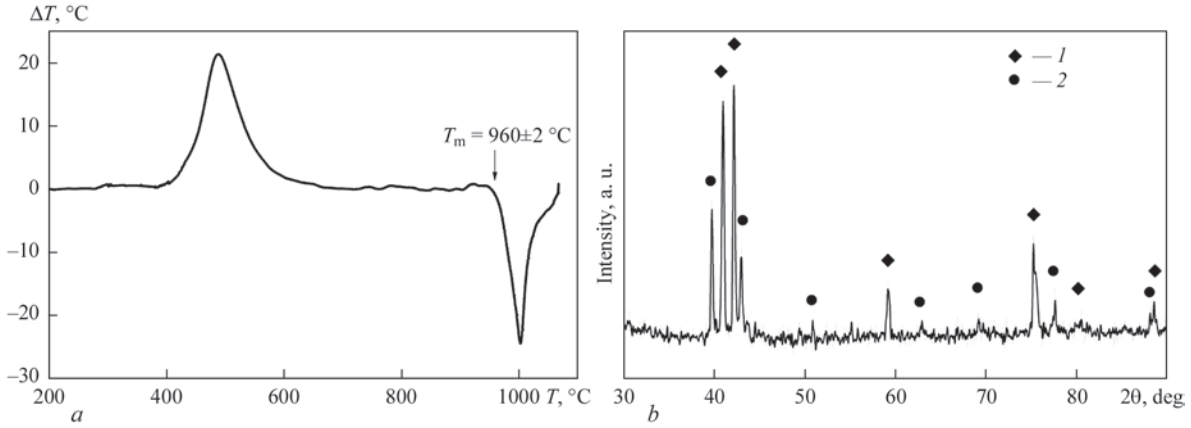

Figure 8. DTA thermogram of MF No. 2 (*a*) and its diffraction pattern after heating to the temperature of 700 °C (*b*): *1* — TiCu; *2* — Ti_2Cu

essary conditions for diffusion interaction between the components, resulting in appearance on the physical contact boundary of diffusion-related volumes of these components, where the chemical composition is close to that of the eutectic [14]. At eutectic temperature such dipoles provide the conditions necessary for appearance of liquid phase nucleus of a critical size on their base. Here, the proportion of the components contacting in the macrovolume is not important. It is clear that the volume fraction of the melt forming in the contact depends on how effectively the established contact will promote diffusion interaction between the components, as well as on the contact area.

Considering that Ti/Cu MF form under vacuum, there are no barriers for their diffusion interaction in the contacts between Ti and Cu layers over the entire area, and the density of contact surfaces per a unit of volume is inversely proportional to layer modulation period, it was anticipated that the volume fraction of the liquid phase can be increased by an order through increase of the number of boundaries between MF component layers due to reduction of the layered structure modulation period, i.e. presence of multiple contacts between MF components with an averaged component ratio, which corresponds to eutectic I, will promote its melting beginning at a temperature close to that of melting of the lower melting eutectic II.

To check this assumption, MF No. 2 with layer modulation period of 150 nm and component ratio close to the composition of eutectic I was studied.

One can see from DTA thermogram from MF No. 2 (Figure 8, *a*) that a heat evolution peak is present in the temperature range from 440 to 600 °C, similar to MF No. 1. At further heating of MF No. 2, however, its melting occurs at the temperature of 960 °C that corresponds to equilibrium melting temperature of the alloy of eutectic composition I. In this case, no low-temperature melting is observed. Results of X-ray diffraction studies of MF No. 2 showed that at heating up to the temperature of 700 °C (Figure 8, *b*) just two intermetallic compounds Ti_2Cu and TiCu form as a result of diffusion interaction. No diffraction indications of formation of additional $TiCu_4$ and Ti_2Cu_3

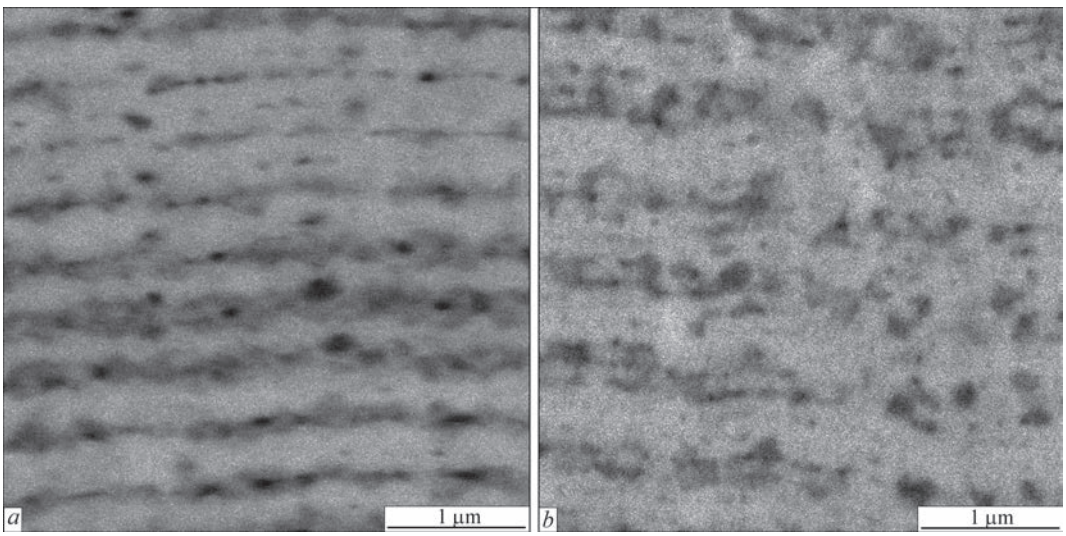

Figure 9. Electron microscopy images of the cross-sectional microstructure of MF No. 1 (*a*) and No. 2 (*b*) after heating to a temperature of 700 °C

intermetallics which are components of low-temperature eutectic II were revealed.

Electron microscopy images of cross-sectional microstructure of MF Nos 1 and 2 after heating up to the temperature of 700 °C are given in Figure 9. In the case of MF No. 1 (Figure 9, *a*) the layered structure is readily visible after heating, but precipitates in the form of individual particles and interlayers, differing by their contrast, appeared in place of titanium layers. On the whole, as one can see from images of MF microstructure, after formation of intermetallic compounds in it component distribution over the foil thickness is rather non-uniform. Analysis of the image of MF No. 2 microstructure (Figure 9, *b*) shows that reduction of the period of layer alternation leads to a more intensive diffusion mixing of the components during heating, which results in the layered structure becoming similar to the composite one (light-coloured regions as matrix, incorporating the dark-coloured inclusions).

Thus, attempts to increase the volume fraction of liquid phase formation in MF through reduction of the layer alternation period will promote more active running of the diffusion interaction between the layer components. It may lead to complete mixing of the component layers in the solid phase and to formation of quasi-equilibrium structure with phase composition of eutectic I already at the stage of heating at temperatures below the melting temperature of eutectic II. As a result, the MF melting temperature will correspond to its chemical composition, i.e. melting will start at the temperature of 960 °C.

In view of that it can be assumed that the layer modulation period should be greater than a certain value that will allow ensuring the conditions for preservation of a metastable structure, forming in the contact zone at the initial stages of diffusion interaction of the components, up to higher temperatures.

Thus, to ensure the conditions necessary for lowering the melting onset temperature of multilayer Ti/Cu foils with eutectic composition I, the modulation period of the layered structure must be greater than a certain critical value, at which the heterogeneous distribution of components across the thickness of the foil will be maintained up to the melting temperature of the more easily fusible eutectic II. It can be assumed that the critical value of the modulation period of the layered structure will depend on the foil heating rate. At lowering of the heating rate, the critical value of the modulation period should become greater.

Lowering of the temperature of the start of melting of MF of eutectic composition I can provide a softening of the conditions of producing permanent joints, both due to lowering of the bonding process temperature, and of the time of soaking at bonding temperature. The latter will be promoted by diffusion mobility of MF components due to heterogeneity and intensive process of intermetallic synthesis. Such a softening of the conditions of producing the joints will prevent lowering of the strength of materials being joined, for instance for titanium alloys after thermomechanical treatment, and reduction of the soaking time at a high temperature will promote preservation of their initial structural state.

CONCLUSIONS

1. It is shown for the first time that the start of melting of Ti/Cu MF with component ratio corresponding to high-temperature eutectic of Ti50–Cu50 (wt.%) composition can take place at a lower temperature, close to melting temperature of low-temperature eutectic of Ti28–Cu78 (wt.%) composition.

2. Lowering of melting temperature of MF of eutectic composition I can be related to formation of a heterogeneous structural state during heating, the composition of which includes metastable $TiCu_4$ and Ti_2Cu_3 intermetallics, which are components of low-temperature eutectic II.

3. To ensure a lowering of melting temperature of MF of eutectic composition I (Ti50–Cu50) the layered structure modulation period should be greater than a certain critical value, which will promote complete mixing of the component layers during heating and formation of the foil homogeneous structure up to the melting temperature of the low-melting eutectic.

REFERENCES

1. Weihs, T.P. (2014) *Fabrication and characterization of reactive multilayer films and foils*. Eds by K. Barmak, K. Coffey. Metallic films for electronic, optical and magnetic applications. Cambridge, Woodhead Publishing Ltd, UK, 160–243. DOI: https://doi.org/10.1533/9780857096296.1.160
2. Adams, D.P. (2015) Reactive multilayers fabricated by vapor deposition: A critical review. *Thin Solid Films*, 576(**16**), 98–128. DOI: https://doi.org/10.1016/j.tsf.2014.09.042
3. Ustinov, A.I., Demchenkov, S.O. (2022) Influence of microstructure of multilayer Al/Ni foils on phase transformations initiated by heating. *Suchasna Elektrometal.,* **1**, 16–23. DOI: https://doi.org/10.37434/sem2022.01.02
4. Yupeng, Zh., Jianglong, Y., Ziyi, L. (2014) Structural view study on diamond and copper bonding with AlNi micro/nano multilayers. *Rare Metal Materials and Eng.*, 43(**11**), 2597–2601. DOI: https://doi.org/10.1016/S1875-5372(15)60009-1
5. Duckham, A., Spey, S.J., Wang, J. et al. (2004) Reactive nanostructured foil used as a heat source for joining titanium. *J. of Applied Physics*, **96**, 2336–2342. DOI: https://doi.org/10.1063/1.1769097
6. Ramos, A.S., Vieira, M.T., Simoes, S. et al. (2009) Joining of superalloys to intermetallics using nanolayers. *Advanced Materials Research*, **59**, 225–229. DOI: https://doi.org/10.4028/www.scientific.net/AMR.59.225
7. Cao, J., Song, X.G., Wu, L.Z. et al. (2012) Characterization of Al/Ni multilayers and their application in diffusion bonding of

TiAl to TiC cermet. *Thin Solid Films*, **520**, 3528–3531. DOI: https://doi.org/10.1016/j.tsf.2012.01.001
8. Ustinov, A.I., Demchenkov, S.A. (2017) Influence of metastable Al9Ni2 phase on the sequence of phase transformations initiated by heating of Al/Ni multilayer foils produced by EBPVD method. *Intermetallics*, **84**, 82–91. DOI: https://doi.org/10.1016/j.intermet.2017.01.005
9. Ming-Fang, W., Chan, Y., Zhi Shuie, Y., Rui Feng, L. (2005) Formation process of liquid in interface of Ti/Cu contact reaction couple. *Transact. Nonferrous Metals Soc. China*, **15**, 125–129.
10. Kocherzhinskyi, Yu.A. et al. (1974) *Experimental-equipment samples for physico-chemical analysis at high temperatures. Devices for examination of physical properties of materials.* Kyiv, Naukova Dumka [in Russian].
11. Massalski, T.B., Okamoto, H., Subramanian, P.R., Kacprzak, L. (1990) *Binary alloy phase diagrams*. 2nd Ed. ASM International, Materials Park, Ohio, USA.
12. Zalkin, V.M. (1987) *Nature of eutectic alloys and effect of contact melting.* Moscow, Metallurgiya [in Russian].
13. Gladkikh, N.T., Kryshtal, A.P., Sukhov, R.V. et al. (2010) About critical thickness of contact melting in lamellar film system Au/Ge. *Visnyk KhNU, Series Physics*, 13(**914**), 109–114 [in Russian].
14. Kukushkin, S.A., Osipov, A.V. (1997) Growth, structure and morphological stability of nuclei growing from melts of eutectic composition. *Fizika Tvyordogo Tela,* 39(**8**), 1464–1469 [in Russian].

ORCID
S.O. Demchenkov: 0000-0002-2412-4214,
T.V. Melnychenko: 0000-0002-1460-5532,
A.I. Ustinov: 0000-0002-8855-3499

CONFLICT OF INTEREST
The Authors declare no conflict of interest

CORRESPONDING AUTHOR
S.O. Demchenkov
E.O. Paton Electric Welding Institute of the NASU
11 Kazymyr Malevych Str., 03150, Kyiv, Ukraine.
E-mail: s_demchenkov@ukr.net

SUGGESTED CITATION
S.O. Demchenkov, T.V. Melnychenko, A.I. Ustinov, O.E. Rudenko, O.V. Samofalov (2024) Phase and structural transformations during heating of multilayer Ti/Cu foils of eutectic composition obtained by the EBPVD method.
The Paton Welding J., **9**, 12–19.
DOI: https://doi.org/10.37434/tpwj2024.09.02

JOURNAL HOME PAGE
https://patonpublishinghouse.com/eng/journals/tpwj

Received: 05.03.2024
Received in revised form: 06.06.2024
Accepted: 25.09.2024

DOI: https://doi.org/10.37434/tpwj2024.09.03

NEUTRON SHIELD MATERIALS BASED ON BORON CARBIDE–TUNGSTEN MULTILAYER COMPOSITES

L. Chkhartishvili[1,2], N. Barbakadze[3], O. Tsagareishvili[2], A. Mikeladze[2], O. Lekashvili[3], K. Kochiashvili[3], R. Chedia[2,3]

[1]Georgian Technical University
77 Merab Kostava Ave., 0160, Tbilisi, Georgia
[2]F. Tavadze Metallurgy and Materials Science Institute
8b Elizbar Mindeli Str., 0186, Tbilisi, Georgia
[3]P. Melikishvili Institute of Physical and Organic Chemistry
31a Anna Politkovskaya Str., 0186, Tbilisi, Georgia

ABSTRACT

Nuclear power industry requires structural materials that effectively absorb neutron radiation. For this purpose, boron and boron-rich compounds and, in particular, boron carbide B_4C and its composites are widely used. Both theoretically and experimentally it has been shown that one such promising class of materials is boron carbide compositions with tungsten B_4C–W: tungsten phase inclusions containing heavy W atoms provide effective attenuation of the secondary gamma-radiation that accompany the absorption of primary neutrons by the boron ^{10}B isotope atoms. In this work, the composites with multilayer morphologies — $W/B_4C/W$, $W/B_4C/W_2B_5$, $W_2B_5/B_4C/W_2B_5$, etc. — in which boron carbide layers alternate with metallic tungsten and/or tungsten pentaboride ones, are produced and investigated. Surface metallization of boron carbide crystals or grains with tungsten powder, plate or coating is done by SPS (Spark-Plasma Sintering) and also by standard thermal sintering. SEM (Scanning Electron Microscopy) structural-morphological, XRD (X-Ray Diffraction) phase- and EDS (Energy Dispersive Spectrometry) chemical-compositions analysis of the obtained samples establishes that transition layers of W_2B_5 are formed on the B_4C–W interfaces, which ensures component-layers strong bonding.

KEYWORDS: boron carbide, tungsten, layered composite, metallization, thermal sintering, spark-plasma-sintering, radiation shield

INTRODUCTION

For structural materials effectively absorbing neutron radiation, nuclear power industry widely uses boron-rich compounds and composites, in particular, boron carbide B_4C and its composites with metals and other ceramics. Experimentally [1–5] and theoretically [6–9] it has been demonstrated that one of such promising class of materials is boron carbide compositions with tungsten B_4C–W. Tungsten and/or tungsten compounds phases, which contain heavy W atoms, provide effective attenuation of the secondary gamma-radiation that accompany the absorption of primary neutrons by the boron ^{10}B isotope nuclei. Composites with (poly-sandwich or multilayer morphologies — $W/B_4C/W$, $W/B_4C/W_2B_5$, $W_2B_5/B_4C/W_2B_5$, etc. — in which boron carbide layers alternate with metallic tungsten and/or tungsten boride ones, were produced and investigated.

As known, tungsten- and boron-based thin films, including B_4C, as well as tungsten carbide WC and boride WB_3, display very high hardness [10]. To expand the superior room-temperature mechanical properties of tungsten foils, the W-containing metallic laminate composites were fabricated [11]. The effect of neutron irradiation on W foil could be investigated to determine their resulting DBTT (Ductile-to-Brittle Transition Temperature) shift. Physical properties, processing techniques, and applications of high-operating temperature (> 1200 °C) materials with multi-layered ceramic/carbon, ceramic, and metal structures were highlighted in [12]. They may have a graceful failure mode and higher toughness as compared to particle-reinforced ceramic composites and, as multi-layered shields, provide better efficacy than single-layered ones. Work [13] aimed to describe the development of an online platform to calculate (in the energy range of 0.015–15 MeV) the 36 GSPs (Gamma Shielding Parameters), which are required to investigate the materials gamma-ray shielding.

The influence of interface roughness on the reflectivity of B_4C–W multilayers varying with bi-layer number N was specially investigated [14]. For such multilayers, fabricated by the DC (Direct Current) magnetron sputtering method, with the same design period thickness of 2.5 nm, a real-structure model was used to calculate the reflectivity variations with $N = 50$, 100, 150 and 200 bi-layers. Their reflectivity and scattering intensity measured by the XRD (X-Ray Diffraction) indicate that reflectivity is a function of N and interface roughness slightly increases from layer to layer in process of multilayer growth.

Coating different types of surfaces with metallic tungsten is used in several modern technologies. In particular, tungsten layer can be obtained [15] by tungsten oxide WO_3 layer formation using the spin coating to reduce it to α-W phase in a hydrogen atmosphere at 600–800 °C. With the aid of chemical vapor transport of $WO_x(OH)_y$, surface morphology is transformed into rod-like, star-shaped cracking, florets, irregularly fibrous structures and, finally, spherical tungsten particles. Usually, semiconductors are coated with a thin layer of tungsten, which is mainly carried out by the CVD (Chemical Vapor Deposition) method, where SiH_4, H_2 and WF_6 are used as precursors, and the vacuum chamber is maintained at pressures of about 20 to 760 Torr to improve the tungsten deposition rate [16]. Tungsten thin film was deposited on Si(100) substrate by using the LPCVD (Low Pressure CVD) technique [17, 18] also using WF_6 and SiH_4 as source and W-reducing gases, respectively.

Pure-W metallic films are often deposited not only by CVD, but also by PVD (Physical Vapor Deposition), by sputtering or evaporation. To avoid the chemical or physical methods drawback of using expensive high-vacuum instrumentation, metallic tungsten in form of thin film was reduced [19] from the water-soluble W–IPA (Inorganic Peroxopolytungstic Acid) composite powder prepared by dissolving metal tungsten in hydrogen peroxide and evaporating the residual solvent. Commonly, metallic tungsten deposition technologies on metal substrates applies [20] aluminum Al, copper Cu and titanium Ti. Deposition by ALD (Atomic Layer Deposition) and PNL (Pulsed Nucleation Layer) techniques may also be used to form tungsten nucleation layers. In industrial conditions, the evolution of the reduction process of tungsten blue oxides ultrafine powder to tungsten thin films under a counter-current flow of hydrogen is described [21] by the following scheme: $WO_{2.90} \rightarrow$ $\rightarrow WO_{2.72} \rightarrow WO_2 \rightarrow W$. It was developed [22] the HWALD (Hot Wire-Assisted ALD) to form W with its filament heated up to 1700–2000 °C in the flow of atomic hydrogen H generated by the dissociation of molecular hydrogen H_2, which reacted with WF_6 at the substrate to deposit.

One of the practical and cheap methods is that metallic tungsten is coated on the ceramic material using [23] the chemical solution deposition to fabricate such films on the inner surface of alumina tubules. This technique involves the preparation of tungsten oxide layers from PTA (PeroxoTungstic Acid) precursor solution and their subsequent reduction to tungsten in the presence of hydrogen. The suitability of using W-matrix coating materials supersaturated with B for stainless steel substrates was tested [24] and all the W–B coated (including W–13 % B and W–23 % B) materials are found to be nearly an order of magnitude more resistant to material loss through corrosion–wear compared to uncoated substrates.

As for the boron carbide–metal B_4C–Me, Me = Mo, W, Ni, etc., sandwich structures in general, they can be obtained by the boron carbide ceramic metallization method [25], which comprises the following steps:

- mixing the metals powder, for example, 10–40 wt.% of Mo, W and Ni, according to their weights ratio, carrying out ball milling, and sieving through 300-mesh sieve;
- preparing paste by mixing the metal powder obtained in the Step 1 with 5 wt.% ethylcellulose solution according to weight ratio of (100–120):30;
- printing the metalized paste obtained in the Step 2 on the 20–30 μm thick boron carbide ceramic part, needing to be metalized, and drying it; and
- metalizing by putting the boron carbide ceramic part dried in the Step 3 into a sintering furnace, introducing hydrogen, keeping the temperature at 1650–1680 °C for 30–35 min, keeping the dew point at 0–10 °C, and cooling along with the furnace.

The formed Mo–W–Ni proportioned metalized layer alloy material to have thermal expansion close to that of B_4C. Then, the bonding strength is high, the metalized stress is small, and due to the sub-μm metal network structure, the metal is not prone to falling off after being brazed.

A method of synthesizing B_4C coatings of metal substrates by using RF (Radio Frequency) plasma source with an external magnetic field is described in [26]. The nanohardness of coated steel surfaces is found in the range of 14.0–16.6 GPa and the B_4C coatings with 1.73–3.89-times higher hardness than uncoated (bare) steels serving as targets. This technique seems useful also for B_4C-coating of W substrates.

In this work, composites with multilayer morphologies — $W/B_4C/W$, $W/B_4C/W_2B_5$, $W_2B_5/B_4C/W_2B_5$, etc. — in which boron carbide B_4C layers alternate with metallic tungsten W and/or tungsten pentaboride W_2B_5 ones, are produced and investigated. The surface metallization of boron carbide crystals or grains with tungsten (*a*) powder, (*b*) plate or (*c*) coating (formed by peroxpolytungstic acid aqueous solution treatment at 600 °C in hydrogen flow) is done by SPS (Spark-Plasma Sintering) at temperature of 1300–1700 °C and pressure of 20–40 MPa for 6–10 min. Such layered composites are also obtained by standard thermal sintering (at temperature of 1300–1500 °C in argon atmosphere or vacuum) of the components bonded with organic compounds aqueous solutions containing 0.5–1.0 % boric acid. SEM

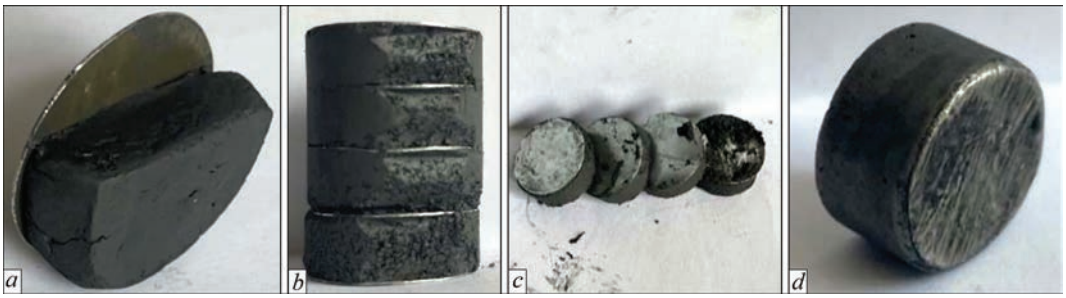

Figure 1. B_4C/W composite sandwich-like structures fabricated from tungsten plate and boron carbide powder: raw (*a*) monosandwich, (*b*) polysandwich and (*c*) its sections, and (*d*) sandwich-like structure produced by SPS at 1500 °C

(Scanning Electron Microscopy) structural-morphological, XRD phase- and EDS (Energy Dispersive Spectrometry) chemical-compositions analysis of obtained samples has established that transition layers of W_2B_5 are formed on the B_4C/W interfaces ensuring the strong component-layers bonding.

OBTAINING OF RAW SANDWICH-LIKE STRUCTURES

We have developed some new methods for obtaining the raw B_4C/W sandwich-like structures. As a tungsten source, tungsten powder and plate are used. Initial tungsten powder is obtained by dissolving tungsten scrap in 15–25 % solution of hydrogen peroxide. PTA is obtained by filtering and drying the solution. By its reducing with hydrogen at 500–600 °C for 4 h, it is obtained the tungsten powder. Both commercial boron carbide and tungsten pentaboride powders, and boron carbide matrix ceramic powders previously synthesized by authors from available inexpensive reagents, are used to prepare these sandwiches.

Here is described the synthesis method for PTA. 5.0 g of tungsten powder is slowly dissolved in 40 ml of 20–25 % H_2O_2. The H_2O_2 solution is added to the tungsten powder in 3 portions during 2 h (Note: The reaction is very exothermic!). Then, 15 ml of hydrogen peroxide solution is added to the reaction mixture again and stirred at room temperature for 5 h. The solution is left for 12 h and then filtered. A yellowish transparent solution is obtained. Excess H_2O_2 is decomposed using a platinum spiral and the solution is evaporated under vacuum. An orange crystalline substance containing 85.4 % tungsten oxide WO_3 is obtained. The sample is heated at 600 °C for 4 h.

As for other liquid-charge chemical synthesis methods that also are used here, they are described elsewhere [27–31]. These methods, previously developed for multi-component B_4C-matrix ceramics containing W compounds, have been modified for the purpose of obtaining B_4C–W layered composites.

The manufacturing technology of B_4C–W layered composite and corresponding (poly)sandwiches is illustrated in Figure 1. First, a paste of boron carbide is prepared using ethylcellulose 1 % solution for binding material, which also contains 0.5–1.0 % boric acid. Tungsten plate discs and B_4C wet (partially dried) powder are then placed alternately in the press-form. After pressing (at 5–10 atm) of the composite, the raw product is dried at room temperature and further processed by SPS at temperature of 1300–1700 °C and pressure of 20–40 MPa for 6–10 min. The thickness of the plates and the neutron absorbing material layers placed between them, as well as the total number of layers are variable.

The powder filling placed between the plates can be composite, consisting of several components. For example, it can be enriched with boron, tungsten, tungsten borides, etc. Some of the sandwiches we made contain 10–30 wt.% W and W_2B_5. Figures 2–4 show diffrectograms of initial powders. In the boron carbide commercial powder diffractogram, there are visible 3 intense B_4C peaks at 2θ = 23.5, 34.8 and 37.7°. In addition, there are also detected the traces of B_6C, $C_{12}BO_2$ and $C_{14}BO_2$ phases. Diffractogram of mixture of boron carbide and tungsten powders shows only 2 of 5 known peaks of W (40.4, 58.4, 73.3, 86.9 and 100.8°): 2θ = 40.4 and 58.4°. In addition to B_4C and W phases, there are also detected the traces of WB_4, W_5O_{14}, WO_3 and WO_4. Peaks of W_2B_5 phase visible in the diffractogram of mixture of boron carbide and tungsten pentaboride powders are placed at 2θ = 25.5, 35.3, 39.9 and 52.7°. In this case, besides main components B_4C and W_2B_5, there is detected a number of trace phases: W, WB_2, WB_4, WC, WO_2, $W_{18}O_{49}$, WO_3, W_3O_{10}, WO_4 and $C_{14}BO_2$.

By a similar method, sandwich composites can be obtained from tungsten and boron carbide powder pastes. In this case, the tungsten powder paste is placed in the mold and pressed with a punch so that the paste does not come out. Then they are added with wet powder of the neutron absorbing (composite) ma-

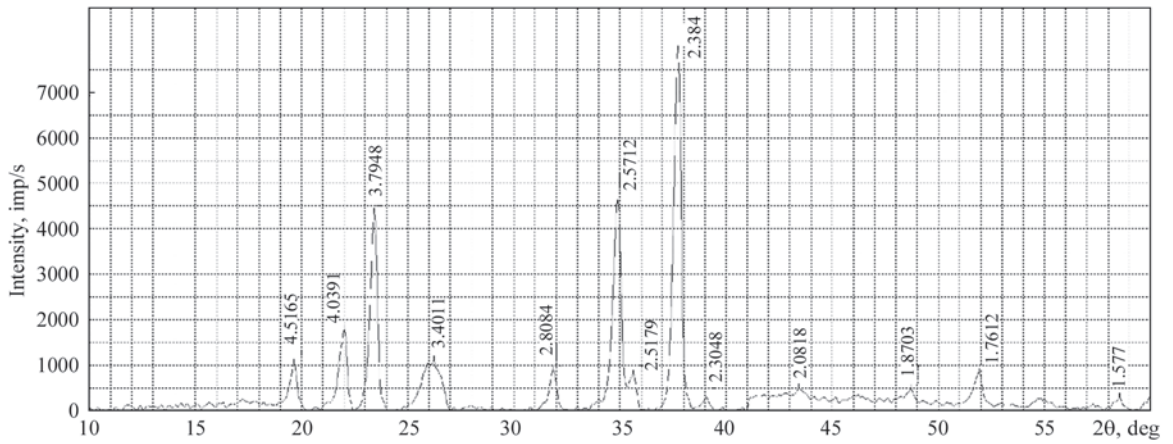

Figure 2. Boron carbide commercial powder diffractogram

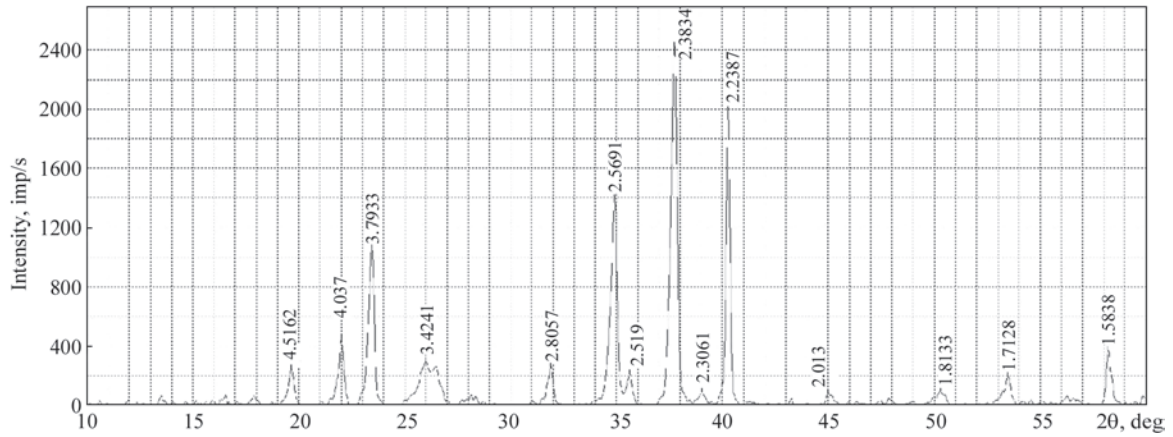

Figure 3. Diffractogram of mixture of boron carbide and tungsten powders

terial and pressed again. An image of the resulting section is shown in Figure 5.

In the next step, these intermediate products should compacted using a sintering method.

DETAILS OF SINTERING METHODS

used to obtain the sandwich-like B_4C/W composites are given below.

For the SPS compacting of W and B_4C powders, the 12 mm diameter graphite press-form lined with graphite foil is placed with a certain amount of commercial W powder and pressed with a punch. Boron carbide powder is added on top of the tungsten powder, which is also pressed with a punch to smooth the surface of the deposited powder. This surface is covered with graphite foil and a graphite punch is placed on top. The pressform is placed in the SPS equipment chamber, and, after its vacuuming, the powder is pressed at 30–50 MPa at temperature 1500–1700 °C for 10 min holding time. Pulsed AC (Alternating Cur-

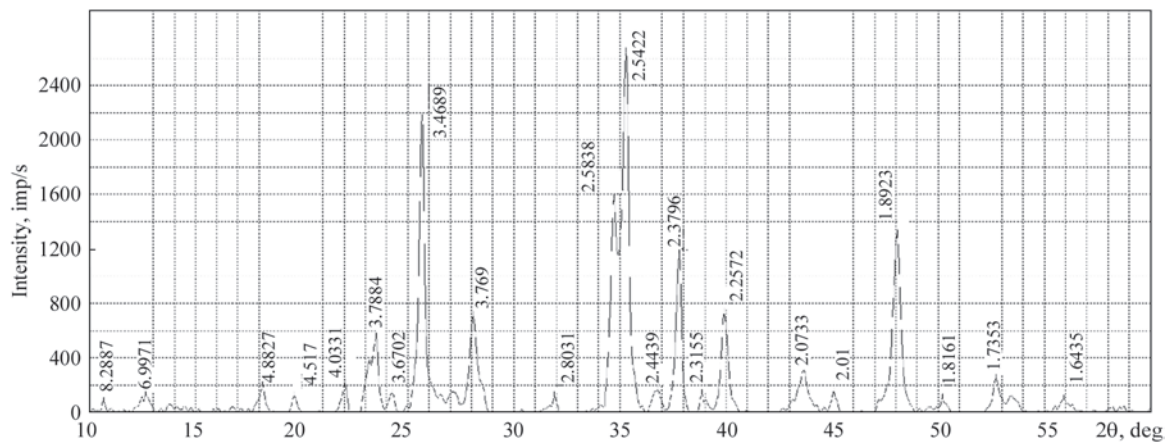

Figure 4. Diffractogram of mixture of boron carbide and tungsten pentaboride powders

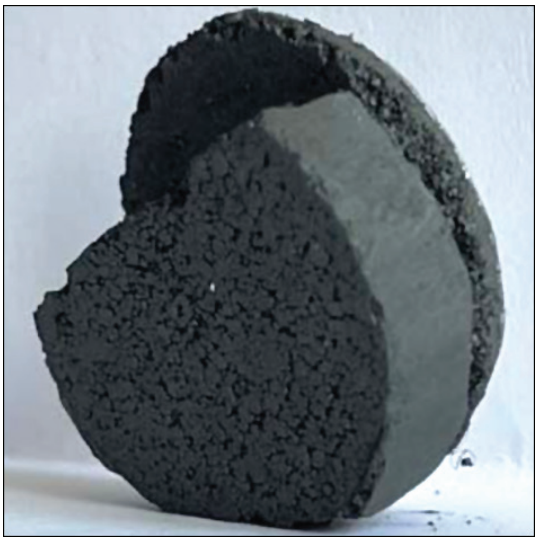

Figure 5. Sandwich made of tungsten (thin) and boron carbide (thick) powder paste layers

rent) mode with pulse duration of 5 μs and pause of 1 μs is used to sinter these ceramics. The sample heating rate reaches 100–200 °C/min. They are cooled in vacuum. Sandwich-like B_4C/W composites are obtained, where the boundary layer between components is well observable.

As for the SPS compacting of W foil and B_4C powder, for its conducting a tungsten disk of 12 mm diameter and thickness of 1–2 mm is placed on a graphite press-form of the same diameter lined with graphite foil and poured with boron carbide powder on top, and pressed with a punch to smooth the surface of the poured powder. Then, the surface is covered with graphite foil and a graphite punch is placed on its top. Sintering is carried out similarly to the described above. The samples are cooled in vacuum. Sandwich-like B_4C/W composites are obtained, where the boundary layer between two components is formed.

The following technological and measuring equipment and devices have been used for realization of above described processes.

To grind the powders there is used planetary mill Pulverisette 7 Premium Line with grinding cup and balls made from WC–Co hard alloy. For the ultrasound treatment and homogenization of suspensions is used an ultrasonic cleaner (45 kHz) and JY92–IIDN Touch Screen Ultrasonic Homogenizer (20–25 kHz, 900 W). Compaction of powder samples or simultaneous synthesis and compaction are carried out by using the SPS equipment manufactured at the Georgian Technical University (with an ability to operate in DC, pulsed DC and pulsed AC modes). Thermal treatment (< 1500 °C) of simples is implemented in high-temperature vacuum furnace Kejia.

X-Ray XRD patterns are obtained with DRON–3M (CuK_α, Ni filter, 2°/min) and XZG–4 (CuK_α, λ = 1.5418 Å) diffractometers. Morphology and microstructure of the powders are studied with SEM JEOL–JSM 6510 LV equipped with energy Dispersive Micro-X-Ray Spectral Analyzer X-MaxN (Oxford Instruments). Particles size of the powders are determined by the Scherrer method and also by photon correlation nanoparticle size analyzer Winner 802 DLS and Malvern Instruments Mastersizer. The specific surface area of the composite powder is measured on a Micromeritics Gemini VII Instrument.

CURRENT DEVELOPMENTS

Such layered composites also can be obtained by standard thermal sintering at temperature of 1300–1500 °C in argon atmosphere or vacuum from the components bonded with aqueous solutions of some organic compounds containing 0.5–1.0 % boric acid.

Now we are developing this new technology for making sandwiches, which will not use the SPS method, but will take the product of required profile under pressure and then sinter/consolidate it using traditional pressureless methods. In this case, it is necessary to use binders to form a raw product. Encouraging preliminary results have been obtained using organic polymer solutions for binding material.

In this approach, expensive finely dispersed commercial powders can be replaced by the commercially available reagents. Boron carbide and multicomponent powders of its composites should be received. Several reports have been already published on this issue. Here, these methods are used by us to obtain neutron capture materials. Their essence is briefly described below.

Target composites are obtained using inexpensive reagent: boric acid, tungsten, titanium and zirconium oxides, metal salts, and organic compounds, which represent a source of carbidizing amorphous carbon, as well as reductants. For example, preceramic precursors are obtained by pyrolysis of a paste made from ammonium paratungstate, zirconium oxide, cobalt acetate, sucrose and amorphous boron at 100–200 °C.

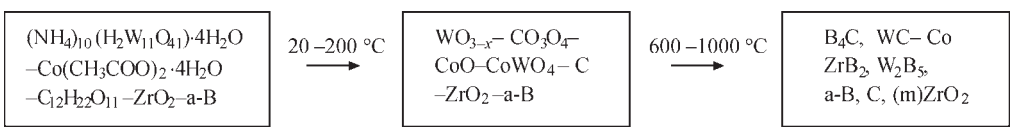

Figure 6. General scheme of obtaining preceramic precursors from mixture of zirconium(IV) oxide–ammonium paratungstenate–cobalt(II) acetate tetrahydrate–amorphous boron–sucrose

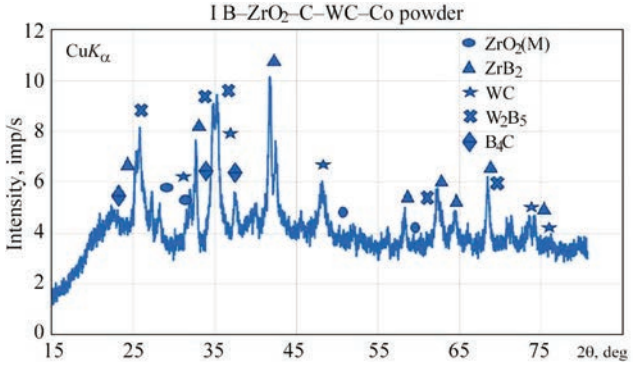

Figure 7. XRD pattern of preceramic precursor obtained from mixture of $(NH_4)_{10}(H_2W_{11}O_{41})\cdot 4H_2O$, $Co(CH_3COO)_2\cdot 4H_2O$, ZrO_2, B and $C_{12}H_{22}O_{11}$ at 1000 °C

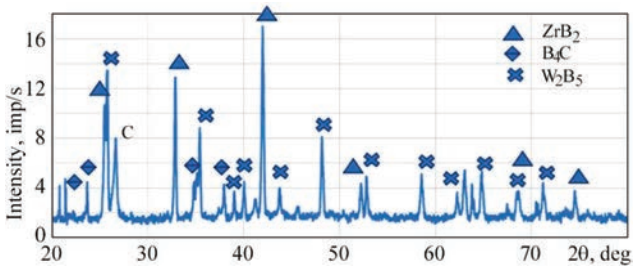

Figure 8. XRD pattern of composite obtained from preceramic precursors by SPS method at 1550 °C

General scheme of this example route is presented in Figure 6. The component phases (B_4C, ZrB_2, W_2B_5 and Co) are obtained by simple technology at relatively moderate temperatures: 800–1000 °C. So far, 1000 °C was the lowest temperature, at which the W_2B_5 phase formation was detected.

It is experimentally established that the starting compounds undergo the certain transformations upon gradual heating to 1000 °C (Figure 7). Raw products are made from preceramic precursors, and

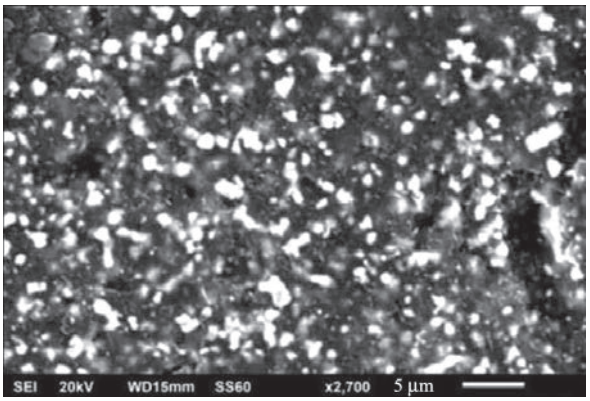

Figure 9. SEM micrograph of simple obtained from preceramic precursors by SPS method at 1700 °C

Figure 10. Raw sandwich made from preceramic precursor paste obtained from zirconium oxide–ammonium paratungstenate–cobalt acetate tetrahydrate–amorphous boron–sucrose system

neutron-capturing sandwiches are obtained by their annealing. It is important that composites containing boron carbide, tungsten boride and zirconium boride are obtained in a single technological process. Tungsten carbide and zirconium diboride (Figure 8), which are boron carbide particle growth inhibitors, are ob-

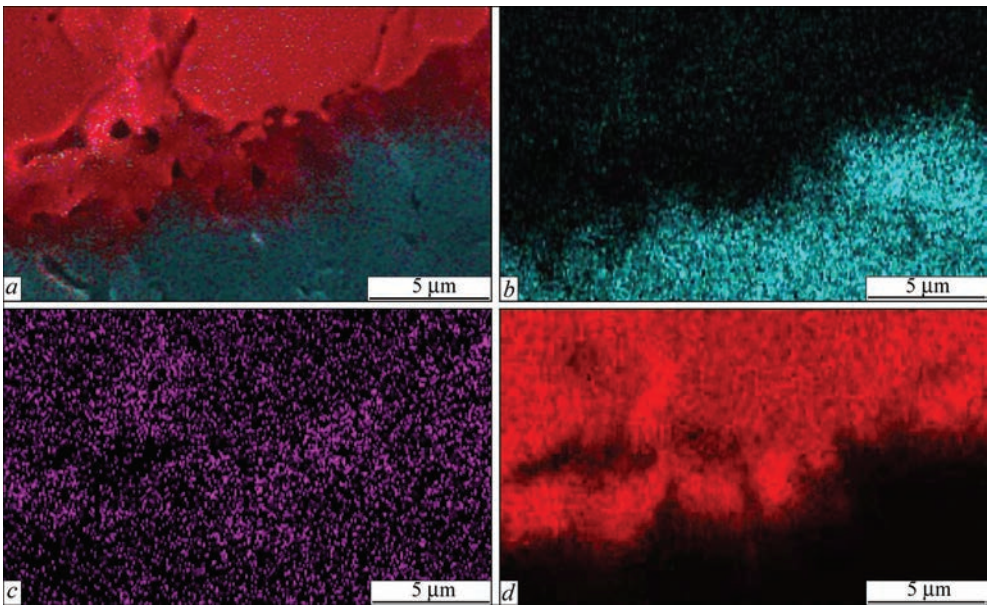

Figure 11. EDS mapping of (*a*) all elements in B_4C/W composite, and separately (*b*) B, (*c*) C and (*d*) W atoms distributions in B_4C and W phases contact regions, respectively

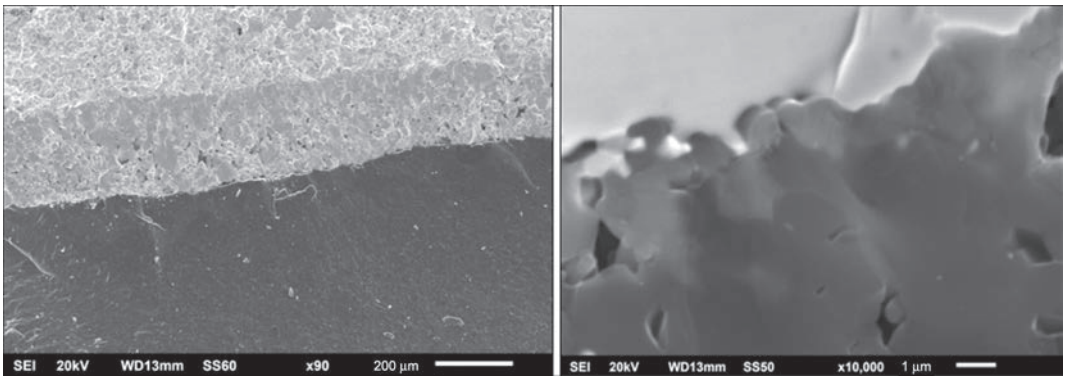

Figure 12. SEM images of fracture surfaces of B_4C–W composite obtained by SPS from B_4C and W powders at 1600 °C in magnifications of (*a*, ×90) and (*b*, ×10000)

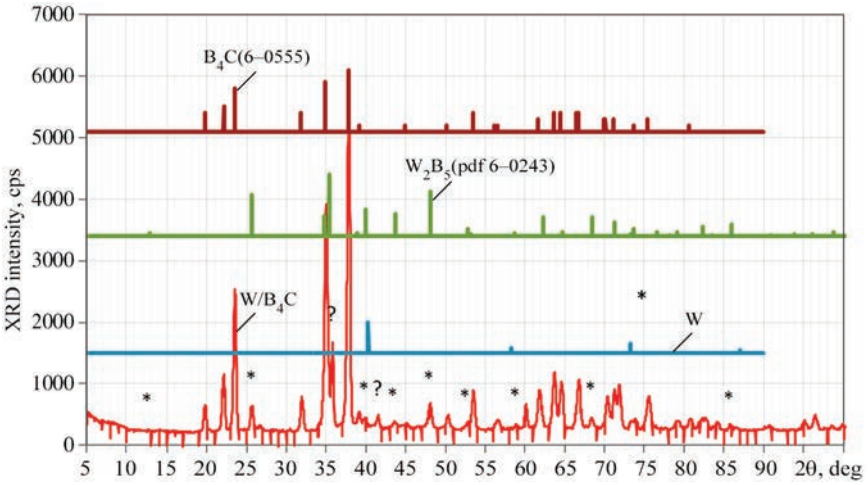

Figure 13. XRD pattern of B_4C–W_2B_5 composite obtained from B_4C–W_2B_5–W sandwich composite after selectively removing of metallic tungsten layer by treatment with hydrogen peroxide 30% solution, where peaks corresponding to B_4C and W_2B_5 component- and W trace-phases are shown separately

tained as intermediate products and contribute to boron carbide sintering.

It is interesting to note that the grains size of the composite are small, ranges within 0.5–2.0 μm (Figure 9) and practically does not change during annealing at 1700 °C. Raw sandwiches are obtained from similar preceramic powders (Figure 10). And by mixing them, B_4C–ZrB_2–W_2B_5 composite is formed, which is a promising material for neutron capture composites.

Preceramic precursors containing titanium and cobalt and boron carbide matrix ceramics are obtained in the same way. It is established that these sandwiches do not undergo exfoliation at the contact boundary of metal and boron carbides and, due to the physical-chemical processes taking place during the components sintering, are materials of high strength and hardness. From the EDS mapping images (Figure 11), it can be seen that at the phase boundary between tungsten and boron carbide (Figure 12) the diffusion of tungsten in the boron carbide layer and the formation of tungsten pentaboride take place (Figure 13). This phase is not detected after the tungsten layer selective removal.

CONCLUSIONS

The favorable properties of tungsten borides for shielding the spherical tokamak fusion power plant central HTS (High-Temperature Superconductor) core have been modelled [32] to minimize the power deposition into the cooled HTS core and to keep its radiation damage to acceptable levels by limiting the neutron and gamma fluxes. The shield materials compared are W_2B, WB, W_2B_5 and WB_4 along with a reactively sintered boride $B_{0.329}C_{0.074}Cr_{0.024}Fe_{0.274}W_{0.299}$, monolithic W and WC. Five shield thicknesses between 253 and 670 mm (corresponding to plasma major radii between 1400 and 2200 mm) are considered. W_2B_5 gives the most favorable results with reduction factor of > 10 in neutron flux and gamma energy deposition as compared to monolithic W. In particular, the W_2B_5 monolithic shields are found to have even better

performance than layered water-cooled ones, which is advantage from the safety perspective due to the risks associated with radio-activation of oxygen in water-cooled shields. The naturally occurring boron ^{10}B isotope 20% fraction gives much lower energy depositions than the 0% fraction, but the improvement largely saturates beyond 40 %. The performance of W_2B_5 is unrivalled by other monolithic shielding materials. This would be due to its trigonal crystal structure giving ^{10}B higher atomic density compared with other borides and, therefore, having just high enough content of ^{10}B to maintain a constant neutron energy spectrum across the shield.

Alternatively, effective radiation shields can be fabricated from tungsten composites with other boron compounds. For example, the tungsten–hexagonal boron nitride core–shell W@h-BN nanoparticles have been synthesized [33] by arc core discharge from tungsten atoms and borazine. The h-BN coats around the W-nanoparticles surface improving in this way their oxidation resistance. The fabricated 20 wt.% W@h-BN/BP-epoxy composite exhibits thermal neutron and gamma-ray shielding with absorption and attenuation coefficients of 3.51 and 0.357 cm^{-1}, respectively. These core–shell nanosystems can effectively shield not only the secondary γ rays emitted by thermal neutrons capture process of ^{10}B, but the primary γ rays as well. The W@h-BN-based materials can be utilized in space or extreme environments, where radiation shielding is critical for human activities.

Sandwich-structures of ^{10}B-enriched layers prepared by PLD (Pulsed Laser Deposition) serve [34] for development of novel neutron detectors showcasing improved efficiency, sensitivity and discrimination against γ background signals arisen from environment or neutron field.

In this work, the ^{10}B-based neutron capturing sandwich and multilayer structures are obtained using powder mixtures of compositions B_4C, B_4C–W and B_4C–W_2B_5. It is established that tungsten pentaboride phase is formed at the contact boundary between tungsten and boron carbide interfaces, which ensures component-layers strong bonding.

ACKNOWLEDGEMENT

Authors are thankful to the Republic Center for Structural Researches (GTU, Tbilisi, Georgia).

REFERENCES

1. Ozer, S.C., Buyuk, B., Tugrul, A.B. et al. (2016) Gamma and neutron shielding behavior of spark plasma sintered boron carbide-tungsten based composites. In: *Proc. of 145th Ann. Meeting Suppl. on TMS*, Cham, Springer Int. Publ., 449–456. DOI: https://doi.org/10.1002/9781119274896.ch54
2. Windsor, C.G., Astbury, J.O., Davidson, J.J. et al. (2021) Tungsten boride shields in a spherical tokamak fusion power plant. *Nucl. Fusion*, **61**, 086018 (1–14). DOI: https://doi.org/10.1088/1741-4326/ac4866
3. Chkhartishvili, L., Chedia, R., Tsagareishvili, O. et al. (2022) Preparation of neutron-capturing boron-containing nanosystems. In: *Proc.of 9th Int. Conf. on Exh. Adv. Nano Mater.*, Victoria, IAEMM, 1–15.
4. Chkhartishvili, L., Makatsaria, Sh., Gogolidze, N. (2023) Boron-containing fine-dispersive composites for neutron-therapy and neutron-shielding. In: *Proc.of Int. Sci. Prac. Conf. on Innov. Mod. Challen.–2022*, 2023, Tbilisi, Tech. Univ., 221–226.
5. Chkhartishvili, L., Makatsaria, Sh., Gogolidze, N. et al. (2023) Obtaining boron carbide and nitride matrix nanocomposites for neutron-shielding and therapy applications. *Condensed Matter*, 8(**4**), 92 (1–27). DOI: https://doi.org/10.3390/condmat8040092
6. Nabakhtiani, G., Chkhartishvili, L., Gigineishvili, A. at al. (2013) Attenuation of gamma-radiation concomitant neutron-absorption in boron–tungsten composite shields. *Nano Studies*, **8**, 259–266.
7. Chkhartishvili, L. (2018) Boron-contained nanostructured materials for neutron-shields. In: *Nanostructured Materials for the Detection of CBRN*. Eds by J. Bonca, S. Kruchinin. Dordrecht, Springer Science, Ch. 11, 133–154. DOI: https://doi.org/10.1007/978-94-024-1304-5_11
8. Evans, B.R., Lian, J., Ji, W. (2018) Evaluation of shielding performance for newly developed composite materials. *Ann. Nucl. Energy*, **116**, 1–9. DOI: https://doi.org/10.1016/j.anucene.2018.01.022
9. Park, J., Hossain, M.M., Jang, S.G., Kim, M.J. (2024) W@ boron nitride core-shell nanoparticles for radiation shielding. *ACS Appl. Nano Mater.*, 7(**9**), 10490–10497. DOI: https://doi.org/10.1021/acsanm.4c00888
10. Martin, P.M. (2018) Active thin films: Applications for graphene and related materials. *Vac. Technol. Coat.*, 19(**11**), 6–14.
11. Zinovev, A., Terentyev, D., Chang, C.-C. et al. (2022) Effect of neutron irradiation on ductility of tungsten foils developed for tungsten–copper laminates. *Nucl. Mater. Energy*, **30**, 101133 (1–10). DOI: doi.org/10.1016/j.nme.2022.101133
12. Sorokin, O., Kuznetsov, B., Lunegova, Y., Erasov, V. (2020) High-temperature composites with a multi-layered structure (Review). *Proc. All-Russian Sci. Res. Inst. Aviat. Mater.*, 88(**4–5**), 42–53 [in Russian].
13. Mann, K.S., Mann, S.S. (2021) Py-MLBUF: Development of an online-platform for gamma-ray shielding calculations and investigations. *Ann. Nucl. Energy*, **150**, 107845 (1–22). DOI: https://doi.org/10.1016/j.anucene.2020.107845
14. Dai, M., Zhang, Z., Zhu, J. et al. (2009) Influence of interface roughness on reflectivity of tungsten/boron-carbide multilayers with variable bi-layer number by X-ray reflection and diffuse scattering. *Chinese Opt. Lett.*, 7(**8**), 738–740. DOI: https://doi.org/10.3788/COL20090708.0738
15. Wang, Y., Long, B.F., Liu, C.Y., Lin, G.A. (2021) Evolution of reduction process from tungsten oxide to ultrafine tungsten powder via hydrogen. *High Temp. Mater. Proc.*, **40**, 171–177. DOI: https://doi.org/10.1515/htmp-2021-0017
16. Chang, M., Leung, C., Wang, D.N., Cheng, D. (1991) *Process for CVD deposition of tungsten layer on semiconductor wafer*. Pat. US, 5028565, July 2.
17. Kim, S.H. (1994) Deposition of tungsten thin film on silicon surface by low pressure chemical vapor deposition method. *J. Korean Chem. Soc.*, 38(**7**), 473–479.
18. Plyushcheva, S.V., Mikhailov, G.M., Shabel'nikov, L.G., Shapoval, S.Yu. (2009) Tungsten thin-film deposition on a silicon wafer: The formation of silicides at W–Si interface.

Inorg. Mater., **45**, 140–144. DOI: https://doi.org/10.1134/S002016850902006X
19. Kim, H.-J., Lee, J.-H., Sohn, I.-H. et al. (2002) Preparation of tungsten metal film by spin coating method. *Korea-Australia Rheol. J.*, 14(**2**), 71–76.
20. Yu, M.L., Ahn, K.Y., Joshi, R.V. (1990) Surface reactions in the chemical vapor deposition of tungsten using WF_6 and SiH_4 on Al, PtSi, and TiN. *J. Appl. Phys.*, **67**, 1055–1061. DOI: https://doi.org/10.1063/1.345791
21. Gao, J., Chan, L.H., Wongsenakhum, P. (2010) *Methods for improving uniformity and resistivity of thin tungsten films*. Pat. US, 7655567B1, February 2.
22. Yang, M., Aarnink, A.A.I., Kovalgin, A.Y. et al. (2016) Comparison of tungsten films grown by CVD and hot-wire assisted atomic layer deposition in a cold-wall reactor. *J. Vac. Sci. Technol. A*, 34(**1**), 01A129 (1–10). DOI: https://doi.org/10.1116/1.4936387
23. Dippel, A.-C., Schneller, T., Lehmann, W., Reichenberg, B., Waser, R. (2008) Tungsten coatings by chemical solution deposition for ceramic electrodes in fluorescent tubes. *J. Mater. Chem.*, **18**, 3501–3506. DOI: https://doi.org/10/1039/B802686F
24. Mallia, B., Dearnley, P. (2013) Exploring new W–B coating materials for the aqueous corrosion-wear protection of austenitic stainless steel. *Thin Solid Films*, **549**, 204–215. DOI: https://doi.org/10.1016/j.tsf.2013.09.035
25. Cao, P., Cao, J.-P., Cao, J.-H. (2021) *Boron carbide ceramic metallization preparation method*. Pat. CN, 110981550B, December 7[in Chinese].
26. Taran, A.V., Garkusha, I.E., Taran, V.S. et al. (2021) Structure and properties of B_4C coatings obtained by RF sputtering with external magnetic field. *Springer Proc. Phys.*, **246**, 51–57. DOI: https://doi.org/10.1007/978-3-030-51905-6_5
27. Barbakadze, N., Sarajishvili, K., Chedia, R. Et al. (2019) Obtaining of ultrafine powders of some boron carbide based nanocomposites using liquid precursors. *Nanotechnol. Percep.*, 15(**3**), 243–256. DOI: https://doi.org/10.4024/N27BA19A.ntp.15.03
28. Chkhartishvili, L., Mikeladze, A., Chedia, R. et al. (2020) Synthesizing fine-grained powders of complex compositions B_4C–TiB_2–WC–Co. *Solid State Sci.*, **108**, 106439 (1–8). DOI: https://doi.org/10.1016/j.solidstatesciences.2020.106439
29. Barbakadze, N., Chkhartishvili, L., Mikeladze, A. et al. (2022) Method of obtaining multicomponent fine-grained powders for boron carbide matrix ceramics production. *Mater. Today Proc.*, 51(**5**), 1863–1871. DOI: https://doi.org/10.1016/j.matpr.2021.08.013
30. Chkhartishvili, L., Mikeladze, A., Jalabadze, N. et el. (2022) New low-temperature method of synthesis of boron carbide matrix ceramics ultra-dispersive powders and their spark plasma sintering. *Solid State Phenom.*, **331**, 173–184. DOI: https://doi.org/10.4028/p-8n6hzy
31. Chkhartishvili, L., Mikeladze, A., Chedia, R. et al. (2022) Combustion synthesis of boron carbide matrix for superhard nanocomposites production. In: *Advances in Combustion Synthesis and Technology.* Eds by M. Bugdayci, L. Oncel. Singapore, Bentham Sci. Publ., Ch. 4, 66–95. DOI: https://doi.org/10.2174/9789815050448122010007
32. Windsor, C.G., Astbury, J.O., Davidson, J.J. et al. (2021) Tungsten boride shields in a spherical tokamak fusion power plant. *Nucl. Fusion*, **61**, 086018 (1–14). DOI: https://doi.org/10.1088/1741-4326/ac4866
33. Park, J., Hossain, M.M., Jang, S.G., Kim, M.J. (2024) W@boron nitride core-shell nanoparticles for radiation shielding. *ACS Appl. Nano Mater.*, 7(**9**), 10490–10497. DOI: https://doi.org/10.1021/acsanm.4c00888
34. Provenzano, Ch., Marra, M., Caricato, A.P. et al. (2023) Development of a high-efficiency device for thermal neutron detection using a sandwich of two high-purity ^{10}B enriched layers. *Sensors*, **23**, 9831 (1–11). DOI: https://doi.org/10.3390/s23249831

ORCID
L. Chkhartishvili: 0000-0003-3926-4524
N. Barbakadze: 0000-0002-5436-8009

CONFLICT OF INTEREST
The Authors declare no conflict of interest

CORRESPONDING AUTHOR
L. Chkhartishvili
Georgian Technical University
77 Merab Kostava Ave., 0160, Tbilisi, Georgia
E-mail: levanchkhartishvili@gtu.ge

SUGGESTED CITATION
L. Chkhartishvili, N. Barbakadze, O. Tsagareishvili, A. Mikeladze, O. Lekashvili, K. Kochiashvili, R. Chedia (2024) Neutron shield materials based on boron carbide–tungsten multilayer composites. *The Paton Welding J.*, **9**, 20–28.
DOI: https://doi.org/10.37434/tpwj2024.09.03

JOURNAL HOME PAGE
https://patonpublishinghouse.com/eng/journals/tpwj

Received: 01.08.2024
Received in revised form: 04.09.2024
Accepted: 07.10.2024

DOI: https://doi.org/10.37434/tpwj2024.09.04

DEVELOPMENT AND APPROVAL OF THE PROCEDURE OF HIGH-TEMPERATURE UNIAXIAL CREEP STRENGTH TESTS OF DIFFICULT-TO-WELD HIGH-TEMPERATURE NICKEL ALLOYS SPECIMENS WITH MICROPLASMA POWDER DEPOSITION

O.V. Yarovytsyn, M.O. Cherviakov, O.O. Nakonechny, O.O. Fomakin, S.O. Voronin, O.F. Yavdoshchyna

E.O. Paton Electric Welding Institute of the NASU
11 Kazymyr Malevych Str., 03150, Kyiv, Ukraine

ABSTRACT

The procedure of high-temperature uniaxial creep testing of welded joints "base-deposited metal" made of difficult-to-weld high-temperature nickel alloys (HTNA) of ZhS32 type, containing more than 60 vol.% of the strengthening γ′-phase, has been developed. It allows using witness specimens to estimate the uniaxial creep strength level at temperatures of 975 and 1000 °C for the conditions of series restoration of edges of the working blades of modern aircraft gas turbine engines with microplasma powder deposition. Its development took into account the need in working with larger sizes and, accordingly, the higher restraint of a welded workpiece for the manufacture of specimens for mechanical tests compared to the typical conditions of series restoration of the blade edge in industry, and also some techniques for hot cracks prevention were proposed. Its feature is the use of "dovetail" type grippers for specimens with a working part of 7.5–9.0 mm^2, which provides a significant reduction in their sizes. The new approach of choosing the shape and dimensions of the specimen for uniaxial creep testing, the technique of preparing and forming the required welded workpieces with microplasma powder deposition allows a significant reduction in heat input and approximation of the deposition modes for witness specimens to the industrial modes of series restoration of edges of working blades of aircraft gas turbine engines. Due to this, in the welded joints "base-deposited metal" of the high-temperature nickel alloys with directional solidification, which represent workpieces for the subsequent production of such witness specimens, it is possible to avoid the known manifestations of the tendency to crack formation during the deposition process and postweld heat treatment. The developed procedure was approved to evaluate the uniaxial creep strength of ZhS32 deposited metal specimens and specimens "50 % of base (ZhS26-VI or Zh32-VI) + 50 % of deposited (ZhS32) metal" at 975 °C and 1000 °C on 40 h base holding and comparison of the relevant experimental data with the technical condition requirements for these cast nickel-based superalloys was carried out.

KEYWORDS: microplasma powder deposition, welded joint "base-deposited metal", difficult-to-weld high-temperature nickel alloys, uniaxial creep testing

INTRODUCTION

In our country, working blades of difficult-to-weld high-temperature nickel alloys (HTNA) ZhS26 and ZhS32 (Table 1), designed for operation in modern aircraft gas turbine engines (GTE) for operating temperatures 950–1100 °C are manufactured in large volumes and remain in operation. At domestic aircraft repair enterprises, series technologies for the restoration of shrouded and unshrouded blades on the base of the process of microplasma powder deposition [1–4] with the use of a filler material of equivalent level of alloying were mastered. Evaluation of the mechanical properties of such welded joints "base-deposited metal", compensating for the losses of damaged material of parts in the local zones of a shroud platform or an airfoil edge (Figure 1), remains to be the relevant task. In particular, this applies to one of the most important indices of such materials — uniaxial creep strength at 975 and 1000 °C [5, 6]. Simultaneous combination of two adverse factors — larger sizes and, accordingly, higher restraint of a welded workpiece compared to the typical conditions for restoration of a blade edge in industry and the known high tendency to crack formation in fusion welding of HTNA with a high content of the strengthening γ′-phase require individual approaches for evaluation of high-temperature creep strength of these welded joints. Similar publications of other authors during the preparation of this article were not found.

The review of the known standards for mechanical tests [7, 8] and their analysis [9] show that they regulate the parameters of the working area of the specimen, and the guidelines on the shape and sizes of its gripping part bear only recommended nature. The consumption of the material to manufacture the specimen for mechanical tests depends on its geometric dimensions (length of the working area and overall dimensions of the gripping part), and also on the required tolerances on its mechanical treatment. But regardless of the type of the specimen for mechanical testing (flat, cylindrical), it can be stated that the need in forming its gripping part during the manufacture significantly increases the overall dimensions of both directly the specimen as well as the corresponding resulting workpiece.

Table 1. Content of base alloying elements in high-temperature nickel alloys

Alloy	wt.%					
	C	Cr	Ni	Co	Al	Ti
ZhS26-VI	0.12–0.18	4.3–5.3	Base	8.7–9.3	5.6–6.1	0.8–1.2
ZhS32-VI	0.12–0.17	4.3–5.3		9.0–9.5	5.7–6.2	–
VZhL12U	0.14–0.19	9.0–10.0		13.5–14.5	5.1–5.7	4.2–4.7
ChS40	≤ 0.05	19.0–21.0		–	2.4–2.7	–

Table 1. Cont.

Alloy	wt.%							
	Mo	W	Nb	Ta	Re	V	Fe	Si, Mn
ZhS26-VI	0.8–1.4	10.9–12.5	1.4–1.8	–	–	0.8–1.2	≤ 0.5	≤ 0.3
ZhS32-VI	0.9–1.3	8.1–8.9	1.4–1.8	3.7–4.7	3.6–4.3	–	≤ 0.5	≤ 0.2
VZhL12U	2.7–3.4	1.0–1.8	0.5–1.0	–	–	0.5–1.0	≤ 1.0	≤ 0.2
ChS40	8.0–10.0	4.5–5.5	–	–	–	–	≤ 5.0	≤ 0.3

The main problems that significantly complicate the use of standard procedures for the preparation of welded workpieces and manufacturing of specimens from them for the welded joint "base-deposited metal" of HTNA, which simulates the conditions for restoration of working blades of aircraft GTE, are the following:

● Limited deformation capacity of the deposited metal of HTNA with a content of the strengthening γ′-phase of more than 50 vol.% in a state directly after surfacing (for example, according to [10–12] $\varepsilon_{1000\ °C} \leq$ ≤ 0.7 %) and a high tendency of the cast base metal to the formation of cracks in fusion welding. This, in turn, prevents the performance of a defect-free deposition with a volume of more than 2–3 cm^3 [12] by an increase in the number of heat inputs into the product due to the components of efficient thermal power of the arc and heat input [13, 14].

● High cost of base metal workpieces and specialized HTNA filler materials, need in their manufacturing by an individual order.

● Complicated mechanical treatment ability of HTNA [15].

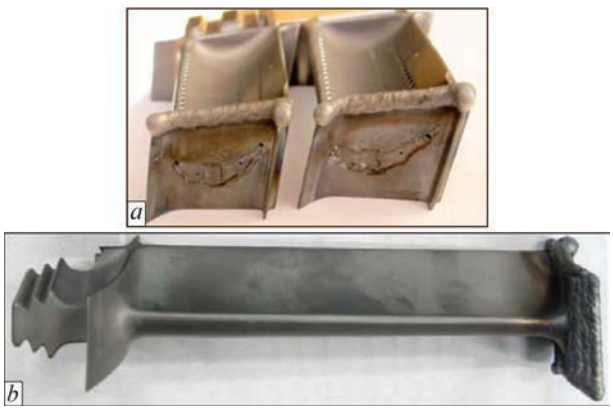

Figure 1. Appearance of restored shrouded working blades of modern aircraft GTE [3]: *a* – working blades of high-pressure turbine, ZhS32-VI alloy; *b* — working blades of medium-pressure turbine, ZhS26-VI alloy

THE AIM

of the work is to develop a procedure of high-temperature tests on uniaxial creep strength of specimens with microplasma powder deposition of working blades of GTE aircraft blades made of difficult-to-weld HTNA.

The preliminary positive experience of using miniature flat proportional specimens for tensile tests at high temperature in the MTS-810 servohydraulic machine at the PWI [9] has been gained. It consist in a significant reduction of the overall dimensions of the gripping part of the flat specimen for mechanical testing, and accordingly the volume required for its manufacture of welded workpiece from HTNA due to the use of "dovetail" type grippers-adapters. In turn, the releavant tasks in the framework of development of a new testing procedure for high-temperature creep strength were the development of a typical specimen and grippers-adapters for the MP-3G test machine, as well as shape, sizes, modes of deposition of initial welded workpiece, which guarantees its producing without crack formation.

DEVELOPMENT OF RESEARCH METHODS

During the preliminary analysis, 3 types of specimens were selected for high-temperature strength tests as initial prototypes. From the flat specimen, which is used at the PWI [16] and has a gripping part with holes under a pin of 8 mm diameter, the shape of the working area was borrowed (25 mm length, 7.5–9.0 mm^2 calculated cross-section, Figure 2, *a*). To specify the necessary geometric characteristics of the gripping part, the following cylindrical prototype specimens were analyzed: with a diameter of 4×M6, 5×M8 and 6×M10 according to ISO 6892-2:2011 [7] (Figure 2, *b*); close to the specimen MI-83 [16] (Figure 2, *c*), which, as is known, is serially used for tests of HTNA VZhL12U and ZhS6U on a high-temperature creep strength. On these specimens, on the base [17], the geometric characteristics of surfaces (Figure 2, *b*) were identified, which in the threaded connection resist to the most dangerous shear [18] and crumpling forces: an area of resistance to shear forces S_{sh} and the equivalent material volume V_{Σ} of a

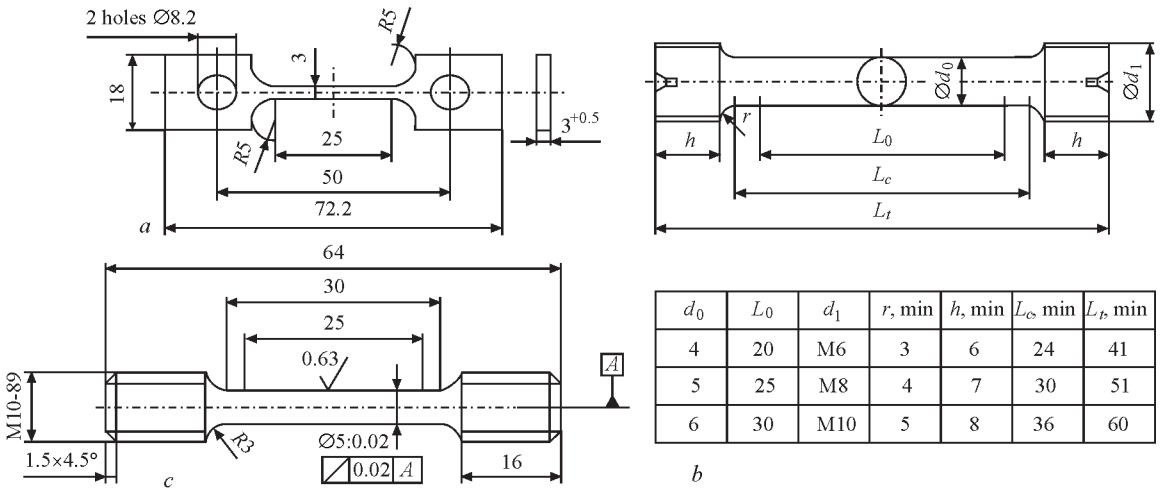

d_0	L_0	d_1	r, min	h, min	L_c, min	L_t, min
4	20	M6	3	6	24	41
5	25	M8	4	7	30	51
6	30	M10	5	8	36	60

Figure 2. Prototype specimens used to design an optimized flat proportional miniature specimen for the task of testing welded joint "base-deposited metal" of HTNA on high-temperature creep strength: *a* — flat proportional specimen of the PWI; *b* — cylindrical specimen according to ISO 6892-2:2011 [7]; *c* — cylindrical specimen for testing HTNA VZhL12U and ZhS6U

gripping part of the specimen (Table 2), which resists to crumpling. Based on the known principles of the theory of similarity [19], the determined indices of metric threads M6 and M8, were converted into the required dimensions of the gripped part of the flat "dovetail" type specimens (Figures 3, 4). Further, for the MP-3G test machine, a set of the specialized fixture made of HTNA VZhL12U with holes under a pin with a diameter of 6 mm was manufactured (Figure 5), which involves the use of the intermediate gripper-adapter to mount flat specimens with a gripped part of the "dovetail" type.

In addition to the performed verification calculations of shear and crumpling strength of a gripping part of the proposed specimen (see Figure 4, *a*), its serviceablility was checked by simulating the static loading process at a temperature of 1000 °C in the SOLIDWORKS Simulation 2015 software package of the corresponding 3D models of a new and a standard specimen with a diameter of 4×M6 (Figure 5). In this case, reference data from the mechanical characteristics of the material of the cast HTNA ZhS32-VI were used according to [20]. The results of physical modeling showed that in the proposed flat specimen (see Figure 6, *a*, *b*), a set level of stresses of 150 and 200 MPa is directly implemented on its working area and is identical to the standard specimen with a diameter of 4×M6 (see Figure 5, *c*, *d*). In places of transition to the gripping part, the concentration of high stresses is not observed.

Checking the manufactured set of a fixture for high-temperature testing of welded joints of difficult-to-weld high-temperature nickel alloys for creep strength was carried out in several stages with a gradual increase in the test temperature and the level of the material heat resistance. At the first stage, for the mentioned tests by multilayered deposition, the "ver-

Table 2. Ratio of basic geometric parameters of cylindrical specimens with a diameter of 6×M10, 5×M8 and 4×M6 according to ISO 6892-2:2011 with the results of calculations of equivalent geometric characteristics for flat proportional specimens: S_0 — cross-sectional area of the working zone of the specimen; S_{sh} — area of the thread, which resists to the shear force in the gripper; V_Σ — equivalent material volume that resists to the buckling and shear force in the gripper (in the thread or flat proportional specimen)

Cylindrical specimen								Flat proportional specimen	
Type	S_0, mm^2	Thread pitch P, mm	Average thread diameter d_2, mm	Inner thread diameter d_1, mm	Number of turns z, pcs	S_{sh}, mm^2	V_Σ, mm^3	According to Figure 4, *a*, S_0 = 9 mm^2	According to Figure 4, *b*, S_0 = 18 mm^2
								V_Σ, mm^3	
Diameter 4×M6	12.56	1	5.35	4.92	12	154.47	69.87	74.0	–
						77.35*	34.93*	37.00*	–
Diameter 5×M8	19.63	1.25	7.188	6.65	9	208.82	110.01	–	110.00
						104.41*	55.00*	–	55.00*
Diameter 6×M10	28.26	1.5	9.026	8.38	8	263.14	176.81	–	–
						131.57*	88.41*	–	–

*For half of the volume of the threaded connection or gripper of the "dovetail" type.

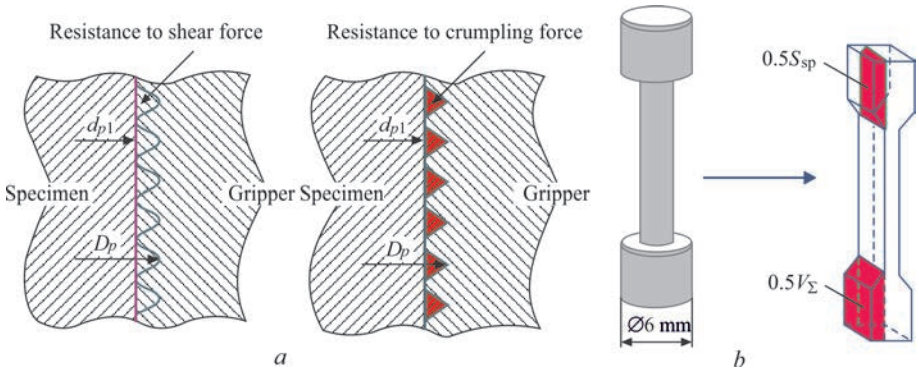

Figure 3. Equivalent surfaces of resistance to shear and crumpling force for the threaded connection of the prototype specimen (*a*) and the scheme of their conversion into the gripping part of the optimized flat proportional specimen of the "dovetail" system (*b*)

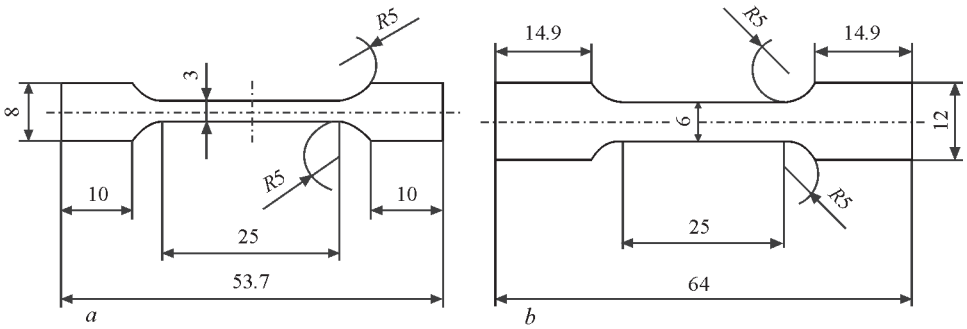

Figure 4. Drawings of designed optimized miniature flat proportional specimens with the gripper of the "dovetail" type for tests on high-temperature creep strength: *a* — with the cross-sectional area of its working part S_0 = 9 mm²; *b* — with the cross-sectional area of its working part of S_0 = 18 mm²

tical wall" workpiece was manufactured, from which after grinding of its side surfaces, the optimized flat proportional specimens were cut out by means of the electrical discharge machining (Figure 7). At the second stage, the preparation of the welded workpiece "50 % of base + 50 % of deposited metal" was practiced, from which the optimized flat proportional specimens were similarly cut out (Figures 8, 9).

RESULTS OF EXPERIMENTS AND THEIR ANALYSIS

The conditions and results of testing the deposited ChS40 metal, layered deposited ZhS32 + ChS40 metal, formed respectively to [21], and deposited ZhS32 metal are presented in Table 3 (experiments Nos 1–3). They proved the proper operation of the manufactured set of the specialized fixture for the test MP-3G machine: at T = 550 °C and σ = 69 kgf/mm² — holding of at least 120 h; at T = 975 °C and σ = 7.5–10.0 kgf/mm² — holding of approximately 20 h. The next stage of the research works was practicing the shape and sizes of the welded workpiece for the welded joint "50 % of base + 50 % of deposited metal".

When using a conventional deposition of ZhS32 alloy to the edge of the plate from the cast HTNA ZhS32-VI or ZhS26-VI to form a gripping part of a flat proportional specimen according to Figure 4, *a*, it is necessary to use a single-layer deposition with the

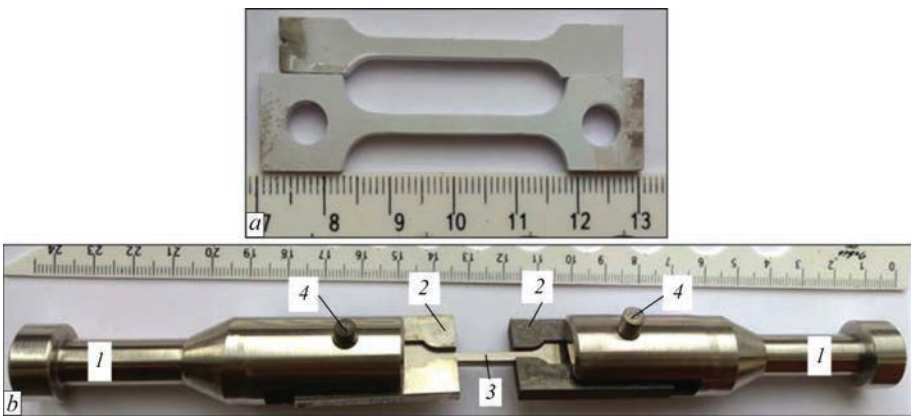

Figure 5. Appearance of the optimized flat proportional specimen compared to the specimen of a conventional shape (*a*) and manufactured assembly of a specialized fixture for the test MP-3G machine (*b*). Designations: *1* — main gripper; *2* — intermediate gripper-adapter; *3* — specimen for mechanical testing; *4* — pin of 6 mm diameter

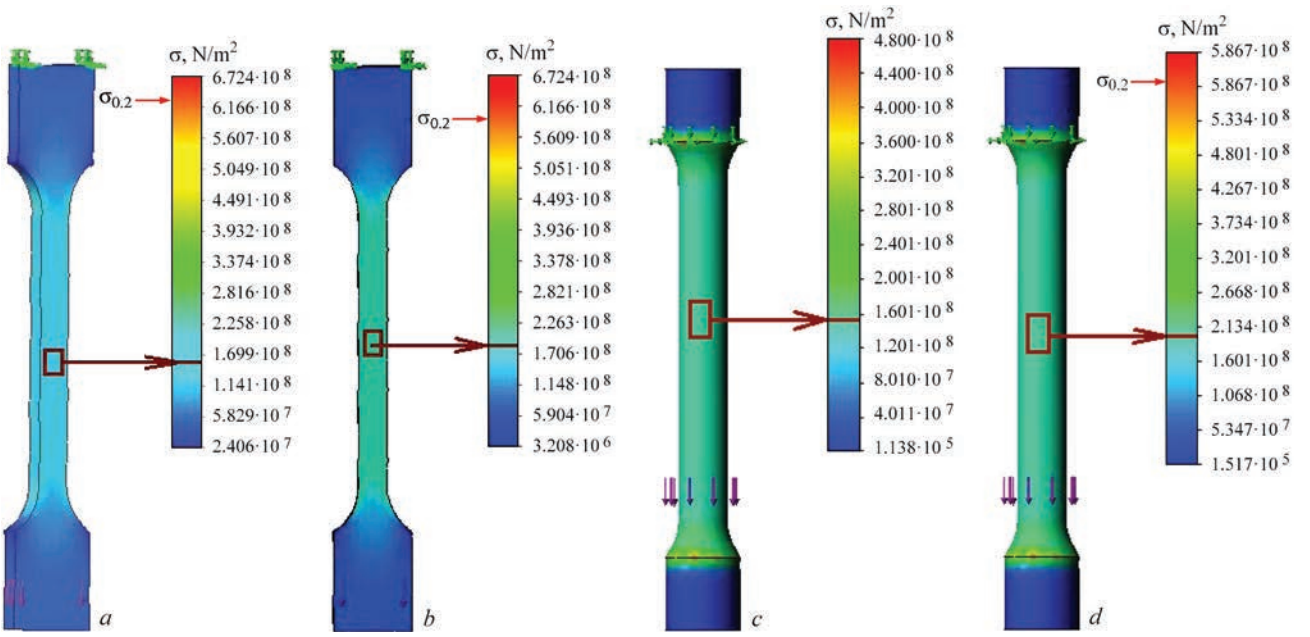

Figure 6. Results of physical simulation of 3D models of a new specimen (*a, b*) and a specimen with a diameter of 4×M6 (*c, d*) from the cast HTNA ZhS32-VI alloy at 1000 °C in the software SOLIDWORKS Simulation 2015 package

bead height of 6–7 mm on the side of the deposited metal (Figure 8, *a*, *b*). However, it turned out that such modes of microplasma powder deposition on the edge of the plate with a thickness of 3.5–5.0 mm, which are characterized by the actual welding current value I = 25–35 A, effective heat power q_s/v = 350–450 W and input power q_s/v = 2000–3000 J/mm, cause the formation of regular cracks (Figure 8, *c*, *d*). According to the data of metallographic testing of 10 sections, they are localized in the deposited metal. Their appearance is explained by the occurrence of tensile deformations in the process of deposition, that exceed the preliminary set limited deformation capacity of the deposited ZhS32 metal [11]. In turn, in view of the preliminary set direct proportionality between the value of the input heat and cross-section of the deposited bead in microplasma powder deposition [14], their appearance may be caused by an increase in the heat input to the product [13] within a longer time of welding pool existence during formation of a bead with a height of 6–7 mm by single-layer deposition.

At the same time, the preliminary formation of the depression on the edge surface of the plate made of HTNA along the shape of the working part profile of the flat proportional specimen (see Figure 4, *a*, *b*) allows ensuring the formation of a gripping part on the side of the deposited metal at a height of the deposited bead reduced to 3–4 mm. Such modes of deposition compared to the first variant are characterized by the heat input q_s/v = = 1000–1500 J/mm, which is accordingly explained by the formation of a much smaller cross-section of the deposited bead [14]. The next heat treatment of such welded workpiece by the modes of aging 1050 °C — 2.5 h and homogenization (1265 °C — 1.5 h for the base metal of ZhS26-VI alloy or 1280 °C — 1.5 h for the base metal of ZhS32-VI alloy) did not reveal any manifestations of the tendency to cracking in it according to the results of liquid penetrant testing and metallographic testing. A typical example of a high-quality microstructure of the base and deposited metal in the fusion line area is presented in Figure 10. After manufacturing specimens for testing on creep strength by means of the electrical discharge machining, the neighborhood of the fusion line between the base and deposited ZhS32 metal was quite evenly distributed in the middle of its working area.

According to the practiced procedure (see Figure 4, *a*, *b*), microplasma powder surfacing of 3 welded workpieces "50 % of base + 50 % of deposited metal" with ZhS32 alloy was performed and after passing of the appointed heat treatment, additional grinding, polishing of electro-erosion cutter surfaces and capillary testing, the specimens were tested for high-temperature creep strength at 975 and 1000 °C.

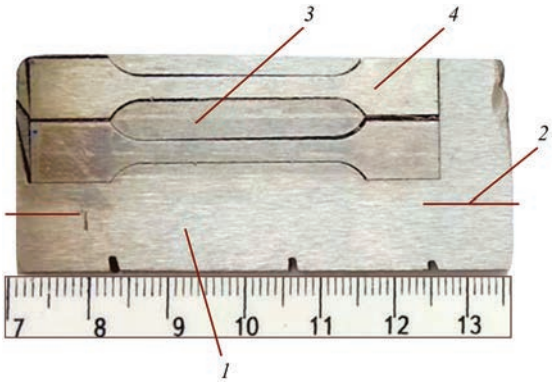

Figure 7. Scheme of producing an optimized flat proportional specimen of deposited metal for high-temperature tests of the deposited metal: *1* — technological base of austenitic stainless steel; *2* — position of the fusion line with the deposited metal; *3* — deposited metal of heat-resistant or high-temperature alloy; *4* — optimized flat proportional specimen

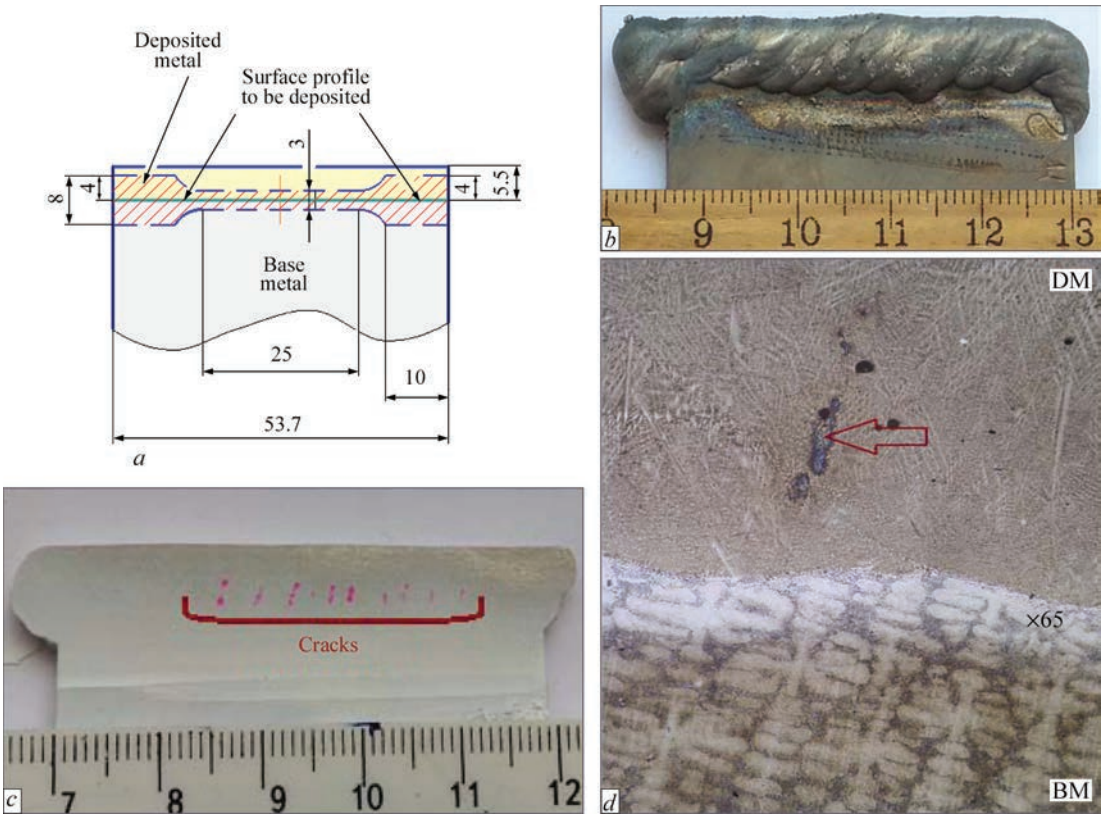

Figure 8. Regularities of crack formation in the welded joint "50 % of base (BM) + 50 % of deposited (DM) metal" made of HTNA of ZhS32 type produced by a single-layer microplasma powder deposition of ZhS32 alloy with q_s/v = 380–450 W and q_s/v = = 2000–3000 J/mm: *a* — scheme of preparation of welded workpiece and cutting of the specimen for mechanical testing; *b* — appearance of a single-layer deposition; *c* — results of liquid penetrant testing after removal of the side reinforcements of the deposited bead; *d* — appearance of cracks in the deposited ZhS32 metal detected during metallographic testing

The test results are presented in Table 3 (experiments Nos 4–6). Their interpretation taking into account the experimental data previously obtained at the PWI [2] and the basic requirements for the minimum level of mechanical properties of the cast HTNA ZhS32-VI and ZhS26-VI according to TS 1-92-177–91 published in [6, 7], is given in Figure 11.

The experimental data of tests of the specimens "50 % of base + 50 % of deposited metal" on creep strength with the participation of the deposited ZhS32 metal, cut out along the fusion line with the cast ZhS26-VI or ZhS32-VI alloy, exhibit that the indices for the basic 40 h creep strength relative to the level of relevant requirements in the acting TS on the cast ZhS32-VI or ZhS26-VI alloys [6, 7], are the following:

- for the specimen "50 % of base (ZhS32-VI) + 50 % of deposited (ZhS32) metal" after heat treatment by aging mode 1050 °C — 2.5 h — approximately 0.5 at 1000 °C;

Table 3. Results of tests on uniaxial creep strength of specimens of welded joints with microplasma powder deposition

Experiment number	Specimen description	Specimen type	Preliminary heat treatment of the specimen	*T*, °C	Load σ, kgf/mm²	Holding time τ, h and min
1	DM of ChS40	According to Figure 4, *a*	1050 °C — 2.5 h + 760 °C — 10 h + 650 °C – 25 h	550	69.0	120 h*
2	DM of ZhS32 + ChS40 (L)	According to Figure 4, *b*	1050 °C — 2.5 h	975	7.5	17 h 25 min**
3	DM of ZhS32	According to Figure 4, *a*	1050 °C — 2.5 h	975	10.0	10 h**
4	50 % BM of ZhS32-VI + + 50 % DM of ZhS32		1050 °C — 2.5 h	1000	14.5	60 h**
5	50 % BM of ZhS32-VI + + 50 % DM of ZhS32		1280 °C — 1.5 h	975	20.0	23 h 30 min**
6	50 % BM of ZhS26-VI + + 50 % DM of ZhS32		1265 °C — 1.5 h	975	20.0	44 h**

*The specimen was removed without fracture.
**Fracture of the specimen occurs over its working part.

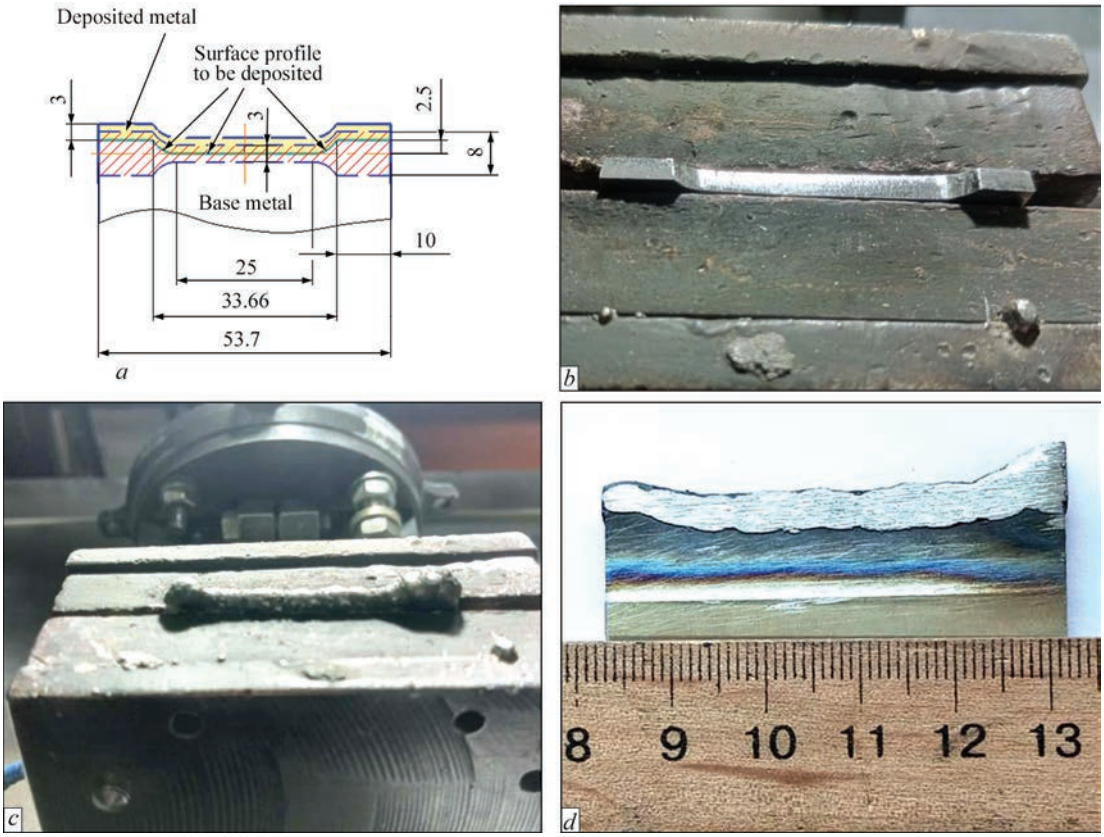

Figure 9. Features of surface preparation and technique of surfacing welded workpiece for welded joint "50 % of base — 50 % of deposited metal" made of HTNA: *a* — scheme of preparation of welded workpiece and cutting of the specimen for mechanical testing; *b* — preliminary formation of depression before deposition; *c* — appearance of a single-layer deposit; *d* — welded workpiece after partial removal of side reinforcements of deposited bead

● for the specimen "50 % of base (ZhS32-VI) + 50 % of deposited (ZhS32) metal" after heat treatment by homogenization mode 1280 °C — 1.5 h — approximately 0.6 at 975 °C;

● for specimen "50 % of base (ZhS26-VI) + 50 % of deposited (ZhS32) metal" after heat treatment by homogenization mode 1265 °C — 1.5 h — approximately 0.77 at 975 °C.

Thus, it was established that the welded joint "base-deposited metal" with the height of the deposited layer of ZhS32 alloy of up to 3 mm in the zone of the fusion line has sufficiently high indices of the creep strength — at a level of 0.5–0.6 at temperatures of 975 and 1000 °C relative to the minimum requirements for the cast ZhS32-VI alloy; at a level of 0.77 at a temperature of 975 °C for the cast ZhS26-VI alloy. For the serviceability of the restored sealing elements of working blades of high- and medium-pressure turbines (edges of shroud platforms and upper edge of the airfoil) made of HTNA ZhS32-VI and ZhS26-VI alloys, a sufficient

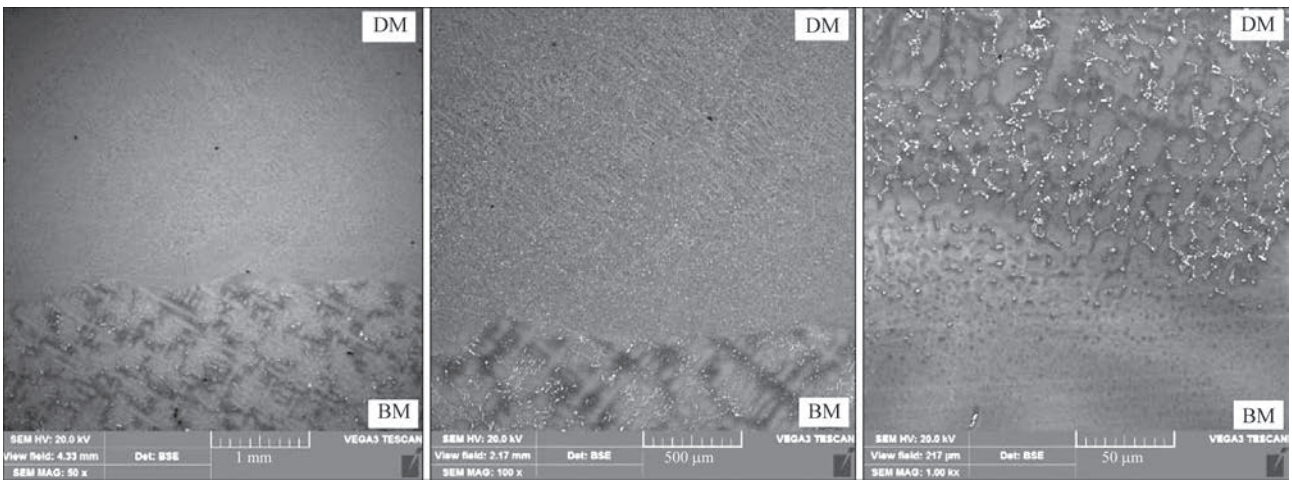

Figure 10. Typical example of a high-quality microstructure of welded joint "50 % of base (BM) +50 % of deposited (DM) metal of ZhS32 alloy

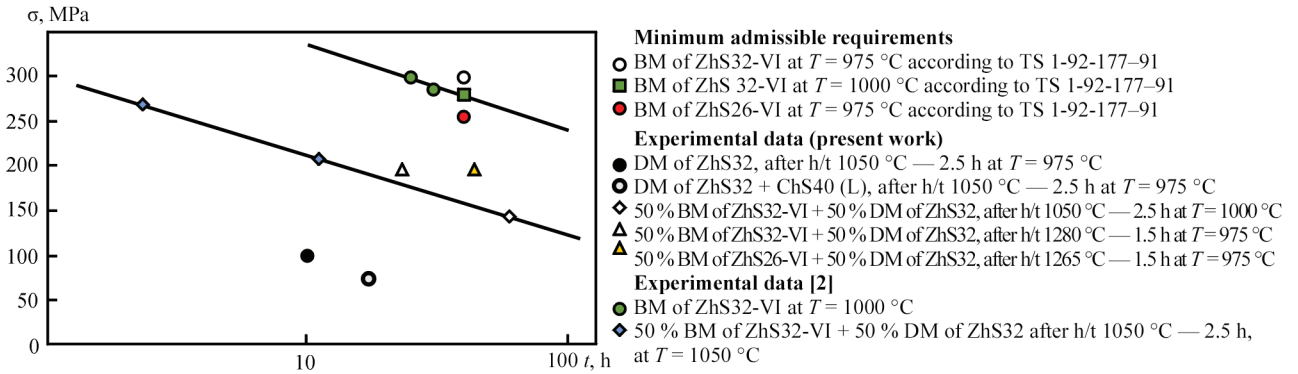

Figure 11. Results of testing specimens of base metal (BM), deposited metal (BM) and "50 % of base (BM) + 50 % of deposited (DM) metal on the creep strength at temperatures of 975 and 1000 °C, produced with microplasma powder deposition of ZhS32 alloy, compared to requirements of acting standard and technical documentation for the cast ZhS32-VI and ZhS26-VI metal

creep strength is achieved at 975 and 1000 °C, which is proved by the practice of long-term operation of the restored working blades on modern aircraft GTE [1–4].

The analysis of the experimental data obtained by the authors of the article and materials of the previously published work [22] allows predicting the presence of a significant decrease in the indices of a high-temperature creep strength, first of all namely for the deposited ZhS32 metal compared to the high-temperature area of the heat-affected-zone of the cast heat-resistant ZhS32-VI and ZhS26-VI alloys. It is assumed that such a decrease in the creep strength of the deposited ZhS32 metal may be predetermined by the excellent conditions of its formation compared to the serial technology of casting HTNA with a directional solidification, in particular, a significant difference (at least by an order [11]) in the cooling rates in the region of the temperature interval of the solidification of ZhS32-VI and ZhS26-VI alloys, which in turn significantly affects the characteristics of the dendritic structure during solidification (see Figure 10), namely the parameter of the distance between the axes of dendrites. Direct causes for reducing the properties of the creep strength namely of the deposited ZhS32 metal at temperatures of 975 and 1000 °C require further research.

CONCLUSIONS

1. The procedure of high-temperature tests for uniaxial creep strength of welded joints "base-deposited metal" made of difficult-to-weld high-temperature nickel alloys of ZhS32 type, based on the use of optimized miniature flat specimens with a cross-section of the working part of 7.5–9.0 mm^2 with a gripping part of the "dovetail" type and intermediate grippers-adaptors has been developed. In this case, under the condition of the same thickness of the welded workpiece, the material consumption compared to a flat prototype specimen is reduced by 2–3 times.

2. For the deposited metal of high-temperature nickel alloys, which has a limited deformation capacity in the process of multilayered deposition, the proposed procedure allows producing specimens without defects and guarantees a high reliability of corresponding experimental data.

3. In order to prevent cracking, during the preparation of a welded workpiece "50 % of base + 50 % of deposited metal" of a high-temperature nickel alloy, it was proposed to preliminary make a sampling-deepening to 2.5–3.0 mm on the edge surface of the plate with a thickness of 3.5–5.0 mm. This allows limiting the height of the deposited bead to 3–4 mm and, by reducing its cross-section and the amount of surfacing material, limiting its heat input to 1000–1500 J/mm at the efficient power of the microplasma arc of 350–450 W by an increse in the rate of microplasma powder deposition.

4. Approval of the developed procedure was carried out when testing the specimens of deposited metal and specimens "base-deposited metal" along the fusion line: at 550 °C — on the base of 100 h; at 975 and 1000 °C — on the base of 40 h.

5. It was established that the welded joint "base-deposited metal" with the participation of the deposited ZhS32 metal, which also includes a high-temperature area of the heat-affected-zone of the base metal, has the following indices of the uniaxial creep strength on the base of 40 h compared to the minimum admissible ones for the cast nickel-based superalloy according to TS: at a level of 0.5–0.6 at temperatures of 975 and 1000 °C relatively to the cast ZhS32-VI alloy; at a level of 0.77 at a temperature of 975 °C relatively to the cast ZhS26-VI alloy.

6. The serviceability of the welded joint "base-deposited metal" made of HTNA of ZhS32type at a level of creep strength determined in the work was proved by the practice of operation during a set interrepair period of a large number of motor sets of working blades of high- and medium-pressure turbines of modern aircraft GTE, restored by the Ukrainian aviation industry since 2005.

REFERENCES

1. Peychev, G.I., Zamkovoy, V.E., Kalashnikov, G.P. et al. (2005) Repair of structural elements worn out in the process of operation of the truss shelves of cast working blades of the turbine made of alloys of the ZS type. *Aviats.-Kosmich. Tekhnika i Tekhnologiya,* 25(**9**), 221–223 [in Russian].

2. Yushchenko, K.A., Savchenko, V.S., Yarovitsyn, A.V. et al. (2010) Development of the technology for repair microplasma powder cladding of flange platform faces of aircraft engine high-pressure turbine blades. *The Paton Welding J.,* **8**, 21–24.
3. Zhemanyuk, P.D., Petrik, I.A., Chigilejchik, S.L. (2015) Experience of introduction of the technology of reconditioning microplasma powder surfacing at repair of high-pressure turbine blades in batch production. *The Paton Welding J.,* **8**, 43–46. DOI: https://doi.org/10.15407/tpwj2015.08.08
4. Yushchenko, K. A., Yarovytsyn, O. V., Khrushchov, G. D. et al. (2022) Research and optimization of refurbishment of HPT blades of the D-18T aircraft gas turbine engine by micro-plasma powder welding. *Kosmichna Nauka i Tekhnologiya,* 28(**3**), 3–16 [in Ukrainian]. DOI: https://doi.org/10.15407/knit2022.03. 01-01
5. Zhemanyuk, P., Klochyhyn, V., Lysenko, N., Naumyk, V. (2015) Structure and properties of cast aircraft engines blades (HA26-VI alloy) from heatproof nickeliferrous alloy after hot isostatic pressing. *Vestnik Dvigatelestroeniya,* **1**, 139–146 [in Russian].
6. Milonin, E. V., Lysenko, N. A., Naumyk, V. V. (2016) Directional solidification cast products of experienced superalloy base HA32-VI, *Aviats.-Kosmich. Tekhnika i Tekhnologiya,* **8**, 83–89 [in Russian].
7. (2011) ISO 6892-2:2011 (E): *Metallic materials — Tensile testing.* Pt 2: Method of test at elevated temperature.
8. (2018) EN ISO 204-2018: *Metallic materials — Uniaxial creep testing in tension — Method of test.*
9. Yushchenko, K.A., Yarovitsyn, A.V., Chervyakov, N.O. et al. (2019) Evaluation of short-term mechanical properties of a joint of difficult-to-weld nickel high-temperature alloys of ZhS6 type. *The Paton Welding J.,* **7**, 29–35. DOI: https://doi.org/10.15407/tpwj2019.07.07
10. Yushchenko, K.A., Zviagintseva, G.V., Yarovytsyn, O.V., Chervyakov, M. O. et al. (2019) New approaches in evaluation of mechanical characteristics and microstructure of restored parts of GTE from nickel heat-resistant alloys. *Metallophysics and Advanced Technologies*, 41(**10**), 1345–1364 [in Ukrainian]. DOI: https:// doi.org //10.15407/mfint.41.10.1345
11. Yarovytsyn, O.V. (2020) About the deformation ability of overlay metal of nickel-base difficult-to-weld high temperature strength alloys with γ′-phase strengthening high content. *Metaloznavstvo ta Obrobka Metaliv,* 94(**26**), 38–48 [in Ukrainian]. DOI: https://doi.org/10.15407/mom2020.02.38
12. Yushchenko, K.A., Yarovitsyn, O.V., Nakonechnyi, O.O. et al. (2020) Development of the technology of reconditioning the sealing element of nozzle blade sector from difficult-to-weld high-temperature nickel alloy of ZhS6 type by microplasma powder surfacing. *The Paton Welding J.,* **11**, 25–28. DOI: https://doi.org/10.37434/tpwj2020.11.05
13. Yushchenko, K.A., Yarovitsyn, A.V., Chervyakov, N.O. (2017) Effect of energy parameters of microplasma powder surfacing modes on susceptibility of nickel alloy ZhS32 to crack formation. *The Paton Welding J.,* **2**, 2–6. DOI: https://doi.org/10.37434/tpwj2017.02.01
14. Yushchenko, K.A., Yarovitsyn, A.V., Chervyakov, N.O. (2016) Dependencies of discrete-additive formation of microvolumes of metal being solidified in multi-layer microplasma powder surfacing of nickel alloys. *The Paton Welding J.,* **5–6**, 143–149. DOI: https://doi.org/10.37434/tpwj2016.06.25
15. Bohuslaev, V.A., Muravchenko, F.M., Zhemanyuk, P.D. et al. (2003) Technological support of service characteristics of GTE parts. In: *Turbine blades.* Pt 2. Zaporozhie: OJSC Motor Sich Publish. House [in Russian].
16. (1978) *Metal Test Specimen Catalog*. PWI of the Academy of Sci. of the Ukr.SSR [in Russian].
17. DSTU ISO 724:2005: ISO *Metric threads of general purpose. Basic dimensions* (ISO 724:1993, IDT), 2007 [in Ukrainian].
18. Birger, I.A., Shor, B.F., Iosilevich, G.B. (1979) *Strength calculation of machine parts*: Refer. Book. 3rd Ed. Moscow, Mashinostroenie [in Russian].
19. Gukhman, A. A. (1973) *Introduction to the theory of similarity*. Moscow, Mashinostroenie [in Russian].
20. Kuznetsov, V.P., Lesnikov, V.P., Konakova, I.P. (2010) *Structure and properties of heat-resistant nickel alloy ZhS32-VI*: Refer. Book. Ekaterinburg, Kvist [in Russian].
21. Yushchenko, K.A., Yarovytsyn, O.V., Nakonechnyi, O.O., Khrushchov G.D. et al. *The method of microplasma powder 3D deposition of parts made of nickel-based superalloys.* Pat. UA 127421, Publ. 16.08.2023 [in Ukrainian].
22. Yushchenko, K.A.,Yarovytsyn, O.V., Chervyakov, M.O. (2022) Development of a set of requirements of methods for evaluating the performance of welded joints "base-overlay metal" from nickel-based superalloys of ZhS6 and ZhS32 type, simulating the repairing of the aircraft gas turbine engines blade edges under industrial conditions. *Metallophysics and Advanced Technologies,* 44(**12**), 1679–1696 [in Ukrainian]. DOI: https:// doi.org //10.15407/ mfint.44.12.1679

ORCID
O.V. Yarovytsyn: 0000-0001-9922-3877,
M.O. Cherviakov: 0000-0003-4440-7665,
O.O. Nakonechny: 0000-0002-6098-0413,
O.O. Fomakin: 0000-0001-8903-3340,
S.O. Voronin: 0009-0003-3360-2710,
O.F. Yavdoshchyna: 0000-0002-8587-7295

CONFLICT OF INTEREST
The Authors declare no conflict of interest

CORRESPONDING AUTHOR
O.V. Yarovytsyn
E.O. Paton Electric Welding Institute of the NASU
11 Kazymyr Malevych Str., 03150, Kyiv, Ukraine
E-mail: yarovytsyn@ukr.net

SUGGESTED CITATION
O.V. Yarovytsyn, M.O. Cherviakov, O.O. Nakonechny, O.O. Fomakin, S.O. Voronin, O.F. Yavdoshchyna (2024) Development and approval of the procedure of high-temperature uniaxial creep strength tests of difficult-to-weld high-temperature nickel alloys specimens with microplasma powder deposition. *The Paton Welding J.*, **9**, 29–37.
DOI: https://doi.org/10.37434/tpwj2024.09.04

JOURNAL HOME PAGE
https://patonpublishinghouse.com/eng/journals/tpwj

Received: 04.04.2024
Received in revised form: 18.05.2024
Accepted: 02.10.2024

DOI: https://doi.org/10.37434/tpwj2024.09.05

IMPROVEMENT OF TECHNOLOGY AND EQUIPMENT FOR WELDING VERTICAL JOINTS WITH FORCED WELD FORMATION

S.A. Reznik, S.M. Kozulin, S.O. Suprun

E.O. Paton Electric Welding Institute of the NASU
11 Kazymyr Malevych Str., 03150, Kyiv, Ukraine

ABSTRACT

The paper presents the results of design and experimental studies carried out to modernize welding equipment to increase the reliability of operation in site conditions and improve ergonomic performance. The results of improving the technology and technique of welding vertical joints with forced weld formation in order to increase the efficiency of the process and expand its technological capabilities, as well as improve the sanitary and hygienic working conditions of the welder-operator are presented. The A-1150 and AD343 machines were modernized and prototypes of the machines were manufactured to create new specialized assembly welding equipment based on a modern element base in compliance with ergonomic requirements. The study of the macrostructure of the welded joints showed that the weld metal is dense, and no defects in the form of lacks of fusion, cracks, pores, nonmetallic inclusions, etc. were found. The main advantages of the proposed method compared to ESW and the method of welding with forced flux-cored wire formation are shown. The technology and equipment for submerged arc welding with forced formation of vertical joints of low-carbon low-alloy steels with a thickness of 12–80 mm have been developed and successfully implemented in factory and site conditions.

KEYWORDS: electroslag welding, electric arc welding with forced weld formation, assembly machines, low-carbon low-alloy steels, fluxes, heat input, impact toughness

INTRODUCTION

At present, in Ukraine, one of the important areas of performing welding works in the workshop and field conditions are the works on the creation and restoration of metal structures manufactured of metal of medium (different dimensional values) and large range of thicknesses. Other indices of welding conditions causing the choice and application of welding and technological process may be: speed of work performance, availability of qualified performers and the possibility of quick production of filler material, technological equipment available in the designated place of works.

In the modern production, vertical welds with forced metal formation are performed mainly with the use of two technological processes: electroslag welding (ESW) and an electric arc process with forced weld metal formation (EAW). Electroslag welding from the time of its invention has become widespread all over the world [1, 2].

ESW is the most widespread in the manufacture of parts of machines and metal structures of large thickness (more than 50 mm), such as housings of rolling mills, frames of jaw crushers, oversized bands of rotary fire kilns, housings blast furnaces, etc. [3]. This is predetermined by the high performance (in terms of melting rate of filler metal, ESW is out of competition) and the stability of the process, deep metallurgical treatment of weld metal (absence of defects in the form of pores and slag inclusions), possibility of welding metal of excessively large thicknesses, cost-effectiveness of the process, low sensitivity to the quality of edge preparation, relatively low cost of welding consumables, which are not scarce, etc.

However, the use of ESW during the construction of large metal structures of large thickness in the field conditions is not always acceptable due to the high heat input of the process that leads to growth of grains of weld metal and heat-affected-zone (HAZ). As a result, the mechanical characteristics of a joint are reduced, especially, impact toughness is noticeably reduced at low temperatures. The situation can be improved by the following high-temperature treatment (HTT), but it requires large-sized furnaces, the use of which for welding of large metal structures, especially in site conditions, is unrealistic.

All this facilitated the development of alternative processes of mechanized welding of small thickness metal in a one pass. One of them turned to be electric arc welding using flux-cored wire with forced weld formation by water-cooled copper shoes, both self-shielding and with additional gas shielding [4]. The method not only provides high performance of wire melting, but also became non-alternative to produce welds in a one/two passes in different spatial positions, both circumferential on pipelines, gas holders, spherical tanks, as well as “on the overhead” when welding horizontal girths of structures of the metal of at least 25 mm thick. However, the method required additional measures to protect the welding zone from drafts, especially at the height, and was too sensitive to side deviation from the vertical. Welding of

metal of more than 30 mm thick using two flux-cored wires turned to be complicated because of the difficulties with the positioning of the wire in depth due to intense radiation and emission of fumes. In addition, production of flux-cored wire is non-serial, it has a high price and a short storage period because of its hygroscopicity.

Therefore, PWI conducted research on the development of welding method with forced formation of vertical welds under a thin layer of molten slag using solid-section wires [5]. The first experiments on practicing of such technique of weld performance showed the prospect of the method, since it combined a stable process course and reliable protection of the welding pool, which was an urgent task.

However, this method did not find an industrial use for several reasons:

- absence of a compact mechanism of drawing two wires for welding in the site conditions, which would provide their reliable and stable feeding to the welding pool;
- lack of mechanism for positioning wires in the slit between welded edges;
- flux AN-47, under which the process was performed, did not ensure its stability.

AIM OF THE WORK:

designing of mobile equipment and industrial technology for joining metal in site conditions with the thickness from 10 mm to the maximum possible in site conditions during the manufacture of tanks of various purposes, bridge spans, etc.

TASKS OF THE WORK:

- modernization of welding equipment in order to increase the reliability of work in these conditions and improve ergonomic indices;
- improvement of technology and technique of welding vertical joints with forced weld formation in order to increase the efficiency of the process and expand its technological capabilities, as well as improve sanitary and hygienic conditions.

MATERIALS AND RESEARCH METHODS

Experimental studies of the process of two-electrode welding with forced formation were carried out as follows:

- welding of specimens of low-alloy structural 09G2 and 10KhSND steels of 12, 20 and 25 mm thick was performed with the use of a prototype of a two-electrode apparatus and VSZh-1600 DC power source;
- electrode wires of Sv-08G2C and Sv-10NMA grades were used;
- fluxes for the process performance were chosen based on the following criteria: electrical conductivity and toughness in the molten state; technological properties, such as stability of the process, wetting of a shoes with the cooled water, which requires the quality formation of the weld metal; visual signal about the need to add another portion of flux to the welding pool; welding was performed with the use of flux grades AN-47, AN-22, AN-60 and AN-67A;
- the main criteria for choosing electrode wire were its diameter, which ensures the stability of the process when welding metal of different thickness; chemical composition that guarantees obtaining of mechanical properties and impact toughness of welded joint, which meet the requirements of standard documentation;
- using the procedure given in [6, 7], in the welding process, the high-speed recording of electrical mode parameters (I_c, U_c, V_{wf}) was performed by means of the Hall sensors, the ADC E-140 module and the Power Graph software. Numerical values of electrical parameters of the welding process were recorded at a frequency of 10 thou records per second. To determine the efficiency coefficient of the process η, during welding, the temperature and water consumption for cooling the copper slider were measured. Water temperature was measured by means of the Doubl Laser Infra Red Thermometer, which provides the measurement accuracy of 0.1 °C;
- tests of the weld metal and HAZ on the impact bending of Charpy specimens were conducted.

PRESENTATION OF THE BASIC MATERIAL

To carry out two-electrode welding of vertical joints with forced weld formation, a complex of works was performed to create the mobile welding equipment. In the process of designing a new apparatus, the design of the apparatus A-1150 was selected as a base, which is trackless, i.e. it moves along the slit between the welded edges of the sheets.

Movement of this apparatus is realized by making cuts in the sharp ribs of the edges of steel sheets by the teeth of the cone-shaped running wheel of the apparatus trolley during its pressing by plate-like springs through the knife fixed to the trolley — the rear suspension on the back side of the joint. This suspension pulls and presses the rear shoes — one of two water-cooled copper shoeses forming a weld. Such an apparatus is the most used one in the construction works.

To provide a two-electrode submerged arc welding process, a compact mechanism for feeding two electrode wires (Figure 1) was designed, which by its sizes did not exceed the standard mechanism for welding using one flux-cored wire. Its joint traction gear has two conical grooves for wires. Each of these wires is pressed with its idle gear with the same conical groove in the teeth, which allowed feeding both wires reliably and at the same speed.

Moreover, there were added mechanisms for adjusting the position of electrode wires in the slit between the edges (and distances between them) both separately and

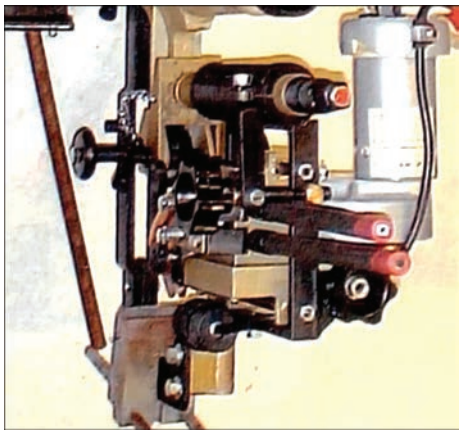

Figure 1. Appearance of upgraded drive for feeding electrode wires

together across the thickness of the joint, and at an angle relative to the weld axis. This, in combination with a standard corrector on the suspension axis, allowed almost plane-parallel displacing of the wires without the danger of "short-circuiting" the tips of the nozzles on welded edges, which would lead to their damage.

The welding voltage supply in such a mechanism is common to both wires, that is, welding is carried out by the so-called "split" arc with power from one current source with remote control.

To ensure the possibility of installing an additional coil with an electrode wire, the design of the coil bracket was changed. Taking into account the twice increased weight of the electrode wire and a load on the running trolley, certain changes were introduced into its design.

For a dosed flux supply, a flux-hopper with a spring-loaded shutoff rod was designed, which makes it possible to use a solenoid and a time relay to determine a portion of flux. The operator had only to determine the moment and frequency of charging, but when the joint deviated from the vertical position at more than 20°, such a flux-hopper did not completely block the flow of flux. Therefore, a flux-hopper was designed with a spring-loaded gate-valve, which reliably blocked the flow of flux during welding of joints when they deviated from the vertical.

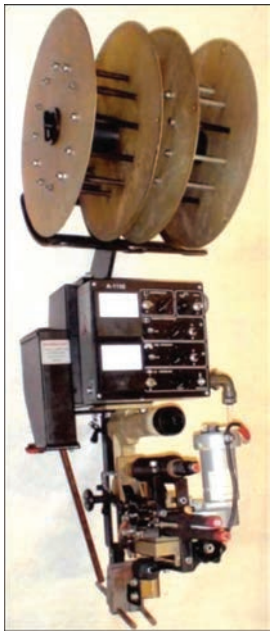

Figure 2. Appearance of prototype of mounting apparatus for welding vertical joints

As a result of the carried out design and experimental works, a prototype of the mounting apparatus for two-electrode welding of vertical welds using solid cross-section wires was designed and manufactured (Figure 2).

Vertical welds and welds inclined to vertical (to 30°) were produced under the minimum possible layer of molten flux, which allowed closing the welding arc from its escaping outside (into the atmosphere). This enabled a visual control (in the gas-cutter glasses) of the positioning of welding wires in the slit-gap between the welding edges, which is important when feeding two wires simultaneously.

The required depth of the molten flux layer depended only on the arc voltage required to melt welded edges at a gap sufficient for safe passing of the nozzle tips, and was determined after stopping the process after the slag solidified above the weld metal. A fairly accurate dependence (approximate equality) of the required height of the molten flux layer and a gap at the joint was noted. Supporting the minimum possible molten flux layer allowed solving two tasks:

- receive a signal about the need in charging the next portion of flux;
- significantly, compared to ESW, reduce the heat input and, as a consequence, increase the impact toughness of welded joint to 27 %.

If slag spattering is absent, the flux during welding was spent only for the formation of a thin (about 1.4–1.5 mm thick) slag crust on the weld surface and proportionally depended on the gap in the joint, and therefore on the voltage. The dependences of flux consumption on an increase in the outlet of welding wires was not observed.

Fluxes, that maintained the electroslag process were not used for conducting research, since the main task of developing the technology was to obtain the process that is as close as possible to the electric arc process. This allows reducing the heat input into the base metal and thus increasing the impact toughness of welded joint, especially at low temperatures. The latter is important when welding metal structures in site conditions, where HTT is impossible.

The first studies of welding with forced formation were performed using fluxes of grades AN-47 and AN-60. Flux AN-60 provided satisfactory results during welding metal of 30–50 mm thick but low stability of the process on the metal of smaller thicknesses. In this case, both in the first and second cases, a tendency to leaking of a melt from under the shoes was observed. During welding under the flux AN-22,

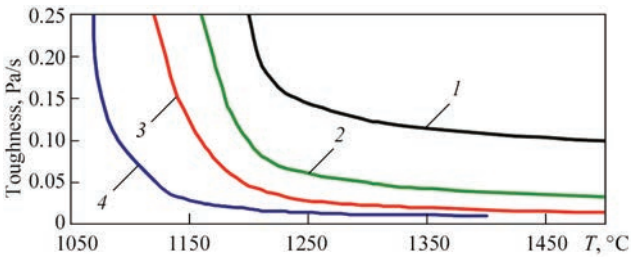

Figure 3. Dependence of flux toughness on temperature [8]: *1* — AN-67A; *2* — AN-348; *3* — AN-60; *4* — AN-22

a high stability of the process and satisfactory (without undercuts) weld surface formation were observed.

However, when using the mentioned flux, leaking of the liquid flux from under the working surface of the shoes was periodically observed, apparently due to the low temperature of its melting, which is unacceptable.

Studies have shown that flux AN-67A has satisfactory technological properties to produce welded joints with forced formation using solid cross-section wires. It provides a high stability of the process, presence of a clear signal about the need in adding another portion of flux, satisfactory formation of the weld surface and easy separation of a skull crust.

The only disadvantage of the flux was its tendency to form undercuts-indents at the edges of the weld due to its high toughness. The problem was solved by changing the configuration of forming weld of the shoes groove.

Thus, fluxes having high electrical conductivity and required toughness are the best for welding vertical joints (Figure 3) [8].

The first studies of submerged arc welding of metal with a thickness of 16 mm were performed using wires of 2 mm diameter [5]. However, a relatively small volume of welding pool did not allow increasing the feed rate of electrode wires of this diameter when welding metal of 14–20 mm thick in order to reduce the heat input, and an increase in the welding gap is not rational from the economic point of view.

It was experimentally established that satisfactory stability of the process can be ensured by using wires of 1.6 mm. Therefore, welding of smaller thicknesses involves the use of electrode wires of even smaller diameter. The use of electrode wires of 2 mm diameter can be recommended for welding metal of more than 20 mm thick.

The use of electrode wires alloyed only by Ni and Mo (for example, Sv-10NMA) did not allow reaching the level of impact toughness of the weld in accordance with regulatory documents. It was experimentally determined that about 1 % Mn should be introduced into the weld metal to provide the required impact toughness. This was achieved by mixing the metal of two electrode wires of Sv-08G2S and Sv-10NMA grades in a joint welding pool. In this case, the weld metal by its chemical composition approaches the surfacing using the wire Sv-08G1NMA.

Figure 4. Submerged arc welding of vertical joint of 20 mm thick with forced formation

Welding of specimens of 12–20 mm thick was performed at the calculated specific input energy E_w = 53.8–60.6 kJ/cm^2 (Figure 4).

Visual inspection of welds showed that the quality of weld formation is satisfactory, undercuts and corrugations are absent (Figure 5).

The examination of welded joint macrostructure showed that the weld metal is dense, no defects in the form of lacks of fusion, cracks, pores, nonmetallic inclusions were detected (Figure 6) [9]. The average depth of the base metal penetration is 7 mm and HAZ width does not exceed 7–8 mm.

The oscillograms of the high-speed recording of electrical mode parameters are shown in Figure 7.

In order to increase the values of impact toughness of welded joints, the technique of welding metal with the thickness of 40 mm in two passes at X-edge preparation was practiced (Figure 8).

In order to expand the technological capabilities of the process, the specimens of a steel of 50 and 64 mm thick were welded (assembled of two sheets of 32 mm thick). Welding of 50 mm thick metal was satisfactory, and for a metal of 64 mm thick, the heat of the arcs was not enough for rapid flux melting — its certain amount remained on the pool surface between the wires. To prevent this, the design of the wire feed mechanism was adjusted for feeding three electrode wires (without changing the dimensions), and the nozzles were replaced by a one solid with the ability to adjust all or one wire

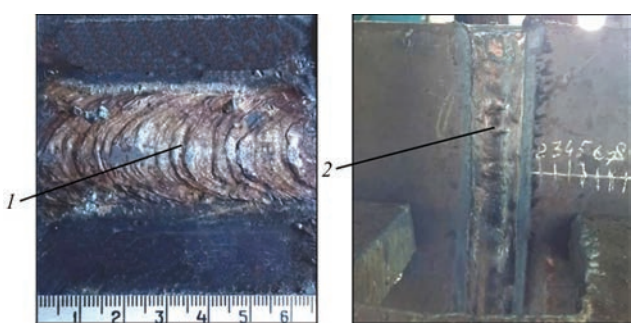

Figure 5. Appearance of welds, produced by welding with forced formation: *1*, *2* — rewelded specimens of 12 and 20 mm thick, respectively

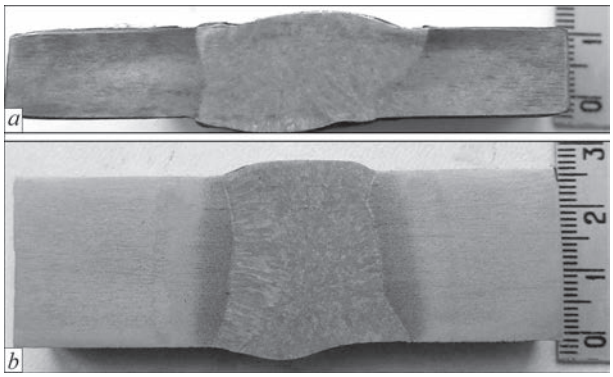

Figure 6. Transverse macrosections of welded joints of 12 (*a*) and 25 mm (*b*) thick

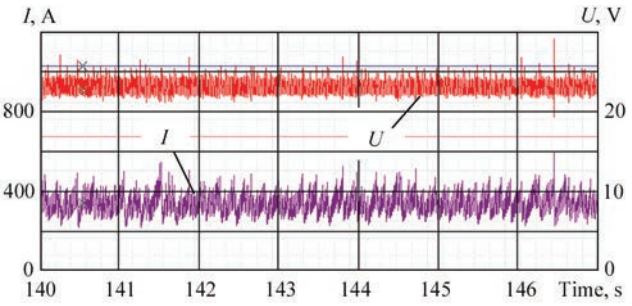

Figure 7. Fragment of welding oscillograms with a stable process

in a depth of the slit simultaneously. The feed mechanism was mounted on the designed suspension already of the rail apparatus on the base of the mechanism for movement of the apparatus AD343. This allowed the Elita-Burji Plant (Tbilisi) to manufacture structural elements of the concert hall Ureki-Natanebi (Figure 9) of 60 and 80 mm thick without angular deformations. The technology of manufacturing square-section pipes with a wall of 20 mm thick with radius rounding along the length was also practiced there.

At present, submerged arc welding was used to produce vertical welds and welds inclided at 30° from the vertical on about 20 span structures of non-standard bridges, overpasses, tunnel walls. Moreover time, the normative service characteristics of joints,

Figure 8. Appearance of weld after the first pass on the metal of 40 mm thick

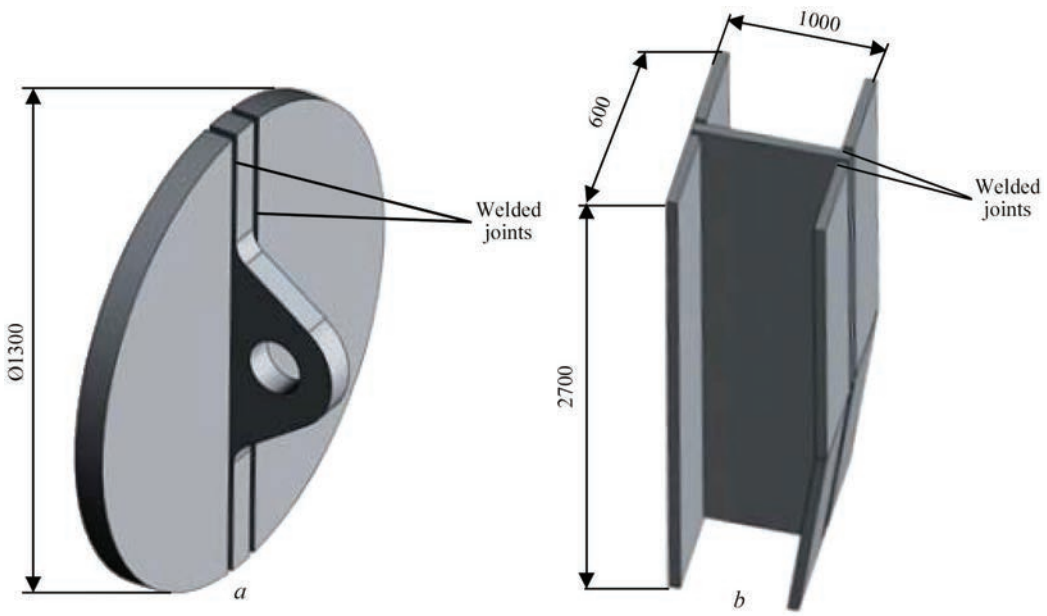

Figure 9. Design schemes of support (*a*) of 80 mm thick and column head (*b*) of 60 mm thick

including impact toughness at temperatures of up to –45 °C were provided.

The main advantages of the proposed method compared to ESW and the method of arc welding using flux-cored wire with forced formation:

- the possibility of refusal from further HTT of welded metal structures due to the low heat input in the base metal [9, 10];
- the possibility of defect-free renewal of the process after an unforeseen (emergency) stop;
- high economical efficiency of the process by more than twice decrease in the welding gap and reduction in flux consumption;
- high efficiency of welding due to a significant increase in the melting coefficient of the electrode wire (welding speed reaches 10 m/h instead of 2.5 m/h when using flux-cored wire);
- providing the quality protection of the welding pool and stable performance of welding process in site conditions in the presence of wind load;
- high cost effectiveness due to the use of non-scarce, not hygroscopic and relatively inexpensive welding consumables;
- improved sanitary and hygienic working conditions of the welder-operator due to the absence of intense radiation and a significant decrease in the volume of emissioned harmful fumes.

CONCLUSIONS

1. As a result of the performed works, the process of welding with forced formation of vertical welds using solid cross-section wire of low-carbon low-alloy steels of 12–80 mm thick was improved in the laboratory conditions. Welding consumables were selected, that provide the necessary mechanical properties of welded joints.

2. A-1150 and AD343 apparatuses were updated and prototypes of apparatuses were manufactured for the creation of a new specialized site welding equipment on a modern elemental base that complies with the requirements of ergonomic indices.

3. Technology and equipment for submerged arc welding with forced formation of vertical joints of low-carbon low-alloy steels of 10–80 mm was developed and successfully implemented in the factory and site conditions.

REFERENCES

1. Kornienko, A.N., Makarenko, N.A. (2019) The birth and formation of electroslag welding. *Avtomatych. Zvaryuvannya*, **10**, 70–73 [in Russian].
2. Paton, B.E., Yushchenko, K.A., Kozulin, S.M., Lychko, I.I. (2019) Electroslag welding process. Analysis of the state and tendencies of development (Review). *The Paton Welding J.,* **10**, 33–40. DOI: https://doi.org/10.37434/tpwg2019.10.05
3. (1980) *Electroslag welding and surfacing*. Ed. by B.E. Paton. Moscow, Mashinostroenie [in Russian].
4. Pokhodnya, I.K., Dubovetsky, V.Ya., Shlepakov, V.N. et al. (1966) Arc welding of vertical seams with forced formation. *Avtomatich. Svarka*, **11**, 67–70 [in Russian].
5. Yablonsky, B.V. (1988) Technique for two-electrode welding of vertical joints with forced formation of a seam under a slag layer. *Avtomatich. Svarka*, **5**, 56–59 [in Russian].
6. Pirumov, A.E., Skachkov, I.O., Suprun, S.A., Maksimov S.Yu. (2007) Specialized information-measuring system for monitoring the process of arc welding. *The Paton Welding J.,* **8**, 34–35.
7. Lychko, I.I., Yushchenko, K.A., Suprun, S.A., Kozulin S.M. (2019) Peculiarities of electrode and base metal melting in electroslag welding. *The Paton Welding J.,* **3**, 12–17. DOI: https://doi.org/10.37434/tpwg2019.03.01.
8. Podgaetsky, V.V., Kuzmenko, V.G. (1988) *Welding slags:* Refer. Book. Kyiv, Naukova Dumka.
9. Pashchin, A.N., Reznik, S.A., Smirnov, O.A., Tokarev, V.S., Goncharov, M.A. (2003) New technology for vertical welding of sheet metal structures using fused flux AN-67B. In: *Proc. of Sci. and Tech. Seminar on Progressive Welding Technologies in Industry, May 20–22, 2003, Kyiv*, Educational Center "Science. Technique. Technology", 69 [in Russian].
10. Maydanchuk, T., Reznik, S. (2021) *The 8th Asian Welding Technology & Application Forum — Intelligent Welding and Surfacing & Additive Manufacturing Technology Remote International Forum, 18.04.2021.* High-performance welding technology of vertical butt joints.

ORCID

S.M. Kozulin: 0000-0002-8368-4545,
S.O. Suprun: 0009-0003-0301-3720

CONFLICT OF INTEREST

The Authors declare no conflict of interest

CORRESPONDING AUTHOR

S.M. Kozulin
E.O. Paton Electric Welding Institute of the NASU
11 Kazymyr Malevych Str., 03150, Kyiv, Ukraine.
E-mail: s.m.kozulin@gmail.com

SUGGESTED CITATION

S.A. Reznik, S.M. Kozulin, S.O. Suprun (2024) Improvement of technology and equipment for welding vertical joints with forced weld formation. *The Paton Welding J*., **9**, 38–43.
DOI: https://doi.org/10.37434/tpwj2024.09.05

JOURNAL HOME PAGE

https://patonpublishinghouse.com/eng/journals/tpwj

Received: 30.04.2024
Received in revised form: 07.06.2024
Accepted: 09.09.2024

DOI: https://doi.org/10.37434/tpwj2024.09.06

REINFORCEMENT OF AN NPP PIPELINE WITH A WALL THINNING DEFECT BY APPLYING EXTERNAL WELD OVERLAY

G.V. Vorona, O.S. Kostenevych, O.S. Milenin, O.V. Makhnenko

E.O. Paton Electric Welding Institute of the NASU
11 Kazymyr Malevych Str., 03150, Kyiv, Ukraine

ABSTRACT

Repair of NPP pipelines with erosive and corrosive wear defects is an urgent problem of the nuclear power industry of Ukraine. When repairing the pipeline, the defective section is cut out and a new pipe coil is installed by welding. However, for a large number of technological pipelines with identified isolated defects, inadmissible wall thinning, replacement of a pipe section is associated with a large volume of repair work. To extend the service life, the defective section of the pipeline can be reinforced, for example, by welding an external overlay, weld deposition, installing a bandage or a welded sleeve. In order to justify the expediency of using reinforcing structures of welded external overlay type at pipeline repair, a finite element analysis of the stress-strain state of a straight section of the pipeline with an erosion-corrosion wear defect under the action of internal pressure before and after repair was carried out. The results of the analysis showed a high efficiency of reinforcement the defective section of the pipeline in the case of using a welded external overlay at repair. The obtained results can be used at justifying the introduction of alternative pipeline repair technologies at NPPs of Ukraine.

KEYWORDS: NPP, pipeline, erosion-corrosion wear, wall thinning defect, reinforcing structure, welded external overlay, stress-strain state, ductile fracture, finite element method

INTRODUCTION

Erosion-corrosion wear (ECW) in pipelines is one of the common problems at long-term operation of NPP. At repair the defective pipeline section is cut out, and a new pipe coil is installed by welding. This process is rather labour consuming and requires draining the transported liquid. As regards pipelines of the primary and secondary circuit of NPP units, such a repair technology is the most reliable and completely restores the pipeline service life. For a large number of technological pipelines, however, replacement of a pipeline section, particularly when individual local wall thinning of inadmissible dimensions is detected, can be excessive. In other sectors, for instance in the main pipeline transportation [1] or in foreign standards [2, 3] there exist several methods of pipeline repair by reinforcement of the defective section, namely welding an external overlay, weld deposition, installing a bandage or welded sleeve. The effectiveness of the defective section reinforcement by mounting a bandage or welded sleeve was considered earlier [4]. In this work the variant of pipeline reinforcement exactly by the welded external overlay is considered. The variant of installing the overlay and its geometrical parameters are shown in Figure 1.

The **objective** of the work is calculation-based assessment from strength viewpoint of the possibility of using an alternative technology of repair of NPP technological pipelines with ECW defects by welding an external overlay.

The admissibility of further operation of a pipeline section with ECW defect was assessed from the viewpoint of ductile fracture, namely, by the results of prediction of the increment of plastic strain intensity (strain criterion) in the defect zone under the action of operational load. The finite element method was used to study the influence of the geometrical parameters, namely initial gap between the pipeline surface and welded overlay

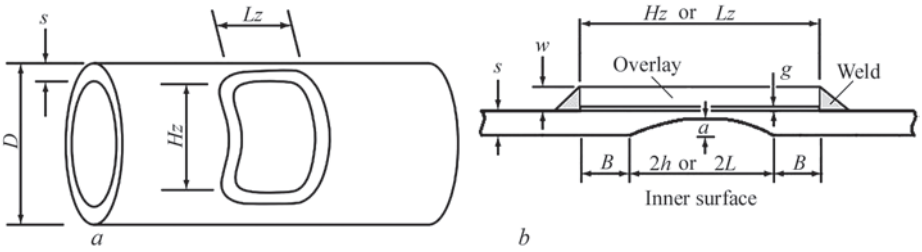

Figure 1. Scheme of reinforcement of the pipeline defective section by a welded external overlay: *a* — general view of the pipeline with the mounted overlay; *b* — section in the external overlay zone

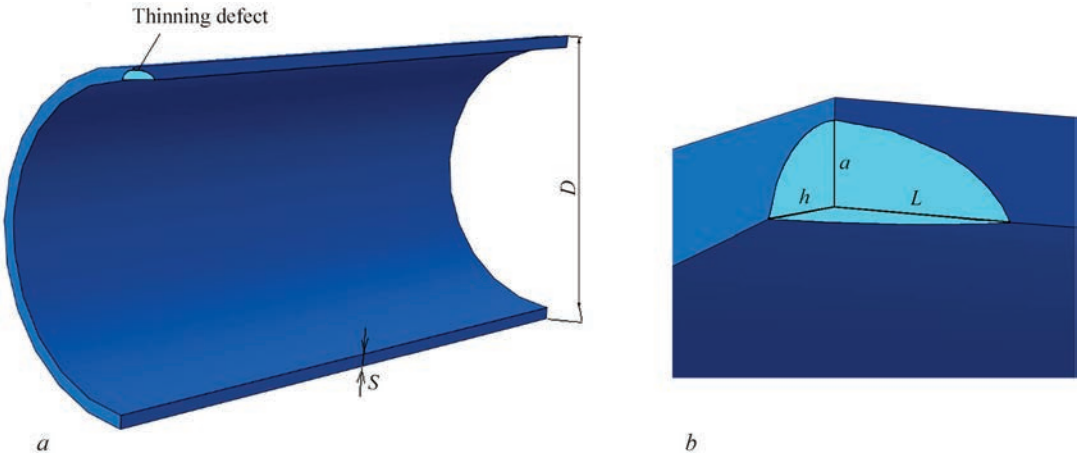

Figure 2. Geometrical model of the straight defective section of the pipeline (1/4 part) (*a*) and inner semi-elliptical defect of wall thinning (*b*)

and linear dimension of the overlay relative to the size of the wall thinning defect, as well as residual welding stresses generated by welding the external overlay on the effectiveness of reinforcement in the straight pipeline section with the wall thinning defect.

PROBLEM DEFINITION

As an example we considered the straight pipeline section having one of the standard dimensions and load parameters for NPP technological pipelines: material was steel 20, pipeline external diameter D = 630 mm, wall thickness s = 25 mm, design pressure P = 11.8 MPa, temperature T = 300 °C.

Critically dangerous geometrical parameters of pipeline wall thinning defect were determined (Figure 2, *b*) by MT-T.0.03.224–18 procedure [5] from the viewpoint of admissibility of further operation of the pipeline section. Dimensions of the critical wall thinning defect (idealized ECW defect of semi-ellipsoid shape) can be as follows: length $L = 2s$ = 50 mm, width $h = s$ = 25 mm, depth a = 20 mm.

The following dimensions of the reinforcing structure of the type of welded external overlay were selected: overlay thickness is equal to pipeline thickness $W = s$ = 25 mm, distance from the thinning edge to overlay edge B = 70 mm, overlay length in the circumferential direction H_z = 190 mm, in the axial direction L_z = 240 mm.

FINITE ELEMENT MODEL

These parameters were used to develop the geometrical and finite element model of the straight pipeline section with ECW defect. Due to symmetry in the two planes (longitudinal and transverse) the developed model consists of 1/4 of the full model (Figure 2, *a*). Mechanical properties of the material are as follows: Young's modulus $E = 2.1 \cdot 10^5$ MPa, Poisson's ratio $\mu = 0.3$, yield limit for steel 20 at the temperature of T = 300 °C, σ_y = 177 MPa [2]. The finite element model with welded overlay application was developed in a similar way.

The problem of the stress-strain state of the defective pipeline section was considered in the elasto-plastic definition, as plastic strains can develop in the zone of ECW defect under the action of internal pressure. In the defect zone the working pressure P = 11.8 MPa is applied to the pipe inner surface. Axial tensile stresses were added to the model end face surface as a boundary condition [8]:

$$\sigma_{zz} = \frac{P D/2}{2s} \rightarrow \sigma_{zz} = 72.6 \text{ MPa}. \quad (1)$$

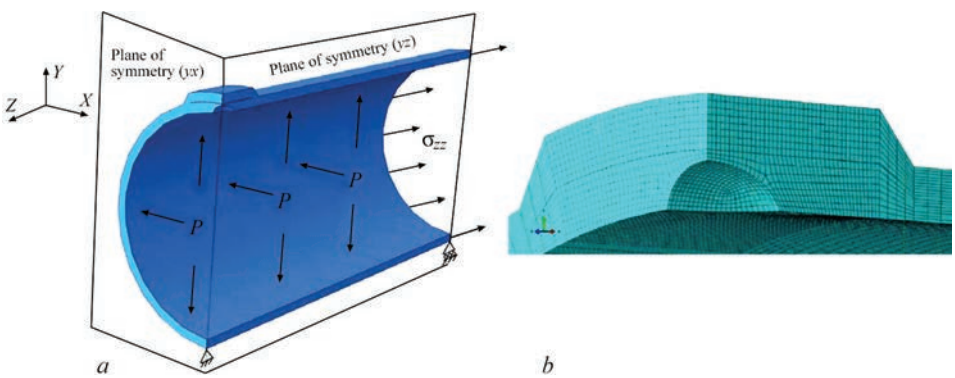

Figure 3. Finite element model of pipeline straight section with a wall thinning defect and reinforcing welded external overlay: *a* — model scheme; *b* — grid of finite elements in the defect zone

Minimal dimension of the finite elements (hexagonal volume element) of the model grid is equal to 3 mm (Figure 3, *b*). Minimal size of the plotted grid elements was selected proceeding from the condition that the value of the maximal equivalent plastic strain changes by less than 5 % at 2 times reduction of the grid minimal dimension.

In pipelines with detected ECW defects the mode of fracture under the impact of internal pressure, is, usually due to the ductile mechanism. The deformation criterion was used to predict the critical condition at ductile fracture under the action of internal pressure in pipeline material with erosion-corrosion wear defect [7]:

$$\int \frac{d\varepsilon_i^p}{\varepsilon_c} \succ 1, \qquad (2)$$

where $d\varepsilon_i^p$ is the increment of plastic strain intensity; ε_c is the critical value of plastic strain, which depends on the rigidity of the stressed state, temperature, material inhomogeneity, etc.

RESULTS OF FINITE ELEMENT ANALYSIS OF SSS

Results of the conducted analysis of SSS of pipeline section without the reinforcing structure showed that under the impact of internal pressure P = 11.78 MPa maximal circumferential stresses of up to 227 MPa (Figure 4) arise in the defective zone, which exceed the material yield limit (177 MPa).

The nominal admissible stress of static strength is determined according to PNAE G 7-002–86 [6], under the condition that

$$[\sigma] = \min\left\{\frac{\sigma_u}{2.6}; \frac{\sigma_y}{1.5}\right\}. \qquad (3)$$

At temperature T = 300 °C the yield limit and ultimate strength are equal to σ_y = 177 and σ_u = 363 MPa, respectively. In keeping with (3), the admissible stress is equal to [σ] = 118 MPa. Such an approach, based on comparison of acting stresses of pipeline wall, developing under internal pressure with admissible stresses for pipeline material in practice is used to establish the nominal dimensions during design. Evaluating the boundary state, determined by development of ductile fracture of pipeline material with a thinning defect, this approach is too conservative. More rational is the above-described approach (2), based on analysis of the results of increment of ductile strain intensity in the defective zone.

By the results of finite element analysis in the case of the defective pipeline section without the reinforcing structure, the maximal circumferential stresses (227 MPa) exceed the admissible stresses and reach the material yield limit (Figure 4, *a*), and the maximal intensity of plastic strains (Figure 5, *a*) in ECW defect zone is equal to $d\varepsilon_i^p$ = 0.011 (1.1 %). Such an increment of the intensity of plastic strains exceeds the established "conditional" limit value ε_c = 0.01 (1%) [7]. Therefore, it can be assumed that conditions are in place for the start of development of ductile fracture of the material.

In the case of a defective section of the pipeline with the mounted external overlay, even though the maximal circumferential stresses (225 MPa) still exceed the admissible stresses and reach the materi-

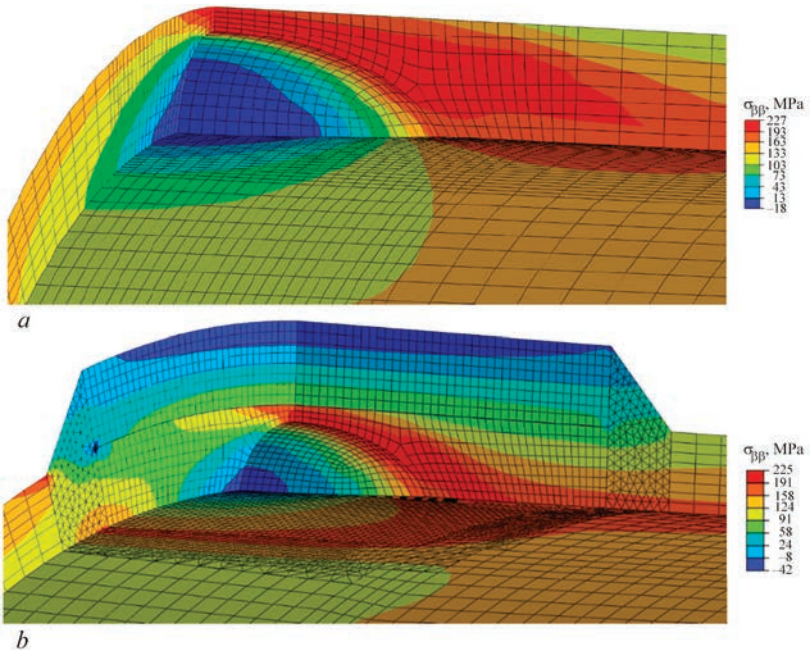

Figure 4. Distribution of circumferential stresses $\sigma_{\beta\beta}$ in the pipeline defective section: *a* — without the reinforcing structure; *b* — with external overlay

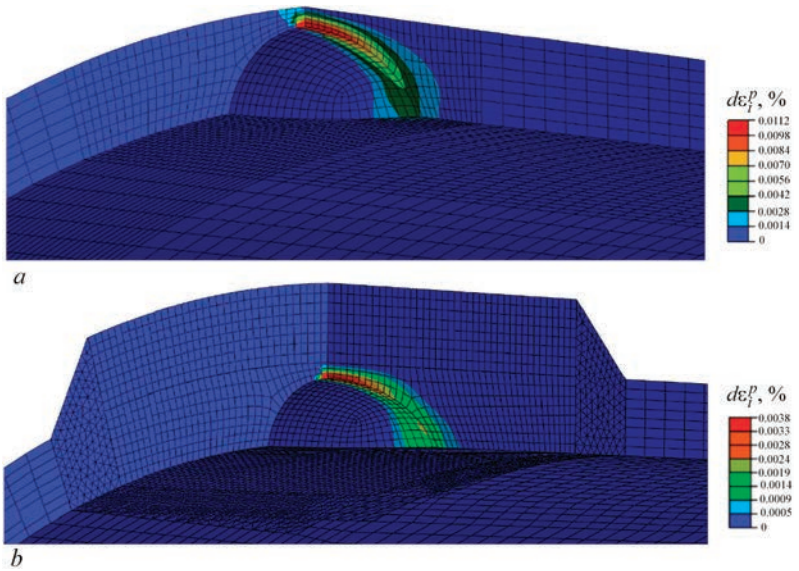

Figure 5. Distribution of the increment of plastic strain intensity in the defective zone of pipeline section: *a* — without the reinforcing structure $d\varepsilon_i^p = 0.011$; *b* — with external overlay $d\varepsilon_i^p = 0.004$

al yield limit (Figure 4, *b*), the maximal intensity of plastic strain (Figure 5, *b*) decreased to $d\varepsilon_i^p = 0.004$ (0.4 %) and is no longer higher than the limit strain of 1 %. Thus, mounting a reinforcing structure of the type of welded external overlay effectively contributes to the prevention of development of plastic strains and pipeline failure in the zone of wall thinning defect under the action of internal pressure.

INFLUENCE OF THE INITIAL GAP

Derived results of numerical prediction of the stress-strain state of the pipeline defective section at its reinforcement by mounting an external overlay showed that the value of gap *g* between the surfaces of the pipeline and the overlap during its mounting does not influence the effectiveness of the defective section unloading (Figure 6, *a*), i.e. unloading occurs not due to contact interaction between the surfaces of the pipeline and the overlay, but as a result of reinforcement of the defective section through the welded joint of the external overlay. This is an important advantage of such a repair technology, as no thorough work on overlay surface preparation and its pressing to the pipeline surface are required before mounting the welded external overlay.

INFLUENCE OF EXTERNAL OVERLAY DIMENSIONS

Another important parameter of the technology of reinforcement of the pipeline defective section by the welded external overlay are the geometrical dimensions of the overlay. The overlay thickness is usually taken equal to the wall thickness of the pipeline being reinforced, as in the case of ECW defect development through the entire wall thickness, the welded external overlay will have the load-carrying capacity, close to that of the pipeline wall. The linear dimension of the external overlay should be greater than that of wall thinning defect. In Figure 1 this increase of the dimensions from each side of the external overlay is marked

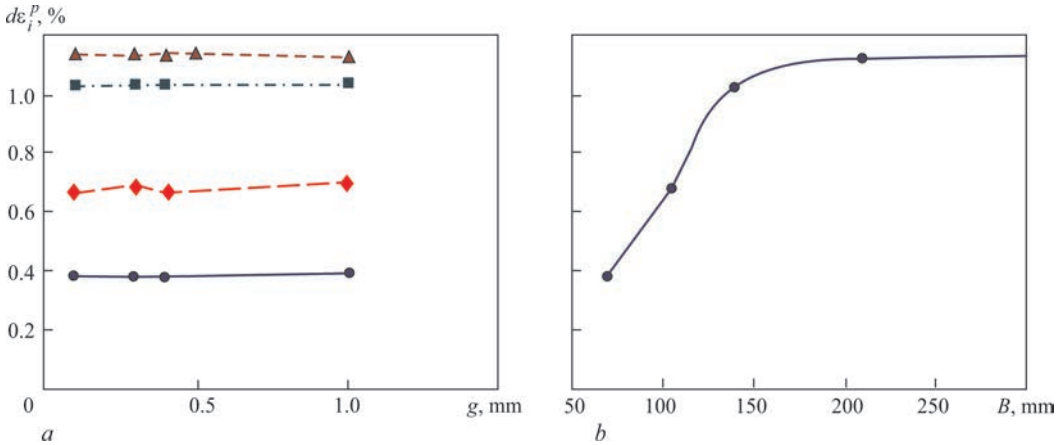

Figure 6. Dependence of maximal values of the increment of intensity of plastic strains $d\varepsilon_i^p$ in the pipeline defect zone on the size of the gap *g* (*a*) and for external overlays of different dimensions (*b*): ● — *B* = 70 mm; ♦ — 105; ■ — 140; ▲ — 210

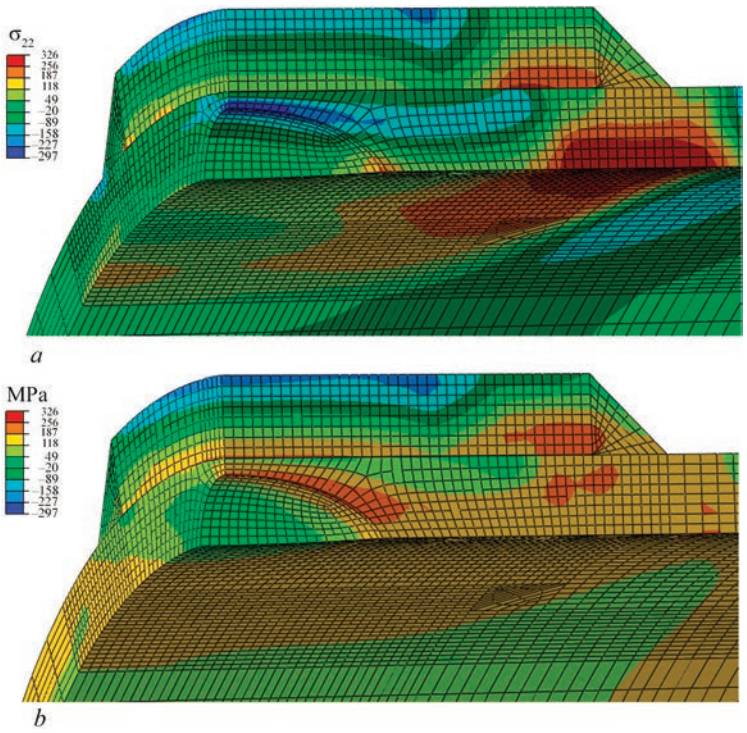

Figure 7. Distribution of circumferential stresses in the zone of pipeline defective section with an external overlay: *a* — residual welding stresses; *b* — from operational load allowing for residual welding stresses

as size B — the distance from the defect edge to that of the overlay. Minimal size B should be [3]:

$$B = \frac{3}{4}\sqrt{\frac{D \cdot s}{2}} = \frac{3}{4}\sqrt{\frac{630 \cdot 25}{2}} \approx 70 \text{ mm}. \quad (4)$$

Results of prediction of the influence of dimension B on unloading of the pipeline defective section (Figure 6) showed that at increase of the linear dimension of the overlay the intensity of increment of ductile strains from operational load in the wall thinning zone becomes much greater, i.e. the effectiveness of the reinforcing structure becomes smaller. This is also explained by the fact that reinforcement of the defective section occurs through the welded joint of the external overlay, and the farther is the welded joint from the wall thinning zone, the lower is the effectiveness of unloading in the thinning zone. Therefore, at repair it is more rational to use minimal admissible linear dimensions of external overlays, which will ensure greater effectiveness of the defective section reinforcement, and will reduce the material cost and welding time.

INFLUENCE OF RESIDUAL WELDING STRESSES

Considering that the welded joints of the external overlay can influence the SSS in the zone of pipelines defect, numerical determination of the residual state of the defective section after welding the external overlay was performed. Welding was conducted by a three-pass fillet weld. Welding speed was 2 mm/s, energy input in the first pass was 23.2 kJ/cm that in the second and third passes was 28.5 kJ/cm.

Residual stresses and strains were determined using thermoplastic analysis by finite element method as a result of following the kinetics of stresses and strains in time under the impact of the thermal cycles of heating and cooling during performance of each welding pass along the external overlay edge.

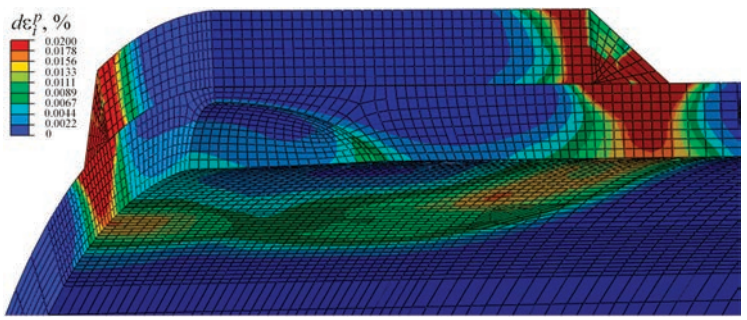

Figure 8. Distribution of the intensity of plastic strains $d\varepsilon_i^p$ in a pipeline section with a wall thinning defect with an external overlay after welding and loading by internal pressure and temperature (in the thinning zone $d\varepsilon_i^p$ = 0.001–0.002)

In keeping with the results of the numerical study (Figure 7), high (up to the yield limit and higher) tensile residual stresses form in the zone of external overlay welded joints, which in the zone of the wall thinning defect cause generate the balancing high compressive stresses of up to 200 MPa. At operational load under the impact of internal pressure $P = 11.8$ MPa and temperature $T = 300$ °C the residual stresses are redistributed, and a stressed state forms in the zone of wall thinning defect (Figure 7), which is characterized by a zone of high tensile stresses (up to the material yield limit) of smaller dimensions, compared with the data without allowing for the residual welding stresses (Figure 4, *b*). Accordingly, the increment of the intensity of plastic strains $d\varepsilon_i^p$ in the zone of wall thinning in the pipeline defective section, from operational load, decreased from 0.004 to 0.001–0.002 (Figure 8). We can come to the conclusion that the compressive residual stresses, developing in the wall thinning zone as a result of welding the external overlay, can contribute to increase of the effectiveness of reinforcement of the pipeline defective section.

CONCLUSIONS

Results of the conducted package of computational studies of the effectiveness of unloading the defective section of a pipeline with ECW defect showed that mounting the welded external overlay can be an effective technology of repair of the technological pipelines with ECW defects for the needs of nuclear power engineering. It was determined that:

1. It is rational to use minimal admissible dimensions of external overlays, that ensures the highest efficiency of reinforcement the pipeline defective section and reduces the material costs and repair time.

2. A significant advantage of welded external overlays over bandages and welded sleeves is the fact that the initial gap between the reinforcing structure and the wall in the case of welded external overlay does not influence the effectiveness of unloading the pipeline defective section. This factor allows greatly reducing the labour consumption of the process of the overlay preparation and mounting (welding) at pipeline repair.

3. Compressive residual stresses, forming in the wall thinning zone as a result of external overlay welding, can contribute to increase of the effectiveness of reinforcement of the pipeline defective section.

REFERENCES

1. (2011) GBN V.3.1-00013741-12:2011. *Main gas pipelines. Repair by arc welding in service conditions.* Ministry of Energy and Coal of Ukraine [in Ukrainian].
2. Jaske, Carl E., Hart, Brian O., Bruce, William A. (2006) *Updated pipeline repair manual.* R2269-01R, United States.
3. *Repair of pressure equipment and piping*. An American national standard. ASME PCC-2-2018 (Revision of ASME PCC-2-2015).
4. Vorona, G.V., Makhnenko, O.V., Milenin, O.S. (2023) Effectiveness of unloading a section of NPS pipeline with a pipe wall thinning defect by mounting a band or welded sleeve. *Tekh. Diahnost. ta Neruiniv. Kontrol*, **4**, 11–19 [in Ukrainian]. DOI: https://doi.org/10.37434/tdnk2023.04.02
5. (2019) MT-T.0.03.224–18: *Procedure for determination of acceptable thicknesses of NPP pipeline elements from carbon steels subjected to erosion-corrosion wear*. NAEK Energoatom [in Russian].
6. (1989) PNAE G-7-002–86: *Norms of strength analysis of equipment and pipelines of nuclear power plants*. Moscow, Energoatomizdat [in Russian].
7. Milenin, A., Velikoivanenko, E., Rozynka, G., Pivtorak, N. (2019) Probabilistic procedure for numerical assessment of corroded pipeline strength and operability. *Int. J. of Pressure Vessels and Piping*, **171**, 60–68. DOI: https://doi.org/10.1016/j.ijpvp.2019.02.003
8. Timoshenko, S.P., Voinovsky-Krieger, S. (1966) *Plates and shells*. Moscow, Nauka [in Russian].

ORCID

G.V. Vorona: 0000-0002-9724-3759,
O.S. Kostenevych: 0000-0002-7427-2805,
O.S. Milenin: 0000-0002-9465-7710,
O.V. Makhnenko: 0000-0002-8583-0163

CONFLICT OF INTEREST

The Authors declare no conflict of interest

CORRESPONDING AUTHOR

O.V. Makhnenko
E.O. Paton Electric Welding Institute of the NASU
11 Kazymyr Malevych Str., 03150, Kyiv, Ukraine.
E-mail: makhnenko@paton.kiev.ua

SUGGESTED CITATION

G.V. Vorona, O.S. Kostenevych, O.S. Milenin, O.V. Makhnenko (2024) Reinforcement of an NPP pipeline with a wall thinning defect by applying external weld overlay. *The Paton Welding J.*, **9**, 44–49.
DOI: https://doi.org/10.37434/tpwj2024.09.06

JOURNAL HOME PAGE

https://patonpublishinghouse.com/eng/journals/tpwj

Received: 23.04.2024
Received in revised form: 10.06.2024
Accepted: 03.09.2024

INTERNATIONAL INSTITUTE OF WELDING AWARD

In 2024, Yevgenia Chvertko, Associate Professor of the Department of Welding Production at Kyiv Polytechnic Institute, PhD, has received the International Institute of Welding award. Yevgenia Chvertko served on the Board of Directors of the International Institute of Welding from 2021 to 2024. In this position, she actively promoted the integration of Ukrainian specialists into the global welding industry. Yevgenia continues her activities as a newly elected member of the International Authorization Board, a joint body of the International Welding Institute and the European Federation for Welding, Joining and Cutting, which deals with training, retraining, certification and qualification of welding personnel and certification of welding companies.

In 2001, Yevgenia Chvertko graduated from the Welding Faculty of the National Technical University of Ukraine "Kyiv Polytechnic Institute" with a Master's Degree in Welding Industrial Systems. After graduation she started working at the Department of Electrical Welding Equipment as an assistant. She worked as a senior lecturer, then as an associate professor, and held the position of deputy dean for work with foreign students and deputy dean for international cooperation. She has been actively involved in career counseling activities. She is a co-organizer of the annual festival "TechnoArt-KPI", developer of thematic lectures and master classes, in particular on welding of decorative structures. In 2018 she became a laureate of the State Prize in Education as a co-author of the work "Development and implementation of innovative teaching technologies for training of specialists in the profession of welder". Currently she works at the Welding Production Department of the E.O. Paton Institute of Materials Science and Welding.

In 2011 she presented her candidate's thesis on monitoring the process of resistance butt welding of concrete reinforcement bars. She holds international professional qualifications of International Welding Engineer, European Welding Engineer and International Welding Inspector.

Since 2008 she has been involved in training, certification and qualification of welding production personnel under the programs of the International Institute of Welding and the European Federation for Welding, Joining and Cutting. She led the creation of an Approved Training Body based on the Welding Faculty. At present, the training body is a part of the E.O. Paton Institute of Materials Science and Welding and has a license to train in the International Welding Engineer, Technologist and Specialist programs. Since its establishment, more than 300 students, graduates and industry representatives have been trained and successfully obtained professional qualifications.

Since 2009 she has been a member of the Ukrainian delegation to the International Institute of Welding and the European Federation, for Welding, Joining and Cutting. She actively participates in the activities of working groups on development and implementation of training programs, qualification and certification of welding personnel. Among the most successful projects are the development of harmonized theoretical and practical examinations for welding coordinators and inspection personnel, participation in the development of the training program for mechanized, orbital and robotic welding, participation in the development of a procedure for re-crediting previous work experience and education for applicants (the procedure for welding coordinators was implemented this year, the procedure for inspectors is currently being developed). The main provisions of the re-crediting procedure were highlighted in a report at the PolyWeld-2023 conference.

In 2018, she became the first representative of Ukraine to the team of assessors who audit the activities of bodies operating under the licenses of the International Institute of Welding and the European Federation for Welding, Joining and Cutting.

In 2021 she was elected to the Board of Directors of the International Institute of Welding. During her tenure on the Board, together with the E.O. Paton Institute of Electric Welding of the National Academy of Sciences of Ukraine, she has significantly intensified cooperation with professional organizations in Ukraine. In particular, the participation of Ukrainian scientists, including young specialists, in professional events has significantly increased, which helps to integrate scientific youth into the international welding community and to inform foreign colleagues about modern developments and research.

At the beginning of the large-scale invasion, she greatly contributed to revoking russia's membership in the International Institute of Welding, as well as the relevant licenses for personnel qualification and certification of welding companies.

We sincerely congratulate Yevgenia and wish her further fruitful work!

Editorial Board

CERTIFIED QUALITY: THE USE OF WELDING WIRE IN THE TRANSPORT INDUSTRY

Today, welding technologies play a crucial role in the manufacturing and repair of transportation, from railway cars to commercial vehicles. The quality of welding materials directly affects the safety, durability, and performance of vehicles. That is why stringent control and adherence to international standards are so important.

A prime example of the application of high-quality welding materials is their use in the railway industry, where safety and reliability are always top priorities. DNIPROMETYZ TAS, a manufacturer specializing in welding wire, has recently been certified by Deutsche Bahn — a leading railway operator in Europe. This certification confirms that our products meet the most stringent requirements and can be safely used in the construction and repair of railway rolling stock.

• Manufacturing Capabilities and Technologies

At DNIPROMETYZ TAS, advanced technologies from the Swedish manufacturer Lämneå Bruk AB and high-quality raw materials are used in the production of welding wire. Quality control of wire rods and testing of finished products are conducted in our own accredited laboratory, equipped with modern instruments for chemical analysis, mechanical tests, and welding technology tests. This ensures the production of the highest quality products, verified by leading industrial enterprises.

The plant employs intelligent production management systems, enhancing efficiency and flexibility, and improving customer orientation at all stages of production. The plant places particular emphasis on product certification and holds several important certifications, including ISO 9001 and TÜV NORD compliance with European standards. Our products also meet the safety and health requirements of the European Union, as confirmed by CE marking.

• Advantages of Welding Wire for Transportation

The welding wire produced at our plant, thanks to stringent quality control standards, is ideal for complex welding tasks in the transport industry. It provides high joint strength, corrosion resistance, and durability, which is critical for vehicles operating in various climatic conditions.

Furthermore, our collaboration with organizations such as Deutsche Bahn allows us to continuously improve production technologies, de-

velop innovative solutions, and ensure unparalleled quality of welding materials. Our plant manufactures welding wire grades 3Si1 and 4Si1, with diameters ranging from 0.6 to 2.0 mm, which have successfully passed Deutsche Bahn certification.

• Reliability of Supplies

Effective logistics and timely delivery of products are key to our success. The plant has its own fleet, which reduces delivery time and improves service quality, ultimately contributing to increased customer satisfaction.

Reliability and speed of delivery play a crucial role in meeting our clients' needs. Therefore, we continuously work on improving operational efficiency, allowing us to provide high-quality products in the shortest possible time.

• Environmental and Social Aspects

DNIPROMETYZ TAS not only strives for excellence in products but also continuously invests in the development of its employees and technologies. Regular training and qualification courses are conducted both internally and with the involvement of external experts. The plant actively collaborates with educational institutions and technical universities to stay abreast of the latest achievements and technologies.

Additionally, we place significant emphasis on sustainable development and environmental responsibility. Energy-efficient technologies are used in the manufacturing process, and we aim to minimize waste. All our operations comply with environmental standards, and environmental audits are conducted regularly. We also invest in the development of environmentally friendly production methods to reduce our impact on the environment.

Deutsche Bahn certification is not only a confirmation of quality but also a commitment to our clients. We continue to improve our technologies to meet the strictest requirements of the transport industry and offer the market products that adhere to the highest standards of reliability. Our plant remains one of the leading manufacturers of fasteners in Ukraine, maintaining a leading position and actively expanding its markets both domestically and internationally.